NOTICE

The quality of this microform is heavily dependent upon the quality of the original thesis submitted for microfilming. Every effort has been made to ensure the highest quality of reproduction possible.

If pages are missing, contact the university which granted the degree.

Some pages may have indistinct print especially if the original pages were typed with a poor typewriter ribbon or if the university sent us an inferior photocopy.

Reproduction in full or in part of this microform is governed by the Canadian Copyright Act, R.S.C. 1970, c. C-30, and subsequent amendments.

AVIS

La qualité de cette microforme dépend grandement de la qualité de la thèse soumise au microfilmage. Nous avons tout fait pour assurer une qualité supérieure de reproduction.

S'il manque des pages, veuillez communiquer avec l'université qui a conféré le grade.

La qualité d'impression de certaines pages peut laisser à désirer, surtout si les pages originales ont été dactylographiées à l'aide d'un ruban usé ou si l'université nous a fait parvenir une photocopie de qualité inférieure.

La reproduction, même partielle, de cette microforme est soumise à la Loi canadienne sur le droit d'auteur, SRC 1970, c. C-30, et ses amendements subséquents.

PHOTOLUMINESCENCE OF HEAVILY Zn-DOPED GaAs AND $Ga_{0.85}In_{0.15}As$ GROWN BY LOW-PRESSURE METAL ORGANIC VAPOUR PHASE EPITAXY

SUBMITTED BY

ROBERTO BENZAQUEN

B.Sc (HONOURS), McGILL UNIVERSITY, 1989

A THESIS SUBMITTED TO THE FACULTY OF GRADUATE STUDIES AND RESEARCH IN PARTIAL FULFILMENT OF THE REQUIREMENTS FOR THE DEGREE OF

MASTER OF SCIENCE

IN PHYSICS

DEPARTMENT OF PHYSICS

UNIVERSITY OF OTTAWA

34 GEORGE GLINSKI

OTTAWA, CANADA

K1N 6N5

1991

ISBN 0-315-70522-1

UNIVERSITÉ D'OTTAWA
UNIVERSITY OF OTTAWA

A MIS MUY QUERIDOS PADRES.

ABSTRACT

Zn-doped, p-type, GaAs and $Ga_{0.85}In_{0.15}As$ samples grown by low-pressure metal organic vapour phase epitaxy with free carrier concentrations in the range of $n=4.3\times10^{14}$ cm^{-3} (nominally undoped)-$p=1.95\times10^{20}$ cm^{-3} at room temperature have been studied by temperature-dependent photoluminescence. At low doping levels, recombinations involving discrete impurity states and free excitons provided measurement of both the 5 K band gap ($E_g(5)=(1.296 \pm 0.003)$ eV) and the zinc acceptor binding energy ($E(Zn^0)=(0.025 \pm 0.003)$ eV) in the $Ga_{0.85}In_{0.15}As$ alloy. At high concentrations, the discrete acceptor levels are replaced by an impurity band which merges with the valence band above the Mott[1] transition. This gives rise to a density of states band tail extending into the gap and containing both extended and localised states. In the presence of such a high density of impurities, potential fluctuations and interparticle interactions result in a band gap shrinkage $|\Delta E_g|$ which has been observed with photoluminescence experiments. A model based on the presence of Kane[2] band tails and on the assumption of a constant matrix element for the relevant optical transitions has been fitted to the photoluminescence spectra of heavily doped layers of GaAs and $Ga_{0.85}In_{0.15}As$ in the range of $p=1.6\times10^{18}$ cm^{-3}-$p=1.95\times10^{20}$ cm^{-3}. This model provided a good description of the experimental results. The 5 K band gap shrinkage has been found to be $|\Delta E_g|=2.7\times10^{-8}p^{1/3}$ for GaAs and $|\Delta E_g|=1.4\times10^{-8}p^{1/3}$ for $Ga_{0.85}In_{0.15}As$ with $|\Delta E_g|$ in eV and p in cm^{-3}.

RÉSUMÉ

Des échantillons d'AsGa et de $Ga_{0.85}In_{0.15}As$ produits par épitaxie à base de composés organométalliques, principalement de type p, dopés au zinc jusqu'à une concentration de l'ordre de $p=1.95x10^{20}$ cm^{-3} à 300 K, sont étudiés par photoluminescence en fonction de la température. A bas dopage, des recombinaisons impliquant des niveaux d'impuretés et des excitons libres permettent de déterminer, dans l'alliage $Ga_{0.85}In_{0.15}As$, l'énergie de liaison du zinc ($E(Zn^0)=(0.025 \pm 0.003)$ eV) ainsi que l'énergie de la bande interdite à 5 K ($E_g=(1.296 \pm 0.003)$ eV). A fort dopage, les niveaux discrets s'élargissent en une bande d'impuretés qui se confond à la bande de valence au-dessus de la transition de Mott[1]. Les fluctuations de potentiel et les interactions entre particules produisent alors un rétrécissement $|\Delta E_g|$ de la bande interdite. Ce phénomène est observé par photoluminescence et analysé sur la base d'un modèle qui inclut des queues de bandes de type Kane[2] et un élément de matrice constant pour les transitions interbandes. Ce modèle reproduit de façon satisfaisante les courbes expérimentales d'échantillons d'AsGa et de $Ga_{0.85}In_{0.15}As$ avec des concentrations variant entre $p=1.6x10^{18}$ cm^{-3} et $p=1.95x10^{20}$ cm^{-3}. Le rétrécissement de la bande interdite à 5 K a été déterminé pour l'AsGa, $|\Delta E_g|=2.7x10^{-8}p^{1/3}$, ainsi que pour l'alliage $Ga_{0.85}In_{0.15}As$, $|\Delta E_g|=1.4x10^{-8}p^{1/3}$, où $|\Delta E_g|$ et p se mesurent respectivement en eV et en cm^{-3}.

ACKNOWLEDGMENTS

This research project was completed at the **Advanced Epitaxy Section** of the **Institute for Microstructural Sciences (IMS)** of the **National Research Council of Canada (NRCC)**. I am indebted to several people for their assistance in preparing the present thesis.

I wish to express my sincere thanks to :

Dr A P. ROTH from the **NRCC** for accepting to direct my work, for providing the help and facilities necessary for its completion and for financial support through a grant from the **NSERC**. I would also like to thank Dr A.P. ROTH for the many informative discussions about the photoluminescence of semiconductors. Merci Alain!

Professor E. FORTIN from the **University of Ottawa** for co-directing my research work and for financial assistance through a grant from the **NSERC**.

Mr C. LACELLE from the **NRCC** for technical assistance and for the growth of a series of GaAs and $Ga_{0.85}In_{0.15}As$ epilayers.

Dr J.J. DUBOWSKI from the **NRCC** for technical assistance and for introducing me to the photoluminescence of CdMnTe.

Dr M. BENZAQUEN from **McGill University** for enlightening discussions on the electronic properties of semiconductors. Gracias Morlin!

TABLE OF CONTENTS

INTRODUCTION

The recent progress in the physics of III-V compound semiconductors is directly related to major advancements in growth and device technologies. The growth of high quality material by molecular beam epitaxy (MBE) and low-pressure metal organic vapour phase epitaxy (LP-MOVPE) and the ability to fabricate thin multi-layer structures using these techniques has led to a rapid development in the production of electronic and opto-electronic devices based on III-V semiconductors. High speed field effect transistors (FETs) and quantum well lasers (QWLs) have been built using direct gap III-V semiconductors. The advantage of having optical and electronic devices based on a single technology provides the driving force for the replacement of the current Si and Ge based technology by the III-V technology. A thorough understanding of the underlying physics is required for the future improvement and advancement of the III-V growth and device technologies.

In this work, we have studied the effect of heavy p-type doping on the band gap of GaAs and $Ga_{0.85}In_{0.15}As$, with temperature-dependent photoluminescence (PL) measurements. GaAs was used as a test material for our numerical analysis while the measurements in $Ga_{0.85}In_{0.15}As$ provided to the best of our knowledge the first determination of the band gap shrinkage in this alloy. The epitaxial layers were grown using conventional LP-MOVPE. The effects of heavy doping on optical and electrical properties of materials such as $Ga_{0.85}In_{0.15}As$ are of interest

both from a fundamental point of view and for device applications. Many devices incorporate heavily doped layers whose properties can affect their performance. $Ga_{0.85}In_{0.85}As$ epitaxial layers grown on GaAs substrates are used in a variety of devices and therefore their properties must be investigated in detail. For example, high performance modulation-doped field-effect transistors (MODFETs) incorporating a single $Ga_{0.85}In_{0.15}As$[3] layer have been achieved.

We have determined the band gap shrinkage in both GaAs and $Ga_{0.85}In_{0.15}As$. Doping levels as high as $p=1.95x10^{20}$ cm^{-3} have been investigated. The measured experimental curves have been analyzed by performing a line shape analysis. This method is based on an approach that has been used for the study of PL spectra of Si[4] by assuming a constant matrix element for the relevant optical transitions. Band tailing effects were included by assuming a Kane-type[2] density of states with parameters to be determined with the experimental data.

Chapter 1 presents a summary of the effect of light and heavy doping on the electronic properties of GaAs and $Ga_{0.85}In_{0.15}As$. This summary describes how discrete impurity states are replaced by an impurity band as the majority impurity concentration N_A of the material is increased. This summary also includes a qualitative description of the band structure, along with a list of the relevant physical material parameters.

Chapter 2 provides an outline of the various luminescent transitions encountered in GaAs and $Ga_{0.85}In_{0.15}As$. The model chosen to describe the PL spectra of heavily doped GaAs and $Ga_{0.85}In_{0.15}As$ is also presented.

Chapter 3 describes the experimental setup.

Chapter 4 discusses the experimental results.

Finally, we give a summary of the conclusions that can be drawn from our experiments.

CHAPTER 1

EFFECT OF LIGHT AND HEAVY DOPING ON THE ELECTRONIC PROPERTIES OF GaAs AND $Ga_{0.85}In_{0.15}As$

1.1 INTRODUCTION

The properties of semiconducting crystals are controlled by its band structure. The fullest information on the properties of such a system, including its energy spectrum, can be obtained by solving Schrödinger's equation for the stationary states of the system. However, we have to deal with a large number of interactions: electrons with other electrons, nuclei with other nuclei, and electrons with nuclei. Because the wavefunction depends on an enormous number ($\sim 10^{23}$) of independent variables, there is no known exact solution to the problem. Nevertheless, many (direct gap) semiconductors show similitudes between the motion of an electron in the crystal and the free electron. In that case, most of the electronic transport properties can be described in classical terms by considering the electrons as free carriers with an effective mass m^*.

Let us consider a three dimensional intrinsic semiconducting crystal with a lattice constant denoted by a. Let $V(r)$ be a periodic crystalline potential where $V(r) = V(r + a)$. In this case, the solutions of the one electron Schrödinger's equation

$$\left(-\frac{\hbar^2}{2m_0} \vec{\nabla}^2 + V(r) \right) \Psi_{n,k}(r) = E \Psi_{n,k}(r) \qquad (1.1.1)$$

are of the form

$$\Psi_{n,\vec{k}}(\vec{r}) = u_{n,\vec{k}}(\vec{r}) \exp(i\vec{k}\cdot\vec{r}) \qquad (1.1.2)$$

where n labels the energy band and $\vec{k}$ is the electron wavevector. The solutions are plane waves modulated by a periodic function $u_{n,\vec{k}}(\vec{r})$ where $u_{n,\vec{k}}(\vec{r}) = u_{n,\vec{k}}(\vec{r}+\vec{a})$. This result is frequently called the Bloch[5] theorem and the functions are known as the Bloch functions.

Due to the form of the functions $\Psi_{n,\vec{k}}(\vec{r})$, we must demand that $\vec{k}$ be real. Indeed, any imaginary $\vec{k}$ would result in function $\Psi_{n,\vec{k}}(\vec{r})$ being infinite in particular directions. Such functions are not acceptable physically. In any given direction of $\vec{k}$, energy regions corresponding to imaginary values of $\vec{k}$ are found, which must be excluded from the energy spectrum of the electron, that is, allowed bands alternate with forbidden bands. In semiconductors, at least one forbidden band (the band gap) exists regardless of the direction of $\vec{k}$.

1.2 BAND STRUCTURE

GaAs and $Ga_{0.85}In_{0.15}As$ are direct gap semiconductors that crystallize in the zincblende lattice. The zincblende lattice can be considered as two interpenetrating face-centred cubic lattices. For a zincblende lattice such as GaAs, the major binding force is from the covalent bonds. However, GaAs has a slight ionic binding force that is an electrostatic attractive force between each Ga^- ion and its four neighbouring As^+ ions, or between each As^+ ion and its four

neighbouring Ga^- ions.

The band model presented here was first proposed by Kane[6]. For very small values of $\vec{K}$ at the vicinity of the Γ point ($\vec{K} = 0$), Kane obtained four parabolic bands. The band structure at the centre of the first Brillouin zone (FBZ) is shown in fig.1.2.1. The energy gap, E_g, is a function of the temperature T and is given by

$$E_g(T) = E_g(0) - \frac{3LT}{R_c}\left(\frac{\partial E_g}{\partial P}\right)_T \qquad (1.2.1)$$

where L and R_c are respectively the coefficients of thermal expansion and compressibility and $(\partial E_g/\partial P)_T$ describes the variation of the band gap with pressure.

As shown in fig.1.2.1, the valence band maximum at $\vec{K}=0$ is doubly degenerate with two $E(\vec{K})$ branches meeting at the centre of the FBZ. The two branches give different effective masses, corresponding to the heavy and light holes, respectively. A third valence band is separated from the two other bands by a value Δ due to spin orbit interaction.

At the Γ point in both GaAs and $Ga_{0.85}In_{0.15}As$, the valence band wavefunctions are p-like and the conduction band wavefunctions are s-like. Hence, electric dipole transitions are allowed and creation of electron hole pairs via absorption of above band gap light is very efficient. Excitation is followed by rapid thermalization of the electrons and holes. The electrons (or holes) quickly lose excess kinetic energy through collisions with other electrons (or holes) and

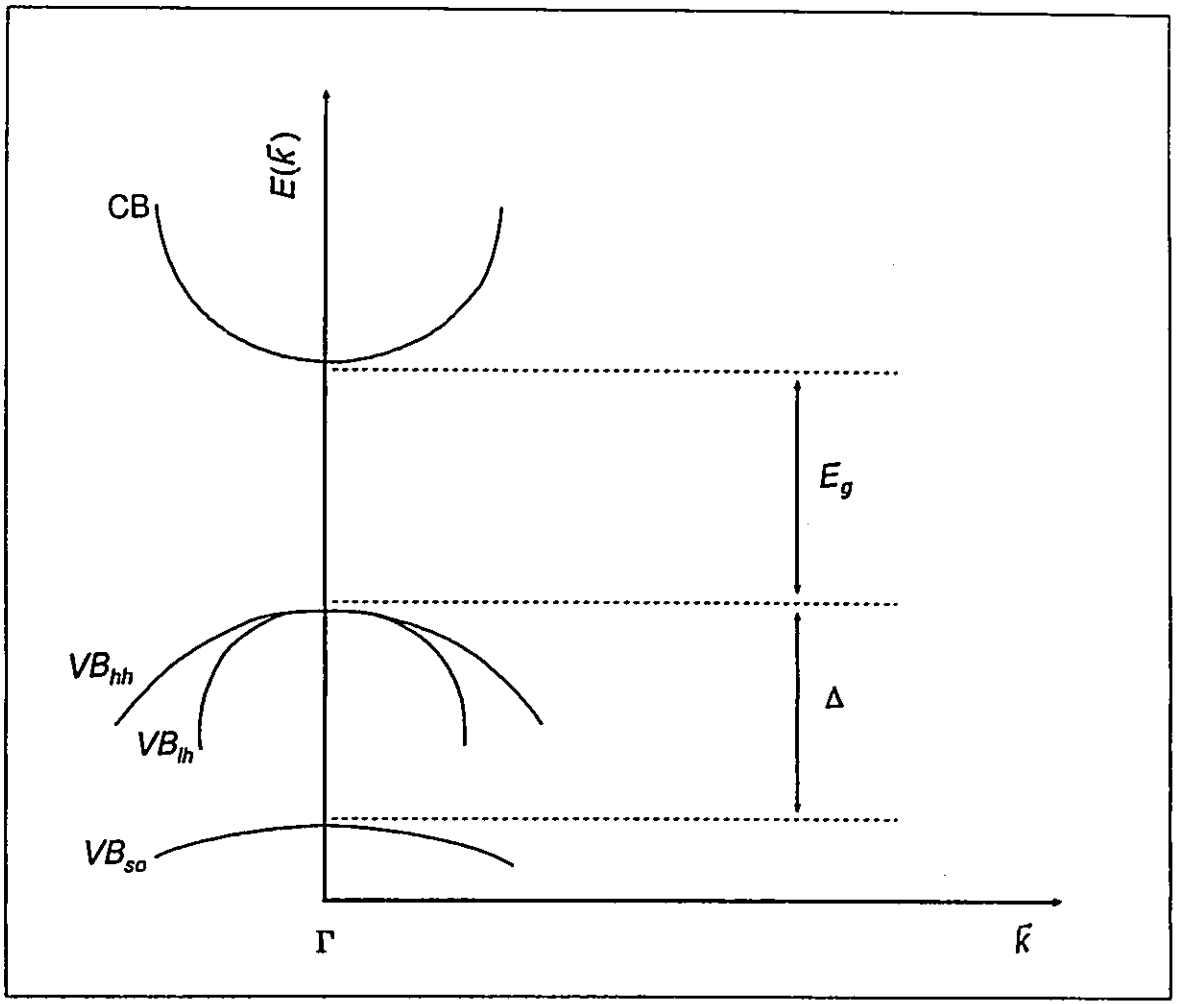

Figure 1.2.1. Conduction band (CB) and valence bands (VB_{hh}, VB_{lh}, VB_{so}) at the Γ point ($\vec{k}=0$) for a semiconductor with zincblende structure. The band gap E_g and the separation Δ due to spin-orbit interaction are also shown.

the emission of acoustic and optical phonons. A quasi-equilibrium distribution of electrons and holes among the existing energy levels is set up under continuous excitation. Excitation is balanced by luminescent and non-radiative recombination processes.

1.3 PHYSICAL PARAMETERS OF GaAs AND OF $Ga_{0.85}In_{0.15}As$

The physical parameters used in this work are presented in table 1.3.1 for GaAs and InAs. These are well established physical parameters found in the scientific literature and they do not require further comments. For the purposes of this work, a linear interpolation[7] between GaAs and InAs is performed in order to determine the relevant physical parameters of the $Ga_{0.85}In_{0.15}As$ alloy.

The following notations have been adopted for the various material parameters :

m_e^* is the electron effective mass,

m_{lh}^* is the light hole effective mass,

m_{hh}^* is the heavy hole effective mass,

m_0 is the free electron mass,

κ is the dielectric constant,

a is the lattice constant.

Table 1.3.1. Physical material parameters of GaAs and $Ga_{0.85}In_{0.15}As$.

Parameters	GaAs	InAs	$Ga_{0.85}In_{0.15}As$
m_e^*	$0.067\,m_0$	$0.023\,m_0$	$0.060\,m_0$
m_{lh}^*	$0.082\,m_0$	$0.026\,m_0$	$0.074\,m_0$
m_{hh}^*	$0.51\,m_0$	$0.41\,m_0$	$0.495\,m_0$
κ	12.74	15.15	13.10
a	5.653 Å	6.058 Å	5.714 Å

1.4 SHALLOW IMPURITY LEVELS

Impurity atoms have a considerable effect on the optical and electrical properties of semiconducting materials. When a semiconductor is doped with donor or acceptor impurities, impurity levels appear in the forbidden band gap. For a donor impurity state, an electron is localized around an impurity atom from which it can be released to the conduction band edge with a rather small expenditure of energy. A donor impurity atom can therefore make an electron

available for conduction. In a similar way, an acceptor state is an energy state linked to an impurity atom which can accept an electron from the valence band. This is equivalent to a hole being created. Since the energies involved in these processes are typically much smaller than the energy required to directly excite an electron from the valence band to the conduction band, the electrons and holes which are thermally excited from impurity states generally dominate the electrical properties of semiconductors at all but the highest temperatures in the absence of illumination (or other external excitation).

The incorporation of Zn in GaAs and $Ga_{0.85}In_{0.15}As$ introduces shallow impurity acceptor states. In both of these materials, Zn is a substitutional impurity atom capable of replacing a Ga atom without significantly distorting the lattice. Zn has one less valence electron than Ga. The corresponding perturbation to the electronic energy spectrum results in an acceptor energy level locally appearing in the forbidden gap at the Zn site. Replacing a Ga atom by a Zn atom is in fact equivalent to expelling an energy state from the valence band into the forbidden gap. In semiconductors, shallow impurity acceptor states have orbits of the order of 50-100 Å in diameter and binding energies in the range of 10-50 meV.

The Hamiltonian of a hole linked to a substitutional acceptor is given by

$$H = -\frac{\hbar^2}{2m_0}\vec{\nabla}^2 + V(r) + U(r) \qquad (1.4.1)$$

where, at large distances from the impurity ion, one can write

$$U(r) = -\frac{e^2}{\kappa r} \tag{1.4.2}$$

Calculations by Kohn[8] in the effective mass approximation (EMA) have shown that the wave function of a charge carrier linked to an impurity centre is of the form $u_{n,\vec{k}}(r)\,F(r)$. In other words, the wave function of an impurity state is the Bloch wave function of the free carrier modulated by a large scale envelope function, $F(r)$. $F(r)$ satisfies the expression

$$\left(-\frac{\hbar^2}{2m^*}\vec{\nabla}^2 - \frac{e^2}{\kappa r}\right)F(r) = EF(r) \tag{1.4.3}$$

which is called the effective mass equation. The energy spectrum of equ.(1.4.3) is

$$E_n = \frac{e^4 m^*}{2\hbar^2\kappa^2 n^2} \tag{1.4.4}$$

The eigenfunctions are similar to the ones of the hydrogen atom. For example, the normalised function for the ground state is

$$F_{1s}(r) = \frac{1}{\sqrt{\pi a^{*3}}}\exp\left(-\frac{r}{a^*}\right) \tag{1.4.5}$$

with

$$a^* = \frac{\hbar^2\kappa}{e^2 m^*} \tag{1.4.6}$$

where a^* is the Bohr radius. The Bohr radius determines the characteristic dimensions in which the wave function is not exponentially small. Because of the large value of the dielectric constant and the small value of the effective mass, the Bohr radius in p-type semiconductors turns out to be quite large. For example, in p-type GaAs where $m^* = m_h^* = 1/2(m_{hh}^* + m_{lh}^*) = 0.296\, m_0$ (we have taken into account the double degeneracy of the valence band at the Γ point by assuming, in a first approximation, an average value between m_{lh}^* and m_{hh}^*.), one finds $a^* = 23$ Å.

1.5 IMPURITY BANDS

We have seen that isolated impurity atoms form discrete energy levels in the forbidden band. The wave function of a hole occupying such a level is localized in the vicinity of the corresponding atom. The notion of independent impurity atoms is only justified when their wave functions do not overlap significantly. This means that the average separation between impurities exceeds the Bohr radius a^* i.e. $N_A\, a^{*3} < 1$ where N_A is the majority impurity concentration. In such a case, a semiconductor is said to be lightly doped.

As discussed in section 1.4, the radius of a hole state near a shallow impurity depends strongly on the nature of the host semiconductor and on the band near which the state is located. Therefore, for shallow impurities, the range of concentrations corresponding to light doping varies from one material to

another. In the same material, it depends on whether the impurities are donors or acceptors.

It is useful to clearly distinguish between heavy and light doping. A criterion for this is given by the static conductivity at low temperatures. The conductivity is metal-like (depends only weakly on temperature) in heavily doped semiconductors whereas in lightly doped semiconductors, it is activated (vanishes exponentially as $T \to 0$). It is reasonable to draw the boundary between light and heavy doping at the impurity concentration N_M, where a nonvanishing conductivity appears in weakly compensated semiconductors at zero temperature. This transition is called metal-insulator or, more specifically, the Mott[1] transition and takes place at a concentration given by

$$N_M^{1/3} a^* \approx 0.25 \qquad (1.5.1)$$

In p-type GaAs doped with Zn impurities, for example, $N_M = 1.3 \times 10^{18}$ cm^{-3}. In p-type $Ga_{0.85}In_{0.15}As$ doped with Zn impurities, $N_M = 1.1 \times 10^{18}$ cm^{-3}. We point out that weak compensation was mentioned intentionally in the definition of N_M. When the compensation is significant, the Mott transition occurs at higher impurity concentrations. In fact, compensation is known to increase local disorder which consequently leads to stronger carrier localisation.

As the electronic wave functions of holes located near different impurities overlap, the discrete impurity levels are replaced by an impurity band which is separated by a gap from the valence band. The very notion of crystal momentum

in the impurity band requires justification since the impurity atoms are not, generally, periodically spaced. One should rather think of them as randomly distributed in the crystal.

Even when the sample is macroscopically homogeneous (the impurity concentration averaged over a large enough volume of the crystal is constant), there may also be appreciable fluctuations of the impurity concentrations on a microscopic scale. This leads to a second mechanism of level broadening, which originates in the fluctuations of the hole potential energy.

Intermediate doping corresponds to the presence of an impurity band well separated from the valence band (p-type material) of the host crystal. The relevant impurity concentration N_A may be obtained experimentally by studying the electrical properties of the material at low enough temperatures.

When the impurity concentration becomes high enough, the activation energy of the holes to the valence band decreases to zero. This means that the impurity band merges with the valence band. This merging results in a band tail extending into the gap and containing both extended and localised states. In such a situation, the notions of valence and impurity bands lose their strict meaning. A material where the impurity band has merged into one of the host bands is said to be heavily doped. This occurs at doping levels such as $N_A\, a^{*3} > 1$.

Heavy doping consequently leads to a drastic change in the valence band edge density of states. In the case of light doping, the holes trapped in the impurity levels play, except at the lowest temperatures, a minor role in the electrical

transport phenomena. The structure of the valence band is not, in such a case, significantly modified by the impurity atoms.

CHAPTER 2

PHOTOLUMINESCENCE OF LIGHTLY AND HEAVILY DOPED GaAs AND $Ga_{0.85}In_{0.15}As$

2.1 INTRODUCTION

Luminescence refers to all de-excitation processes whereby a crystal in an excited state undergoes a radiative transition to a lower energy state. In semiconductors, the absorption spectrum of light is strongly dependent on the wavelength of the incident light. The dependence on the wavelength is almost entirely due to the presence of the band gap in semiconductors. The band gap will effectively reduce the amount of free carrier absorption which occurs since the band gap will reduce the amount of energy available to excite free carriers to $\hbar\omega - E_g$, where $\hbar\omega$ is the incoming photon energy and E_g is the band gap energy.

For semiconductors there are few cases of primary interest. First, let us suppose that $\hbar\omega < E_g$. In this case the electrons in the valence band will not be excited to the conduction band by the absorption of radiation. The electron is excited to a metastable state and decays by either reradiating the light or by electron-phonon scattering.

Next, let us suppose $\hbar\omega \leq E_g$. In this case, the electrons will be excited from the valence band close to the bottom of the conduction band and may be thermally excited into the conduction band. It may also be possible for the excited electrons to interact with the lattice and absorb a phonon, again allowing the electrons to reach the conduction band. Electrons which are excited into the conduction band may undergo free carrier absorption to higher electronic states or they may decay by passing their energy on to the lattice. The decay process

will be one of electron-phonon scattering (nonradiative decay) until the electron reaches the conduction band minimum. The system will then decay by the radiation of a photon of energy E_g. When the carriers excited to the conduction band decay back to the valence band, they recombine with the hole that was left behind upon excitation and may transfer this energy to the lattice via phonon scattering (nonradiative recombination). In addition, the electron-hole recombination energy may be transferred to another electron via Auger recombination, or, the electron-hole energy may be emitted as a photon which may then excite another valence electron or excite an electron in the conduction band resulting in photoemission from the solid.

The case $\hbar\omega > E_g$ is similar to the previous case except that electrons are excited very high above the conduction band minimum.

In a photoluminescence experiment on a semiconducting crystal, light with energy $\hbar\omega_l$ near or above the band gap is incident on the sample. The absorption process involves an interaction between the electron and the electromagnetic radiation. This interaction is treated as a perturbation to the electronic Hamiltonian. The interaction Hamiltonian $H_{elec-phot}$ is expressed as[9]

$$H_{elec-phot} = \frac{e}{m_0}\vec{A}\cdot\vec{p} + \frac{e^2}{2m_0}\vec{A}^2 \qquad (2.1.1)$$

where $\vec{A}$ is the vector potential operator, $\vec{p}$ is the electron momentum operator and e is the electronic charge. The second term in this expression is neglected here. An analysis of the perturbation problem leads to the following expressions

for the conservation of wavevector and energy[9]

$$\vec{K}_f = \vec{K}_i + \vec{K}_{phot} \tag{2.1.2}$$

$$E_f(\vec{K}_f) = E_i(\vec{K}_i) + \hbar\omega \tag{2.1.3}$$

The photon wavevector $\vec{K}_{phot}$ is in general much smaller in value than the initial and final wavevectors of the transition, $\vec{K}_i$ and $\vec{K}_f$, respectively. Hence, the above expressions are replaced, to a good approximation, by the expressions

$$\vec{K}_f = \vec{K}_i = \vec{K}_r \tag{2.1.4}$$

$$E_f(\vec{K}_r) = E_i(\vec{K}_r) + \hbar\omega \tag{2.1.5}$$

Electronic transitions involving only photon absorption (or emission) are known as direct transitions, since the electron wavevector remains unchanged in going from the initial to the final state. Transitions, in which photon absorption (or emission) is accompanied by the simultaneous absorption (or emission) of a phonon of wavevector $\vec{q}$, are known as indirect transitions. Indirect transitions are second order processes and therefore have a lower probability of occurring than direct transitions.

In sections 2.2 to 2.5, the various near band gap light emitting transitions encountered in lightly doped semiconductors will be explained in detail. In section 2.6 we present the model chosen to describe the PL spectra of heavily doped semiconductors.

2.2 FREE EXCITONS

At energies lower than the energy gap, there are emission peaks which correspond to processes in which the conduction electron and the valence hole are bound to one another via the long range Coulomb interaction in states within the forbidden energy gap. Such mutually bound electron-hole pair states are called free excitons (FEs). FEs are mobile electron-hole pairs. The centre of mass of the exciton can move through the crystal by diffusion, just like the individual electronic particles. However, this exciton migration does not produce electrical conductivity since each exciton contains a pair of charges of opposite sign.

Because the exciton is a two-body system, the general problem of calculating its energy levels and wavefunctions is, in principle, more complicated than the one electron problem. However, in the limit where the electron and hole are separated by many lattice spacings, one can use the EMA and the problem simplifies enormously. In the EMA, the electron and hole behave as though they possessed the effective masses of the conduction and valence band extrema, m_e^* and m_h^* respectively, and interact with each other via the Coulomb force modified by κ the dielectric constant of the crystal.

Let us assume that a free hole and electron are created in a direct gap material and attract each other. If they are so far apart that the atomic structure of the crystal can be ignored, the Hamiltonian for the FE system $H_{FE}(r_e, r_h)$ can be written as[10]

$$H_{FE}(\vec{r}_e,\vec{r}_h) = -\frac{\hbar^2}{2m_e^*}\vec{\nabla}_e^2 - \frac{\hbar^2}{2m_h^*}\vec{\nabla}_h^2 - \frac{e^2}{\kappa|\vec{r}_e - \vec{r}_h|} \qquad (2.2.1)$$

where $\vec{r}_e$ and $\vec{r}_h$ are the position vectors of the electron and hole, respectively. $\vec{\nabla}_e^2$ and $\vec{\nabla}_h^2$ are the Laplacian operators with respect to the electron and hole coordinates, respectively. The solution of Schrödinger's equation with an Hamiltonian like equ.(2.2.1) gives rise to an infinite series of discrete hydrogenic bound states, with energies given by[10]

$$E_{x,n}(\vec{K}) = E_g - E_{x,n} + \frac{\hbar^2\vec{K}^2}{2M} \qquad (2.2.2)$$

with

$$E_{x,n} = \frac{e^4\mu}{2\hbar^2\kappa^2 n^2} \qquad (2.2.3)$$

where $n=1,2,\ldots\infty$, $\mu^{-1}=(m_e^*)^{-1}+(m_h^*)^{-1}$, $M=m_e^*+m_h^*$, $E_{x,n}$ is the FE binding energy and $\hbar\vec{K}$ is the momentum of the centre of mass. $E_{x,n}(\vec{K})$ is measured from the top of the valence band. The transition probability associated with the excited states of the exciton decreases as n^{-3} relative to the ground state exciton transition probability[10]. Pursuing the analogy with the hydrogen atom, one could evaluate the wave function of the $n=1$ exciton ground state to be[10]

$$\eta_{1s}(\vec{r}) = \frac{1}{\sqrt{\pi a_x^3}}\exp\left(-\frac{r}{a_x}\right) \qquad (2.2.4)$$

where the most probable value of r is a_x, the FE Bohr radius, given by

$$a_x = \frac{\hbar^2 \kappa}{\mu e^2} \tag{2.2.5}$$

The binding energy of the $n=1$ FE, relative to a free electron-hole pair at the band gap edge, often called the exciton Rydberg, is

$$R_x = \frac{\hbar^2}{2\mu a_x^2} \tag{2.2.6}$$

R_x can be very small; for example, in GaAs, for which $a_x=150$ Å, $\kappa=12.74$ and $\mu=0.045 m_0$ (we have taken into account the double degeneracy of the valence band at the Γ point by replacing in a first approximation, $(m_h^*)^{-1}$ by $1/2((m_{lh}^*)^{-1}+(m_{hh}^*)^{-1})$, one obtains $R_x=3.80$ meV. Such an exciton is clearly only going to be stable at very low temperatures.

Ultimately, the electron and the hole forming the FE can radiatively recombine creating a slightly below band gap photon. Since the wavevector must be conserved upon FE annihilation, momentum selection rules require that only zero kinetic energy excitons can recombine radiatively. However, this condition does not prevent excitons from possessing kinetic energy. Exciton emission at other than zero kinetic energy can occur through phonon participation. Phonons provide additional means of satisfying the momentum selection rules and thereby reduce the restriction on the exciton momentum allowing excitons of finite K to

annihilate.

FE recombination is the dominant luminescent transition at low temperatures only in intrinsic or extremely pure semiconductors. Ionized impurities present in less pure materials create local fields which act to tear apart the excitons. The FE transition is important only if the temperature is sufficiently low such that $k_B T$ is smaller or equal to the exciton binding energy. Excitons are broken up when the thermal energy exceeds the FE binding energy. Thus, at higher temperatures, the electron-hole pairs remain as free carriers in the conduction and valence bands. Luminescence resulting from the recombination of the unbound electron-hole pairs, that is, the band to band transition, is then dominant. Since FEs are mobile and therefore have kinetic energy, the radiative decay of FEs results in a luminescence band. In Zn-doped p-type GaAs, the FE emission line is found to be at $E_{x,1}(0)=(1.5152 \pm 0.0003)$ eV with a linewidth (FWHM) of ~ 0.6 meV at $T=5$ K (see fig.4.2.4, Chapter 4). Contrary to GaAs where the FE emission line is clearly observed, the FE emission in $Ga_{0.85}In_{0.15}As$ is not resolved into a sharp line. Intrinsic alloy broadening due to the random distribution of In and Ga atoms on the group III sublattice sites affects all the interband optical structures which overlap and therefore cannot be resolved (see fig.4.2.5, Chapter 4).

Under certain circumstances, the binding energy of an exciton can be decreased by the presence of a point defect or an impurity such as a donor or an acceptor. Energy is the fundamental criterion that determines whether or not an exciton can be trapped on an impurity. If the total energy of the system is

reduced when the exciton is in the vicinity of an impurity, then it is energetically favourable for the FE to remain near the defect; at a low enough temperature the exciton becomes bound to the impurity to form a bound exciton.

2.3 BOUND EXCITONS

The simplest bound exciton (BE) system consists of an electron and a hole bound to an ionized donor (or acceptor). This system has been subject to detailed theoretical analysis by many authors[11,12]. In the EMA, the Hamiltonian for the BE system $H_{BE}(\vec{r}_e,\vec{r}_h)$ is given by[11,12]

$$H_{BE}(\vec{r}_e,\vec{r}_h) = -\frac{\hbar^2}{2m_e^*}\vec{\nabla}_e^2 - \frac{\hbar^2}{2m_h^*}\vec{\nabla}_h^2 - \frac{Ze^2}{\kappa r_e} + \frac{Ze^2}{\kappa r_h} - \frac{e^2}{\kappa|\vec{r}_e - \vec{r}_h|} \qquad (2.3.1)$$

where the origin is taken at the nucleus of the singly ionized donor ($Z > 0$) (or acceptor($Z < 0$)) . Since the BE is a three-body system, the general problem of calculating its energy levels and wavefunctions has yet no known analytical solution. For a donor impurity (or an acceptor impurity) we can get an estimate for the result in various limits. For example, if $m_h^* > m_e^*$ (or if $m_e^* > m_h^*$) i.e when the electron and hole masses are very different, the more massive particle will move quite close to the ionized impurity so that the remaining lighter particle which is more remote will see only a neutral impurity and thus will be weakly bound. In this approximation, the system is analogous to a hydrogen molecule ion. The

binding energy of the BE is then a considerable fraction of the exciton Rydberg. On the other hand, if m_h^* is light ($\sim m_e^*$), it is a reasonable approximation to consider the exciton as an entity weakly bound to the impurity. Then, the wavefunction of the BE system $\Psi_{BE}(\vec{r}_e,\vec{r}_h)$ separates into $\eta(r)\chi(\vec{R})$ where $\eta(r)$ is the usual exciton wavefunction of relative motion and $\chi(\vec{R})$ represents the wavefunction describing the motion of the centre of mass of the exciton. In this limit, the system is analogous to the FE problem encountered in section 2.2.

Detailed calculations by Hopfield[13] and Herbert[14] have shown that the BE stability criterion depended on the electron-hole effective mass ratio $\sigma = m_e^*/m_h^*$. They concluded that excitons bound to ionized impurities were stable only for restricted values of σ. In GaAs, for example, where $m_e^* < m_h^*$, an exciton bound to an ionized donor is stable while an exciton bound to an ionized acceptor is not.

Relatively pure semiconductors containing low concentrations of impurities are characterized by a low temperature PL spectrum in which the dominant luminescent transitions are those involving the radiative decay of excitons localized at donor or acceptor impurities. Emission lines arising from the decay of BEs are downshifted in energy relative to the FE emission peak by amounts equal to the binding or localization energies of the exciton to the corresponding impurities. The linewidths (FWHM) of BE luminescence peaks are substantially reduced from that observed for the FE emission peak, since localization implies that the exciton has essentially no kinetic energy. The limiting linewidths (FWHM) of BE transitions in

Zn doped p-type GaAs are approximately of 0.4 meV at $T=5$ K and are found to be at $E(Zn^0,X)=(1.5127 \pm 0.0003)$ eV for the acceptor BE and at $E(D^0,X)=(1.5145 \pm 0.0003)$ eV for the donor BE (see fig.4.2.4, Chapter 4).

Impurity broadening effects present at higher impurity concentrations effectively increase the linewidth of BEs. Also, in the heteroepitaxial growth of $Ga_{0.85}In_{0.15}As$ on GaAs substrates, intrinsic alloy broadening arising from the random distribution of In and Ga atoms on the group III sublattice sites act to greatly increase the width of BE emission lines.

Besides the FE and BE PL lines observed in semiconductors, other non-excitonic recombinations are also seen in the near band gap r gion. These transitions will be discussed in the next section.

2.4 DONOR-ACCEPTOR PAIR TRANSITIONS

Low temperature PL spectra of semiconductors containing both donor and acceptor impurities include luminescence bands associated with electronic transitions between the excited and ground states of donor-acceptor pair (DAP) systems. The DAP transitions become increasingly important and eventually dominate over the excitonic transitions as the impurity concentration in the material is increased. DAP recombinations can also occur with the simultaneous emission of phonons. The coupling of electrons to LO phonons is particularly strong in compound semiconductors. Hence a series of progressively less intense LO

phonon replicas of the main DAP emission band is present in the PL spectra.

DAP complexes differ from exciton complexes bound to impurities, but they also retain many similarities. Like the neutral BE complex, the DAP complex consists of four point charges. It differs in that two of them are immobile, the donor ion D^+ and the acceptor ion A^- and the remaining two charges, the electron and the hole, are mobile.

When a donor and an acceptor impurity form a pair, the normal ionization energy $E(D^0)$ (or $E(A^0)$) of an isolated donor (or acceptor) is reduced due to the Coulombic interaction between the electron and the hole bound to the impurities. The recombination energy of pair-band luminescence is given by the well-known and often quoted formula[15]

$$\hbar\omega(R) = E_g - E(D^0) - E(A^0) + \frac{e^2}{\kappa R} \qquad (2.4.1)$$

This equation is easily understood from simple conservation of energy arguments. Consider a donor which has been compensated by an acceptor so that both are ionized and taking this state as the zero of energy. The energy required to form the complex is the energy E_g required to excite an electron to the conduction band and leaving a hole in the valence band, reduced by the energy gained by binding the electron on D^+ in the presence of A^- at a distance R away, $-E(D^0)+e^2/\kappa R$, and then binding the hole on A^- in the presence of D^0, $-E(A^0)$. In other words, the binding energy of the donor $E(D^0)$ is reduced by the repulsive potential $-e^2/\kappa R$ arising from the ionized acceptor at a distance R, but the

subsequent process of placing a hole on the acceptor is not altered by the presence of the distant neutral donor and hence involves only the acceptor binding energy $E(A^0)$.

Since the donor and acceptor impurities can only be on well-defined lattice sites, R can only assume certain discrete values. For relatively small R corresponding to, say, 10 to 50 lattice spacings, the change in the energy between lattice shells can be resolved and the spectrum $\hbar\omega(R) = E_g - E(A^0) - E(D^0) + e^2/\kappa R$ appears as a discrete set of emission lines corresponding to the allowed values of R. As R increases, $e^2/\kappa R \rightarrow 0$ and the emission lines from neighbouring lattice shells become increasingly closed together, eventually merging to form a broad band of emission energies with the low energy limit occurring for $\hbar\omega(\infty) = E_g - E(A^0) - E(D^0)$ as R approaches infinity. The intensities of the various lines of the spectrum are determined by the overlap of the donor and acceptor wavefunctions and the number of interacting pairs. Over 300 sharp lines corresponding to discrete DAP separations have been identified in GaP, along with the merging of the discrete lines to form the broad band emission as $R \rightarrow \infty$[16].

However, the conditions required to observe both of these features of pair spectra are not met in all materials. For example, in GaAs the sum of the shallow donor and shallow acceptor binding energies is typically small (~30 meV). Emission energies of sharp isolated pair lines would lie above the band gap energy because $e^2/\kappa R > E(D^0) + E(A^0)$ for the corresponding values of R. Only the unresolved broad band portion of the pair spectra is expected to be

observable. For example, in the low temperature (T=5 K) PL spectrum of nominally undoped, n-type GaAs, the emission band observed at $E(D^0,A^0)$ = (1.490 ± 0.001) eV is associated with DAPs involving C acceptors (see fig.4.2.1, Chapter 4). At this energy, the mean separation R between the donors and the acceptors is ~400 Å. In fact, sharp line spectra attributable to the discrete values of R have not yet been identified in any direct gap III-V compound, probably because of the small impurity binding energies associated with the light electron and hole masses.

Finally, free to bound transitions, such as free-electron to neutral acceptor or free hole to neutral donor, are also observed in the near band gap PL spectrum of various semiconductors. These transitions are discussed in the next section.

2.5 FREE TO BOUND TRANSITIONS

Radiative recombination processes whereby a free electron in the conduction band recombines with a hole bound to an acceptor (transition denoted by the symbol (e,A^0)) or a free hole in the valence band recombines with an electron bound to a donor (transition denoted by the symbol (D^0,h)) are referred to as free to bound (FTB) transitions. The transition results in the emission of a photon of energy[17]

$$\hbar\omega = E_g - E(A^0) + \frac{1}{2}k_B T \qquad (3.5.1)$$

$$\hbar\omega = E_g - E(D^0) + \frac{1}{2}k_B T \qquad (3.5.2)$$

for the (e,A^0) and (D^0,h) transitions respectively. A simple correction has been made for the initial energy of the free electron (or free hole) and its capture cross section at the acceptor site (or donor site). Such corrections have the equivalent effect of increasing the band gap energy by $1/2k_BT$. FTB transitions may also occur with the simultaneous emission of LO phonons.

Transitions involving the recombination of free electrons with holes bound to shallow acceptors are important in the temperature range where significant donor ionization occurs and acceptors remain neutral. However, at very low temperatures most of the electrons are trapped into shallow lying donor levels for lightly doped crystal. As a result, the intensity of the DAP transitions is increased at the expense of the FTB transitions. In GaAs the relative intensities of these emissions vary rapidly in the range T=2 K to T=20 K and this variation is used to make certain of the important distinction between the two types of emission, FTB and DAP, a distinction which, if ignored, can give rise to errors of the order of several meV. For example, in the low temperature PL spectrum (T=5 K) of nominally undoped, n-type GaAs, the emission line observed at $E(e,A^0)$=(1.494 ± 0.001) eV is associated with a FTB transition involving C acceptors (see fig.4.2.1, Chapter 4).

2.6 PHOTOLUMINESCENCE OF HEAVILY DOPED SEMICONDUCTORS

The luminescence emitted by the radiative recombination of photogenerated minority carriers in heavily doped p-type material is schematically depicted in fig.2.6.1. The luminescence extends from the reduced band gap energy E_g (low energy edge) to the energy of the optical gap $E_{g,o}$ (high energy cutoff). The width of the emission band represents the Fermi energy E_F (see fig.2.6.1), which is the difference between $E_{g,o}$ and E_g.

The luminescence line shape has been calculated according to the expression[18,19]

$$I(E) \sim \int_{-\infty}^{+\infty} G_c(E_e)\, G_v(E_h)\, |M(E_e,E_h)|^2\, F_c(E_e)\, F_v(E_h)\, \delta(E - \hbar\omega)\, dE_e \quad (2.6.1)$$

where $G_c(E_e)$ and $G_v(E_h)$ are the densities of states of the electrons and the holes, respectively. $|M(E_e,E_h)|^2$ represents the matrix element of the interband transition. $E = E_e - E_h$ is the energy of the transition. E_e and E_h are the energies of the electrons and the holes, respectively. $F_c(E_e)$ and $F_h(E_h)$ are the Fermi-Dirac distribution functions of the electrons and the holes, respectively, and are given by

$$F_c(E_e) = \frac{1}{1 + \exp\left(\frac{E_e - E_F}{k_B T}\right)} \quad (2.6.2)$$

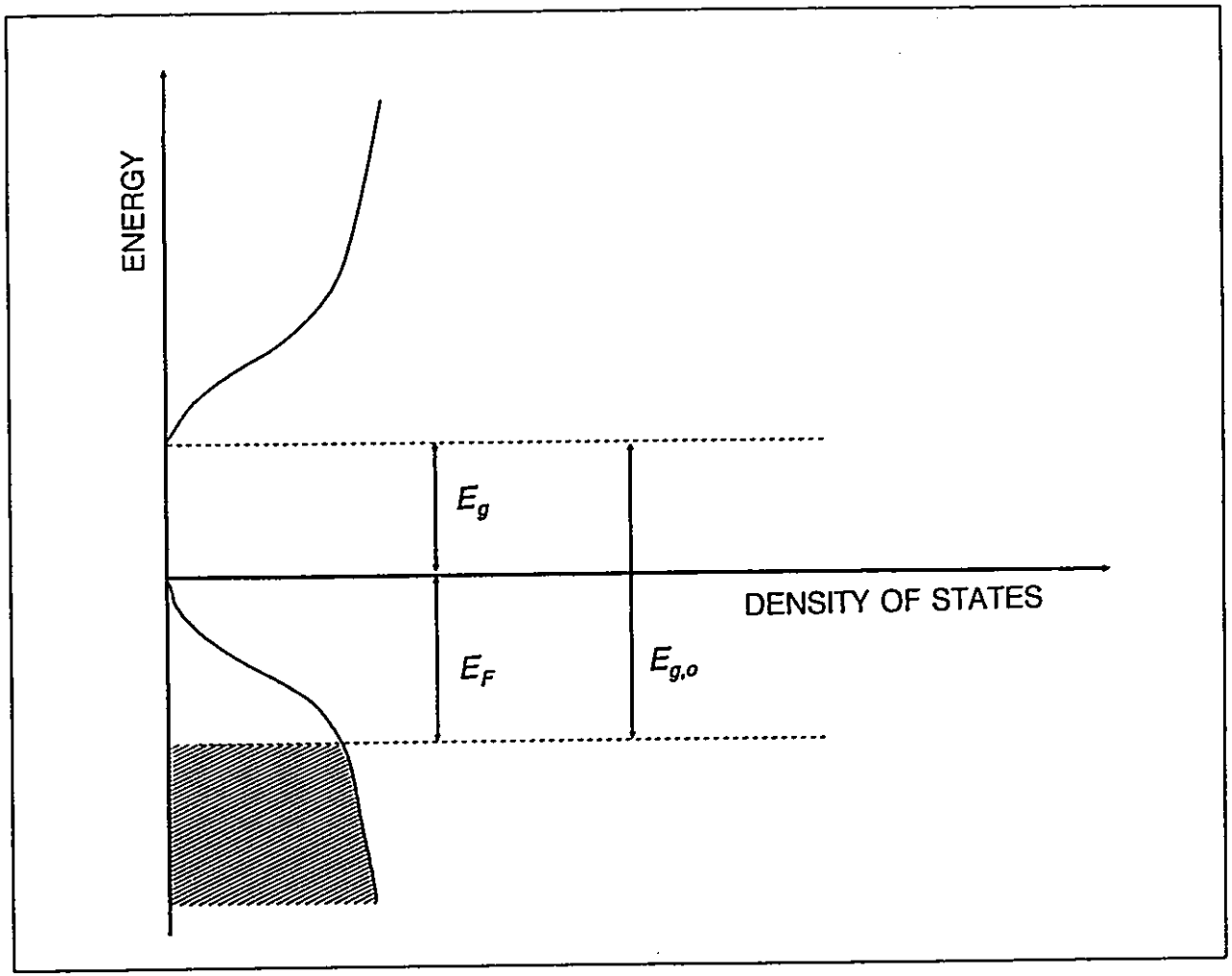

Figure 2.6.1. Schematic drawing of the band structure of a heavily doped p-type semiconductor. Optical gap $E_{g,o}$ and reduced band gap E_g as well as the Fermi energy E_F are indicated

$$F_v(E_h) = \frac{1}{1 + \exp\left(\frac{E_F - E_h}{k_B T}\right)} \qquad (2.6.3)$$

The photocreated minority carriers are assumed to thermalize completely before radiative recombination with holes of the valence band occurs. This is justified when the recombination time is large compared to the thermalization time[20]. However, this may not be the case for minority carriers excited high above the conduction band minimum. Equ.(2.6.1) can, for the case of p-doping, be written as

$$I(E) \sim G_v(E_h)\, F_v(E_h)\, |M(E_e,E_h)|^2 \qquad (2.6.4)$$

The interband matrix element has been assumed to be constant by many authors[4,18,19,21,22]. This approximation provided a good fit to their data and was found adequate. Nevertheless, the constant-matrix-element approximation fails when the photon energy is significantly larger than the reduced band gap. With this approximation equ.(2.6.4) may now be written as

$$I(E) \sim G_v(E_h)\, F_v(E_h) \qquad (2.6.5)$$

The luminescence spectra of heavily doped semiconductors has been interpreted as a mixture of $\vec{k}$-conserving and $\vec{k}$-nonconserving optical transitions[21]. Lasher and co-workers[23] have mentioned that states deep in the tail will have appreciable matrix elements with states in the opposite band over a wider

range of values of $\vec{K}$ than does a simple hydrogenic level. Such an effect is due to the randomness in the distribution of the impurity levels. The $\vec{K}$-conserving transition is represented by a Lorentzian line shape which is introduced in equ.(2.6.5) to give

$$I(E) \sim \frac{1}{\left[1+\left(\frac{E-B_0}{C_0}\right)^2\right]} + G_v(E_h)\,F_v(E_h) \tag{2.6.6}$$

where C_0 is a broadening parameter and B_0 is the peak maximum.

The band structure of heavily doped semiconductors has been considered by many authors[1,2]. Kane[2] has considered the case of charge carriers with low kinetic energy. Those carriers can follow the fluctuations of the impurity potential whose root mean square is denoted by V_{rms}. A valence-band density of states of the Kane form reads[2,18,19]

$$G_v(E_h) = \sqrt{\pi}\; Y\left(\frac{E_h - E_v}{\eta}\right) \tag{2.6.7}$$

with

$$Y(x) = \frac{1}{\sqrt{\pi}} \int_{-\infty}^{x} \sqrt{x-\xi}\,\exp(-\xi^2)\,d\xi \tag{2.6.8}$$

where $\eta = \sqrt{2}\,V_{rms}$, and E_v is the valence band edge for a parabolic density of states in the absence of narrowing effects. η represents the band tail parameter

to be determined with our data analysis. Despite the fact that Kane's theory is well known to overestimate the magnitude of the band tails[20], a Kane-like expression is used as it has the advantage of giving a fair representation of the density of states both in the band and in the tail. This is clearly seen by taking the asymptotic limit of equ.(2.6.7). For $E_h \to \infty$, $G_v(E_h) \sim \sqrt{E_h - E_v}$ as in the unperturbed band, whereas for $E_h \to -\infty$, $G_v(E_h) \sim \exp -((E_h - E_v)/\eta)^2$ i.e. the density of states reflecting the Gaussian statistics of the potential in the low-energy states which form a band tail. The function $Y(x)$ is plotted in fig.2.6.2.

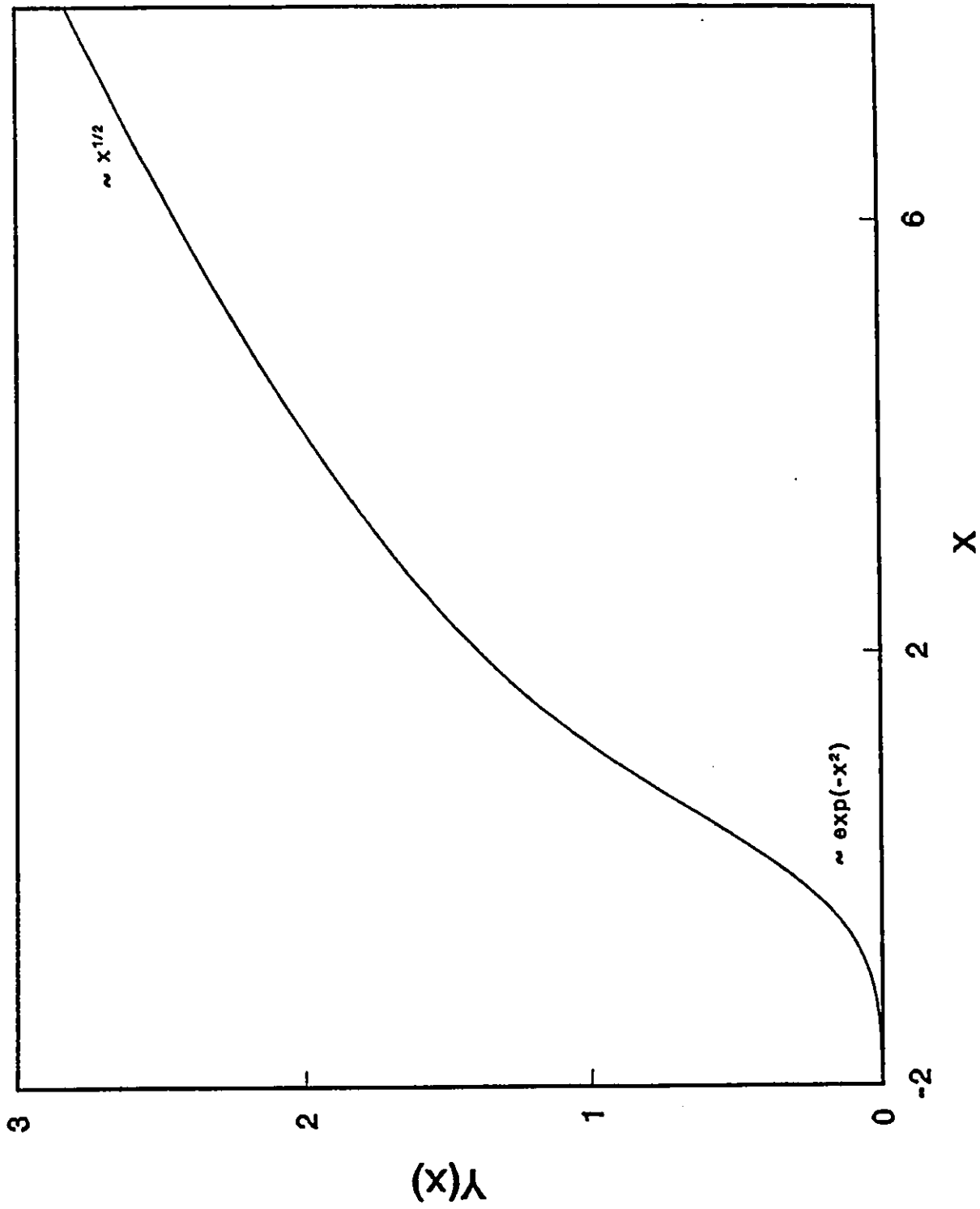

Figure 2.6.2. The function $Y(x)$ of equ. (2.6.8)

CHAPTER 3

EXPERIMENTAL SETUP

3.1 PHOTOLUMINESCENCE SETUP

A brief discussion of the experimental setup for the PL measurements is presented below. A schematic of the setup is shown in fig.3.1.1

The PL excitation source is a Coherent Innova 90K Krypton ion laser (L). The continuous wave output in the visible may be selected from several available lines in the wavelength range 3507-7993 Å. For the purposes of this work the laser was tuned to output red light of wavelength 6471 Å with excitation power densities in the range of 0.2-2 W/cm^2 as measured at the sample surface. The intensity of the output was attenuated using neutral density filters (NDF). In order to avoid laser background gas emission lines in the infrared a spike filter (SF) has been placed at the output of the laser. The laser beam is directed through a quartz focussing lens (QFL) onto a mirror (M_2) by a beam steering instrument (BSI) and a mirror (M_1). The orientation of the mirrors is controlled by micrometer adjustments. The laser beam is focused onto the sample surface (SS). The PL is collected by spherical mirror (SM_1) with an f number closely matched to the corresponding f number of the monochromator. The PL is spectrally analyzed using a 3/4 m Spex monochromator equipped with two spherical mirrors, (SM_2) and (SM_3), and a 1200 grooves/mm grating (GRA) blazed at 7500 Å or a 600 grooves/mm grating blazed at 12500 Å. The two slits (S_1) and (S_2) in the monochromator are independently adjustable. The resolution obtained using a 200 μm slit width is 2 Å. The total resolution of the system was set to 5 Å and

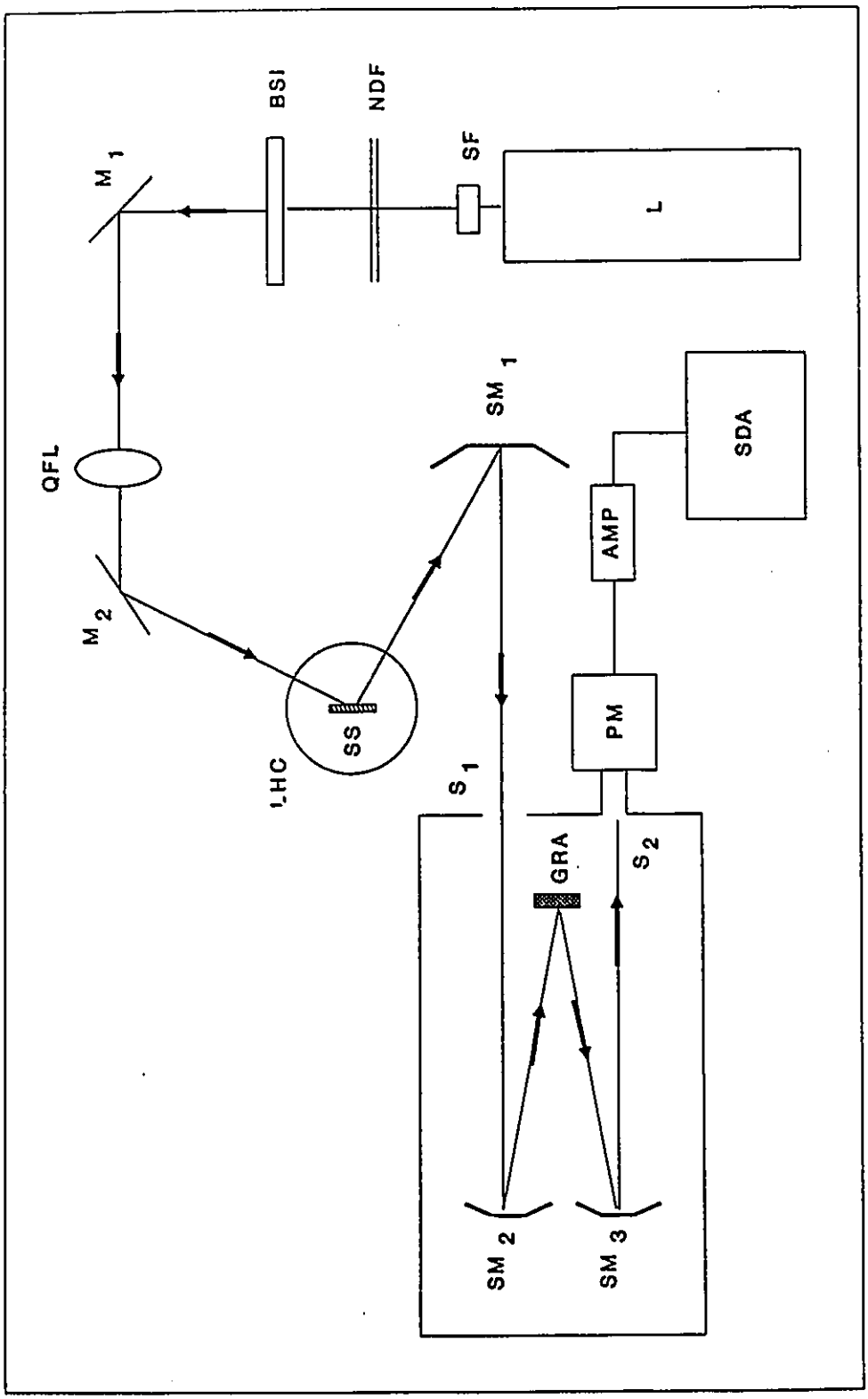

Figure 3.1.1. Photoluminescence setup

occasionally to 1 Å. The exit slit (S_2) is coupled to a Hamamatsu R1767 photomultiplier (PM) tube with spectral response in the range of 4000-12000 Å or with a Hamamatsu R943-02 PM tube with spectral response in the range of 1600-9300 Å. The photocurrent generated by the PM tube undergoes a voltage to frequency conversion by an amplifier (AMP). This frequency is proportional to the intensity of the light incident on the PM tube. The Spex data acquisition system (SDA) records the PM signal amplitude (as a frequency) and the monochromator position to a file on a hard disk. The user inputs the desired values of the sampling time, scanning range, increment and scan number. The sample is mounted on a copper holder with the aid of a small quantity of vacuum grease deposited on the reverse side of the sample. The sample is cooled by helium exchange gas, using a continuous flow liquid-helium cryostat (LHC). The temperature could be varied between T=300 K and T=5 K. The Si diode temperature sensor (DTS) is attached to the copper holder of the sample. A constant current passes through the diode. The voltage drop across the diode varies with temperature. The voltage is measured using a digital voltmeter and converted by means of a calibration table to a temperature value. The sample temperature may be maintained at any value within the range of the cryostat by controlling the flow of the coolant and the power to the electrical heater with an overall accuracy of ± 1 K.

CHAPTER 4

RESULTS AND DISCUSSIONS

4.1 INTRODUCTION

All fifteen epitaxial layers investigated in this work were grown in a horizontal LP-MOVPE reactor[24] using either trimethylgallium (TMG) or trimethylindium (TMI) and arsine (AsH_3), diluted (5%) in hydrogen. The GaAs layers (samples 1 to 8; see table 4.1.1) were grown directly on semi-insulating Cr-doped (100) GaAs substrates. The $Ga_{0.85}In_{0.15}As$ layers (samples 9 to 15; see table 4.1.1) were grown on GaAs substrates oriented 2° off (001) towards [011]. The composition of the ternary layers has been deduced from a combined study of energy-dispersive X-ray spectra (EDS) and of X-ray diffraction experiments. The precision on the composition is ± 0.5% of In. All the layers had a thickness of 3-4 μm and were doped with Zn using diethylzinc. The carrier concentration was determined from Hall effect measurements at room temperature. We estimate the overall accuracy of the doping concentration to be 5%. All the PL spectra were obtained with excitation power densities of 2 W/cm^2 and with resolutions of ± 1 meV (except when differently mentioned in the text).

In section 4.2, we will study the effect of light doping on the PL spectra of GaAs (samples 1 to 5) and $Ga_{0.85}In_{0.15}As$ (samples 9 to 11). Particular attention has been given to samples 1 and 2. These high purity samples provide detailed near band gap optical structures and are therefore suitable for observing the evolution of the PL spectra upon initiating Zn doping. Also, low doped $Ga_{0.85}In_{0.15}As$ (sample 9) will provide measurement of both the Zn acceptor binding energy and the 5 K

Table 4.1.1. List of samples investigated in this work

GaAs (Sample Nº)	p (cm^{-3})	$Ga_{0.85}In_{0.15}As$ (Sample Nº)	p (cm^{-3})
1	$1.00x10^{14}$ (*)	9	$3.22x10^{15}$
2	$4.30x10^{14}$	10	$5.00x10^{16}$
3	$7.30x10^{15}$	11	$1.50x10^{17}$
4	$1.30x10^{16}$	12	$1.60x10^{19}$
5	$9.00x10^{16}$	13	$4.60x10^{19}$
6	$1.60x10^{18}$	14	$5.31x10^{19}$
7	$1.10x10^{19}$	15	$1.95x10^{20}$
8	$1.97x10^{19}$	...	...

* n-type, nominally undoped.

reference band gap. This reference band gap will be used in section 4.3 to determined the 5 K band gap shrinkage in the $Ga_{0.85}In_{0.15}As$ alloy.

In section 4.3, we will study the effect of heavy doping on the PL spectra of GaAs (samples 6 to 8) and $Ga_{0.85}In_{0.15}As$ (samples 12 to 15). A detailed analysis of the data provided the free hole dependence of the band gap shrinkage $|\Delta E_g|$ for both of these materials. All the PL spectra of heavily doped GaAs and $Ga_{0.85}In_{0.15}As$ have been fitted as a function of doping and of temperature using equ.(2.6.6).

4.2 LIGHTLY DOPED GaAs AND $Ga_{0.85}In_{0.15}As$

In fig.4.2.1, we show the luminescence spectrum of a nominally undoped GaAs layer (sample 1). The luminescence consists of three spectral structures. The high energy structure (a) centred around 1.515 eV is due to exciton recombinations, while the second structure (b), near 1.49 eV, is due to FTB and DAP recombinations involving residual C acceptors. A third structure not shown in fig.4.2.1, but observed in all spectra at 1.45 eV, is a LO phonon replica of the 1.49 eV emissions. The excitonic structure (a) is dominated by an exciton bound to a neutral donor (D^0,X) at 1.515 eV (k), followed at higher energy by a shoulder around 1.518 eV (m) due to FE recombinations. The structure (b) is dominated by (e,C^0) transitions at 1.494 eV (e), followed at lower energy by a less intense peak occurring at 1.490 eV (c) and attributed to (D^0,C^0) transitions. In fig.4.2.2,

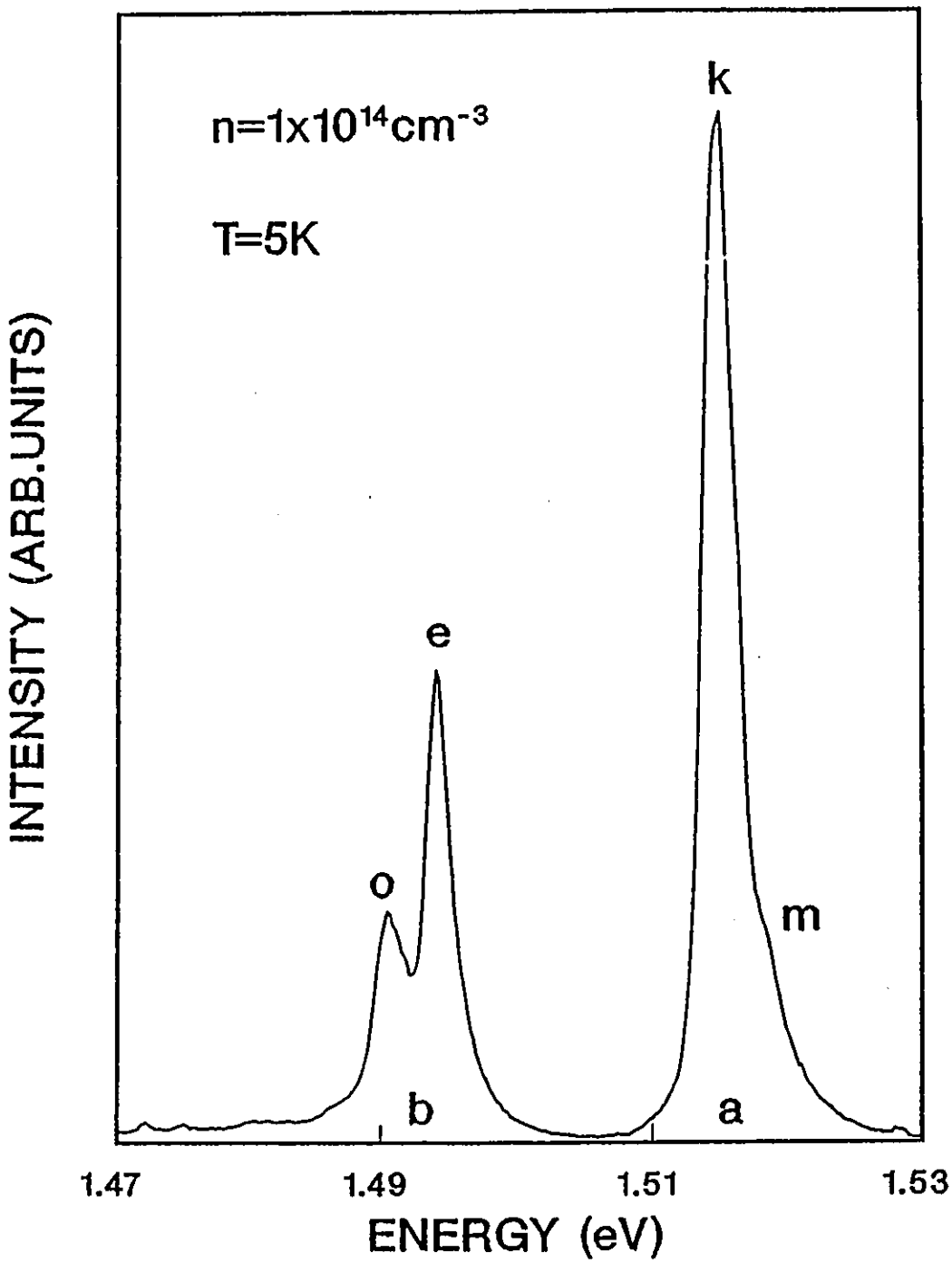

Figure 4.2.1. 5 K luminescence spectrum of nominally undoped GaAs with $1x10^{14}$ electrons cm^{-3}.

a = m (FEs), k (D^0,X)

b = e (e,C^0), o (D^0,C^0)

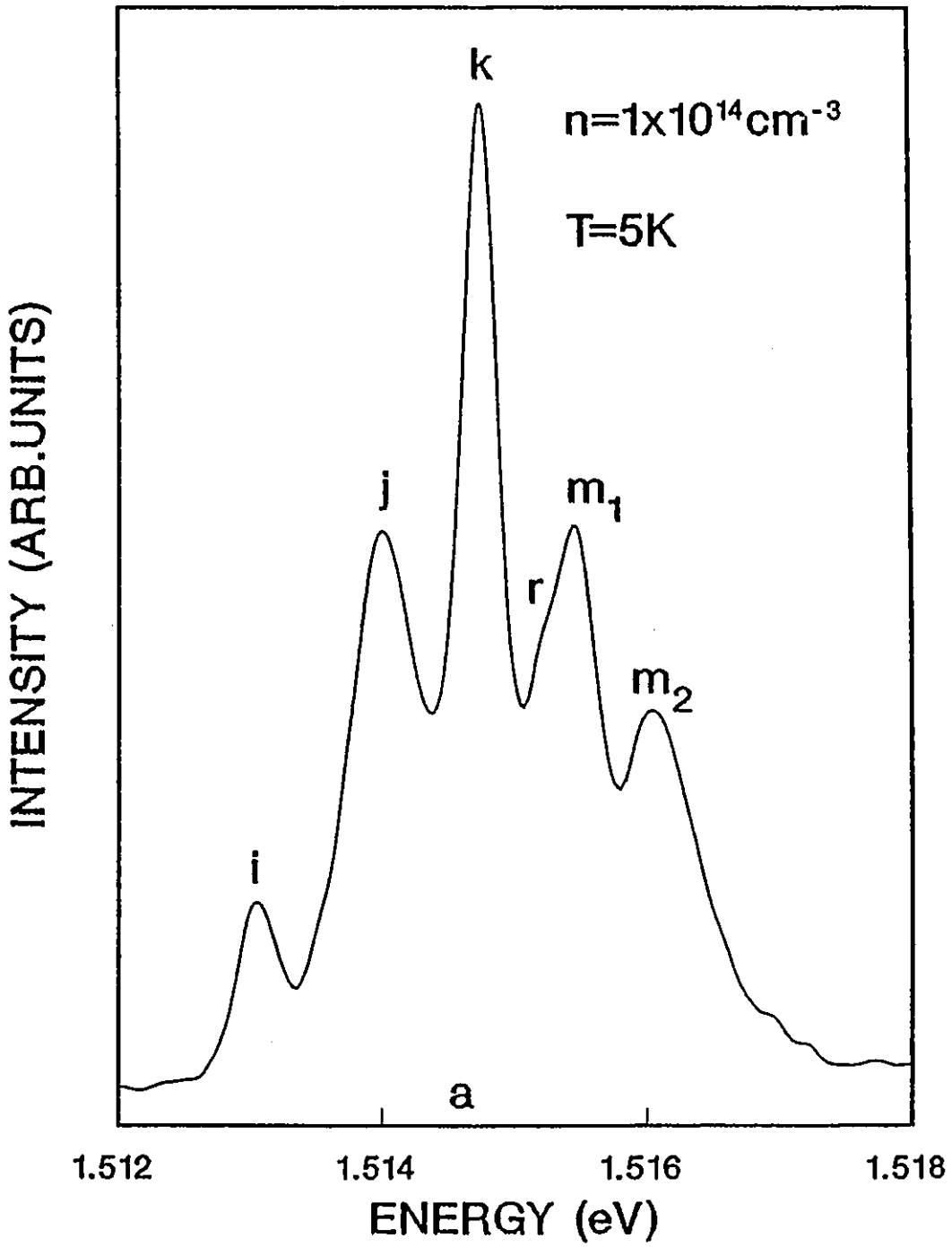

Figure 4.2.2. 5 K luminescence spectrum of the excitonic structure (a) of nominally undoped GaAs with $1x10^{14}$ electrons cm^{-3}. i = (C^0,X), j = (D^+,X), (D^0,h), k = (D^0,X), r = $(D^0,X)^*$, m_1 = FE-LPB, and m_2 = FE-UPB

we show a high resolution (~0.3 meV) spectrum obtained with low laser excitation power density (0.2 W/cm^2) of the excitonic structure (a) in GaAs (sample 1). The spectrum displays the features normally observed in high purity n-type GaAs. The $n=1$ state of the FE-upper polariton branch (FE-UPB) along with the associated FE-lower polariton (FE-LPB) branch occur at 1.5160 eV (m_2) and at 1.5155 eV (m_1), respectively. The shoulder at 1.5152 eV (r) and the intense and narrow peak at 1.5147 eV (k) are respectively attributed to a rotational excited state (rotational excited states correspond to the p-like distributions of the hole around the donor) of the donor BE $(D^0,X)^*$ and to an exciton bound to a neutral donor (D^0,X). The structure at 1.5140 eV (j) is either due to an exciton bound to an ionized donor (D^+,X) or to a FTB transition (D^0,h). Finally, at lower energy, an exciton bound to a neutral residual C acceptor (C^0,X) is found to be at 1.5131 eV (i).

In fig.4.2.3, we present the luminescence spectrum of lightly Zn-doped GaAs (sample 2). The luminescence consists of three spectral structures. The high energy structure (a) centred around 1.515 eV is due to exciton recombinations, while the second structure around (b), close to 1.49 eV, is due to FTB and DAP recombinations involving both Zn and residual C acceptors. A third structure not shown in fig.4.2.3, but observed in all spectra at 1.45 eV, is a LO phonon replica of the 1.49 eV emissions. The excitonic structure (a) is dominated by (D^0,X) transitions occurring at 1.515 eV (k), followed at lower energy by a less intense peak attributed to (A^0,X) transitions involving Zn acceptors and found to be at 1.513 eV (q). At higher energy, the usual FE recombinations occur near 1.518 eV

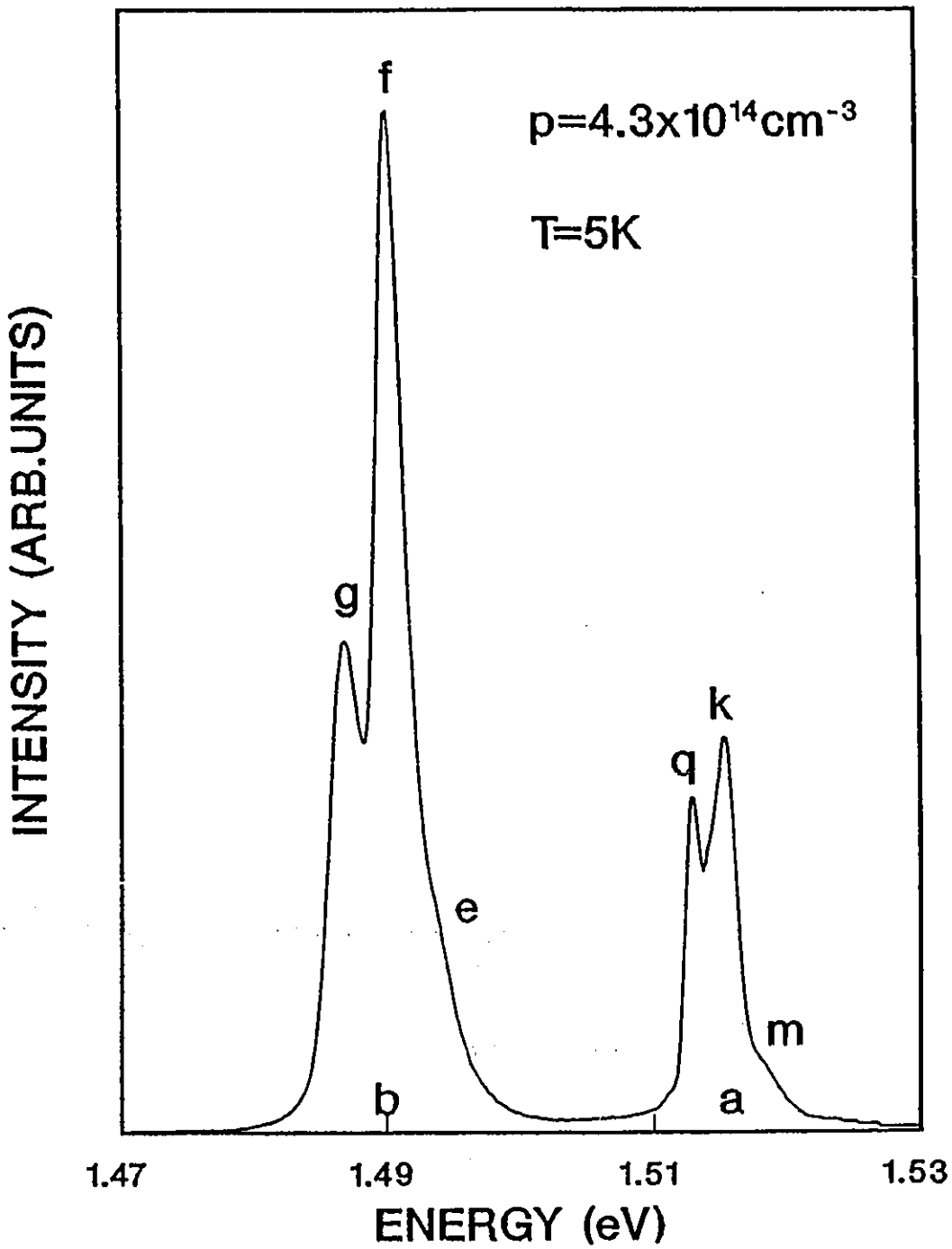

Figure 4.2.3. 5 K luminescence spectrum of Zn-doped GaAs with $4.3x10^{14}$ holes cm^{-3}.

a = m (FEs), k (D^0,X), q (Zn^0,X)

b = e (e,C^0), f (e,Zn^0), g (D^0,Zn^0)

(m). The structure (b) is dominated by (e,Zn^0) transitions occurring at 1.490 eV (f), followed at lower energy by (D^0,Zn^0) recombinations found to be at 1.487 eV (g); also present on the high energy side of the spectrum, is a shoulder associated with (e,C^0) transitions and occurring around 1.494 eV (e). In fig.4.2.4, we show a high resolution (~0.3 meV) obtained with low laser excitation power density (0.2 W/cm^2) of the excitonic structure (a) in GaAs (sample 2). The spectrum displays the features normally observed in high purity p-type GaAs. The spectrum is similar to the nominally undoped GaAs layer (sample 1). The n=1 state of the FE-UPB and the associated FE-LPB occur at 1.5158 (m_2) and at 1.5152 eV (m_1), respectively. The $(D^0,X)^*$ and (D^0,X) transitions are found to be at 1.5150 eV (r) and at 1.5145 eV (k), respectively. The peak occurring at 1.5136 eV (j) is either due to a (D^0,h) or to a (D^+,X) transition, followed at lower energy by a shoulder due to a (C^0,X) transition occurring at 1.5132 eV (i). Finally, the intense and narrow peak found to be at 1.5127 eV (q) is attributed to (Zn^0,X) recombinations.

Therefore, as the Zn concentration increases, two main changes are observed in the PL spectra of very low doped GaAs (see figs.4.2.1 to 4.2.4). On the one hand, FTB and DAP recombinations involving residual C acceptors are diminished at the expense of FTB and DAP transitions involving Zn acceptors. On the other hand, acceptor BE transitions involving Zn acceptors dominate the spectrum. All of these spectral changes can be explained on the basis of very simple arguments: as the incorporation of Zn is increased, recombinations involving Zn states are enhanced (at the expense of other recombination channels)

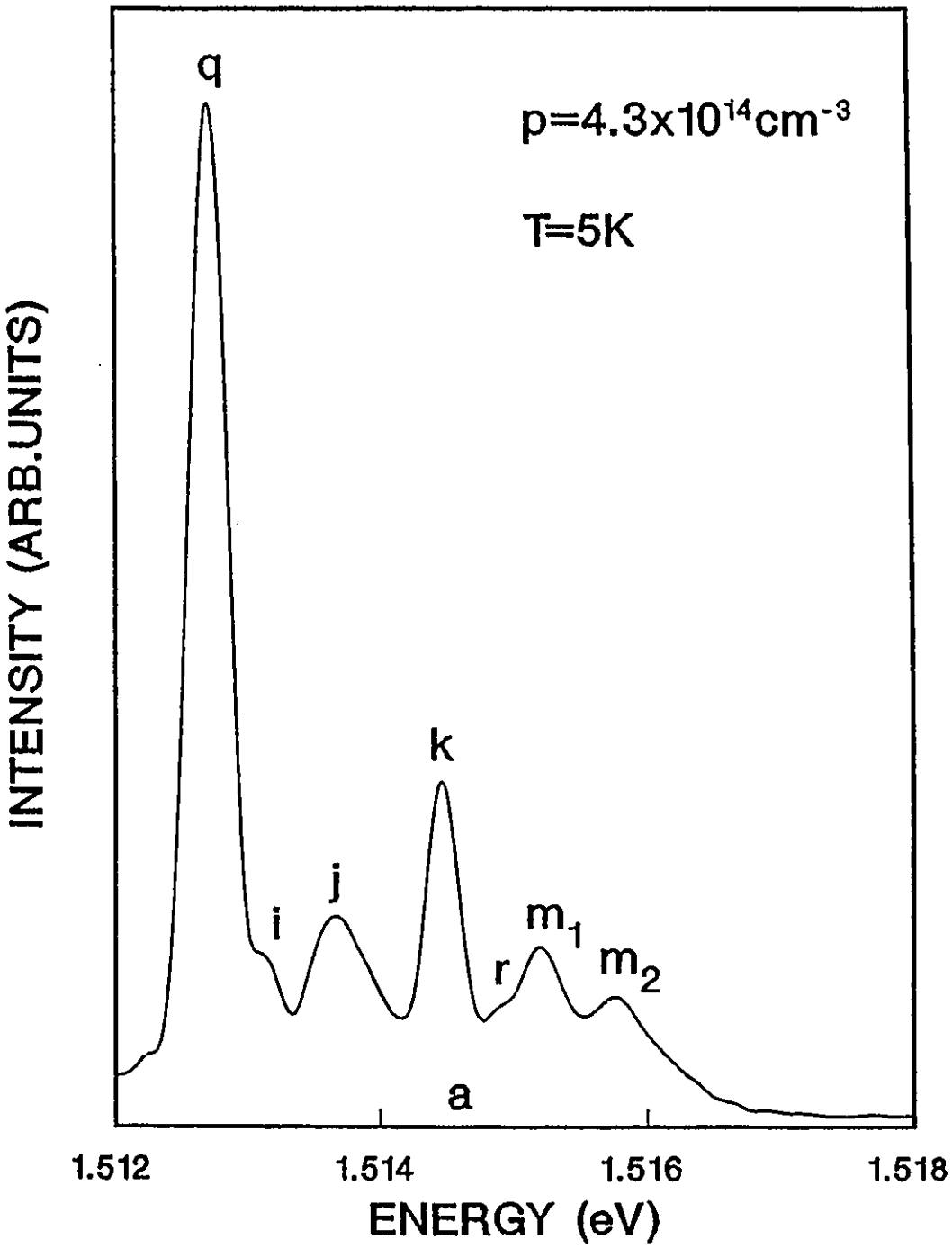

Figure 4.2.4. 5 K luminescence spectrum of the excitonic structure (a) of Zn-doped GaAs with 4.30×10^{14} holes cm^{-3}.

q = (Zn^0,X), i = (C^0,X), j = (D^+,X), (D^0,h), k = (D^0,X),

r = $(D^0,X)^*$, m = FE-LPB, and m = FE-UPB

and eventually will dominate the emission spectrum. Spectra such as that of figs.4.2.1 to 4.2.4 have been discussed in detail in the scientific literature[25,26] and we will only consider the features relevant to the present work.

In fig.4.2.5, we show the spectrum of a lightly Zn-doped $Ga_{0.85}In_{0.15}As$ layer (sample 9), consisting of an intense and narrow emission (a), followed at lower energy by a much more weak and broad structure (b). The energy of the intense peak is a function of the alloy composition x, its intensity does not vary with x and is comparable to exciton recombination in high purity GaAs[27]. All the ternary layers under consideration are much thicker than the critical thickness (~ 0.5 μm) for non elastic lattice-mismatch accommodation. In these high quality layers, misfit dislocations are concentrated within ~100 nm from the interface and most of the layer thickness is fully relaxed, showing the properties of bulk, high quality $Ga_{0.85}In_{0.15}As$[27]. However, the intense PL peak is not resolved into several sharp emissions as it is the case in GaAs, where both free and bound excitons are easily observed. In the ternary alloy layer, as already mentioned, the random distribution of In and Ga atoms on the group-III sublattice sites creates local potential variations that result in local band gap fluctuations. These fluctuations induce a broadening of excitonic luminescence lines when the diameter of the exciton is comparable to the spatial extension of the fluctuations. This affects all the interband optical structures which overlap and therefore cannot be resolved. To determine whether the PL of very low doped $Ga_{0.85}In_{0.15}As$ (sample 9) is dominated by free or bound excitons, we have studied the spectrum as a function of

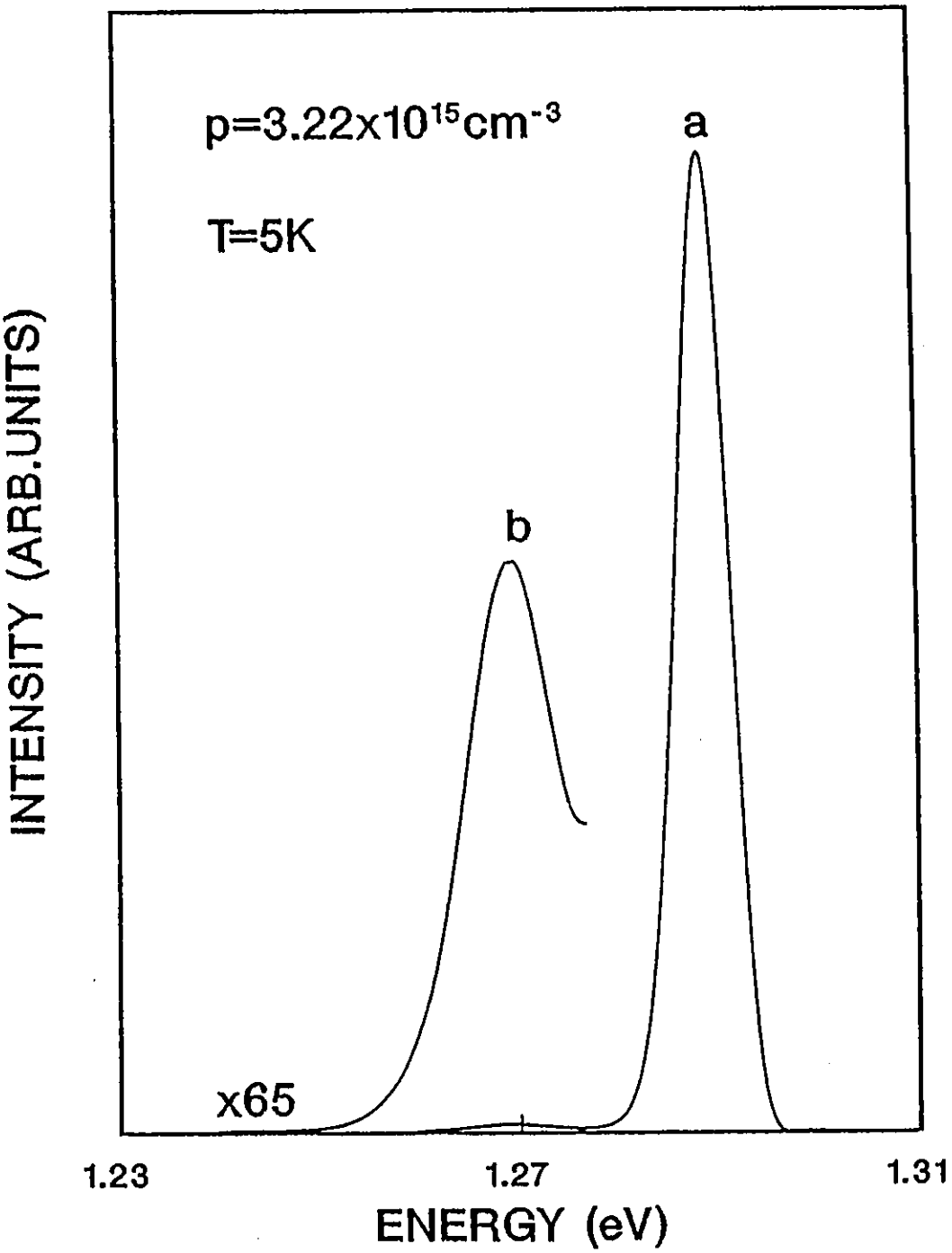

Figure 4.2.5. 5 K luminescence spectrum of Zn-doped $Ga_{0.85}In_{0.15}As$ with $3.22x10^{15}$ holes cm^{-3}.

a = unresolved exciton recombinations.

b = (e, Zn^0), (D^0, Zn^0)

temperature. The temperature dependence of the energy maximum (a) is plotted in fig.4.2.6. The energy of the maximum shifts very little for temperature less than ~30 K. Above that temperature, the energy decreases and follows the typical temperature dependence of III-V compounds. This behaviour is characteristic of BEs, which thermalize at relatively low temperatures. The intense PL emission (a) is therefore attributed to unresolved excitonic recombinations dominated by excitons bound to neutral Zn impurities. Similar to GaAs, the weak structure (b) at about 20 meV below the excitonic peak is due to a mixture of conduction band-acceptor and DAP recombinations.

At low doping level, recombinations involving impurity states and FEs can provide the first energy measurement of both the Zn acceptor binding energy $E(Zn^0)$ and the 5 K reference band gap in the $Ga_{0.85}In_{0.15}As$ alloy. First, $E(Zn^0)$ is obtained by solving the following set of equations[17,28]

$$E(Zn^0) = E_g - E(e,Zn^0) + \frac{1}{2}k_B T \qquad (4.2.1)$$

$$E_g = E_{peak} + E_{x,1} + \beta' E(Zn^0) \qquad (4.2.2)$$

where $E(e,Zn^0)$ is the energy of the maximum of the weak emission observed at T=30 K (see fig.4.2.7), where the contribution of the DAP recombinations is negligible. E_{peak} represents the energy of the acceptor BE as can be seen in fig.4.2.7. Using a linear interpolation between GaAs and InAs parameters, the value of $E_{x,1}$ for $Ga_{0.85}In_{0.15}As$ is found to be 3.25 meV. The coefficient β' in equ.(4.2.2) which is a measure of the localization energy of the exciton has a value

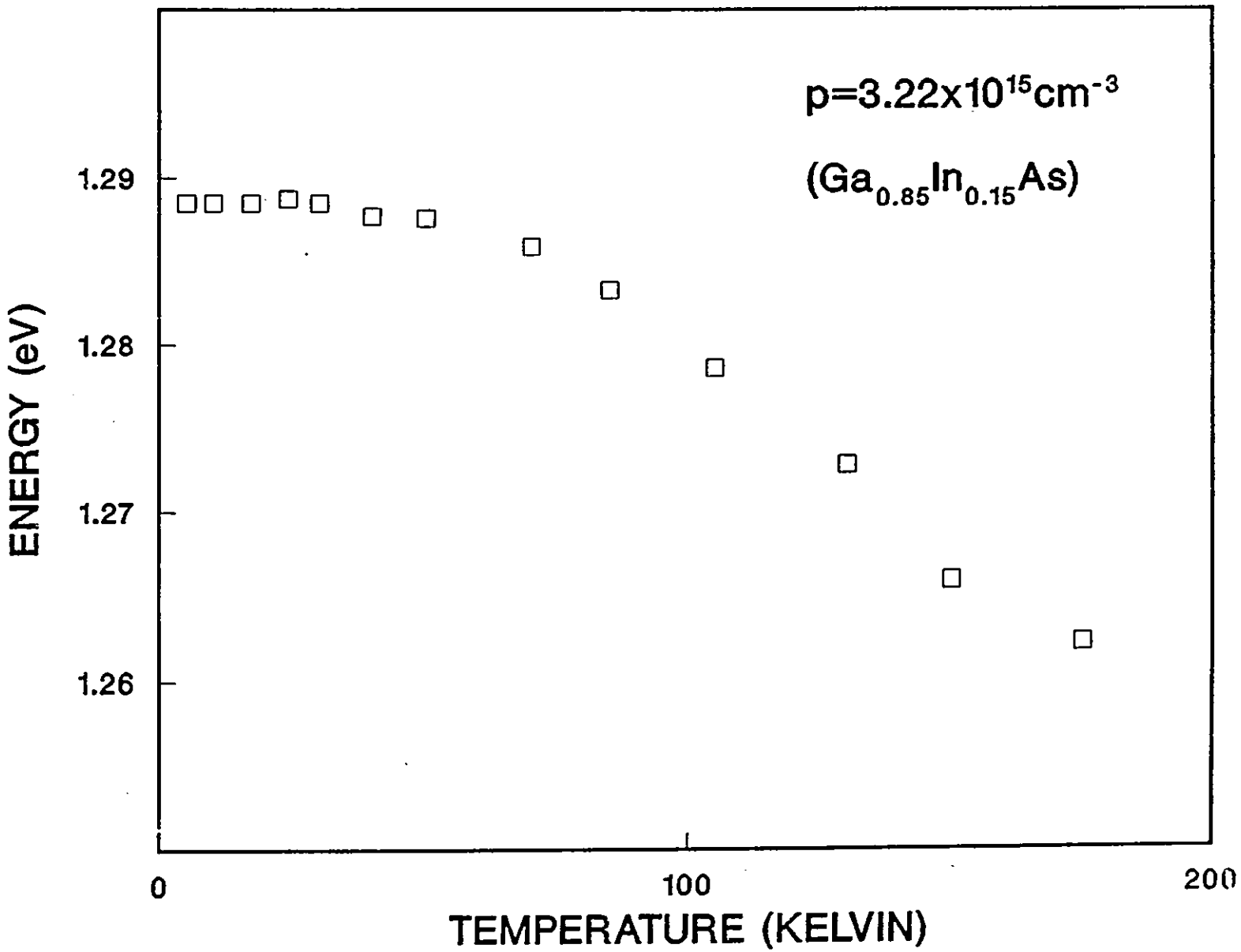

Figure 4.2.6. Temperature dependence of the excitonic structure (a) of Zn-doped $Ga_{0.85}In_{0.15}As$ with $3.22x10^{15}$ holes cm^{-3}

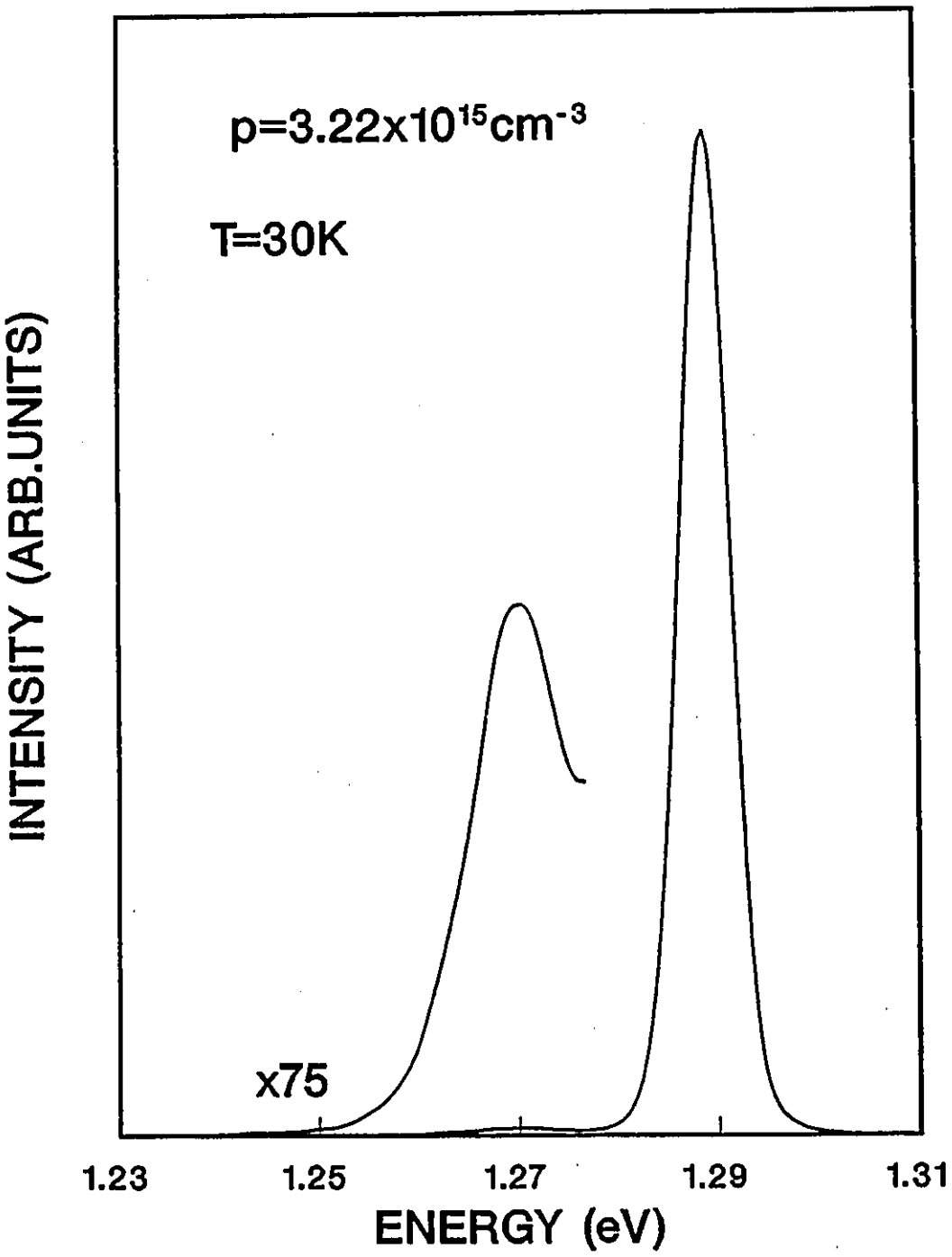

Figure 4.2.7. 30 K luminescence spectrum of Zn-doped $Ga_{0.85}In_{0.15}As$ with $3.22x10^{15}$ holes cm^{-3}

of about 0.1 according to Haynes' rule[28]. The resulting binding energy is $E(Zn^0)$ =25 meV. The corresponding error is ± 3 meV, and is mainly due to the uncertainty in the values of E_{peak} and $E(e,Zn^0)$. Using a linear interpolation between the experimental values for GaAs[26] and $Ga_{0.47}In_{0.53}As$[29] a value of 28 meV is obtained, which is somewhat higher than the experimental value of $E(Zn^0)$. Replacing the material parameters for $Ga_{0.85}In_{0.15}As$ into equ.(1.4.4) (see Chapter 1) we get a value of 23 meV which slightly underestimates the experimental value of $E(Zn^0)$. This discrepancy is due to the fact that equ.(1.4.4) does not take into account the chemical nature of the impurity.

Next, using equ.(4.2.2) with $E(Zn^0)$ =25 meV and E_{peak} =1.288 eV , we can readily obtain the 5 K band gap in the $Ga_{0.85}In_{0.15}As$ alloy (see fig.4.2.5). However, one cannot measure the true sample temperature under illumination (excitation power density 2 W/cm^2) at T=5 K. Consequently, we have determined the band gap at T=5 K in the $Ga_{0.85}In_{0.15}As$ alloy from a fit of its variation with temperature in the range of 20-300 K where illumination heating effects are relatively less important[19].

The temperature dependence of the band gap in most of the group IV and III-V semiconductors has been shown to be well described by the Varshni[30] equation

$$E_g(T) = E_g(0) - \frac{\alpha T^2}{(\beta + T)} \qquad (4.2.3)$$

where $E_g(0)$, α and β are assumed adjustable parameters. The function $E_g(T)$, corresponding to sample 9, is provided by a set of PL spectra collected at different temperatures. For a given temperature T, $E_g(T)$ is obtained using equ.(4.2.2). The fitting of equ.(4.2.3) to the experimental $E_g(T)$ provides $E_g(0)$, α and β for sample 9. Fig.4.2.8 reproduces the temperature dependence of $E_g(T)$ for sample 9. The dashed and solid lines are theoretical fits obtained using the Varshni equation in the temperature range of 5-300 K and 20-300 K, respectively. Further, the solid line for sample 9 is significantly above the dashed line, in the temperature range of 0-20 K, due to the inclusion of illumination heating effects (see fig.4.2.8). In table 4.2.1, we list for sample 9, the parameters $E_g(0)$, α and β obtained in the temperature range of 20-300 K. The resulting 5 K band gap is $E_g(5)=(1.296 \pm 0.003)$ eV. In table 4.2.3 we display the measured hole concentration and E_g at $T=5$ K, as calculated from equ.(4.2.3), for sample 9.

As the doping concentration increases up to $p=9\text{x}10^{16}$ cm^{-3} for GaAs and $p=1.5\text{x}10^{17}$ cm^{-3} for $Ga_{0.85}In_{0.15}As$, a progressive displacement of structure (a) to lower energy becomes noticeable, indicating the onset of band gap shrinkage (see figs.4.2.9 and 4.2.10). However, for the ternary layers some of the displacement may be attributed to a small increase of In content as suggested from a combined study of EDS and of X-ray diffraction experiments. The high energy structure (a) in figs.4.2.9 and 4.2.10 for the low doped samples, $p=7.3\text{x}10^{15}$ cm^{-3} to $p=5\text{x}10^{16}$ cm^{-3}, is dominated by acceptor BE at the expense of donor bound and free excitons. The band gap in this range is related to the experimental peak energy E_{peak} by equ.(4.2.2). Using equ.(4.2.2), with $E_{x,1}=3.8$ meV and $E(Zn^0)=30.7$ meV[26] for

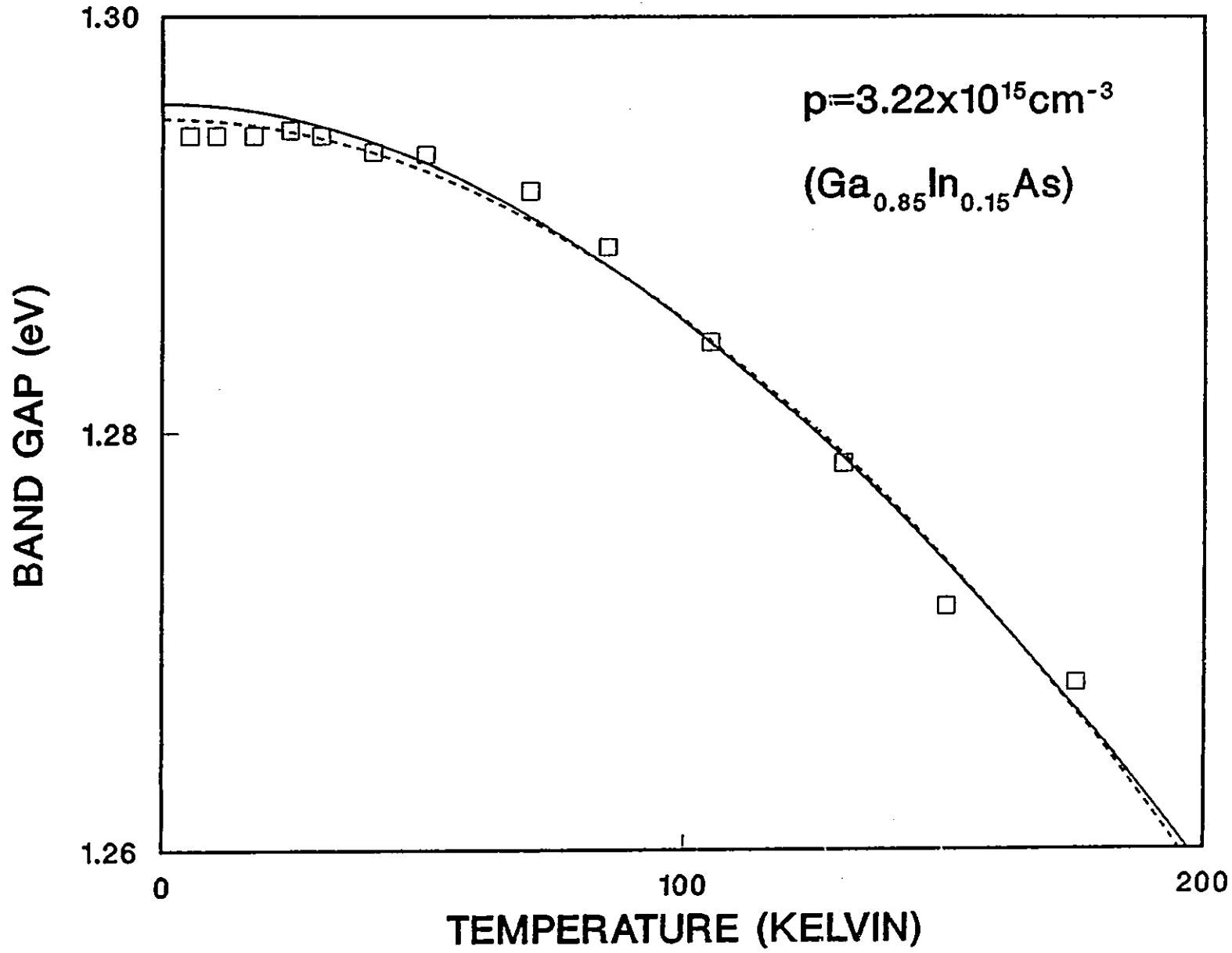

Figure 4.2.8. Temperature dependence of the band gap (open squares) of Zn-doped $Ga_{0.85}In_{0.15}As$ with 3.22×10^{15} holes cm^{-3}. The dashed and solid lines represent fits with Varshni's equation in the temperature range of 5-300 K and of 20-300 K, respectively.

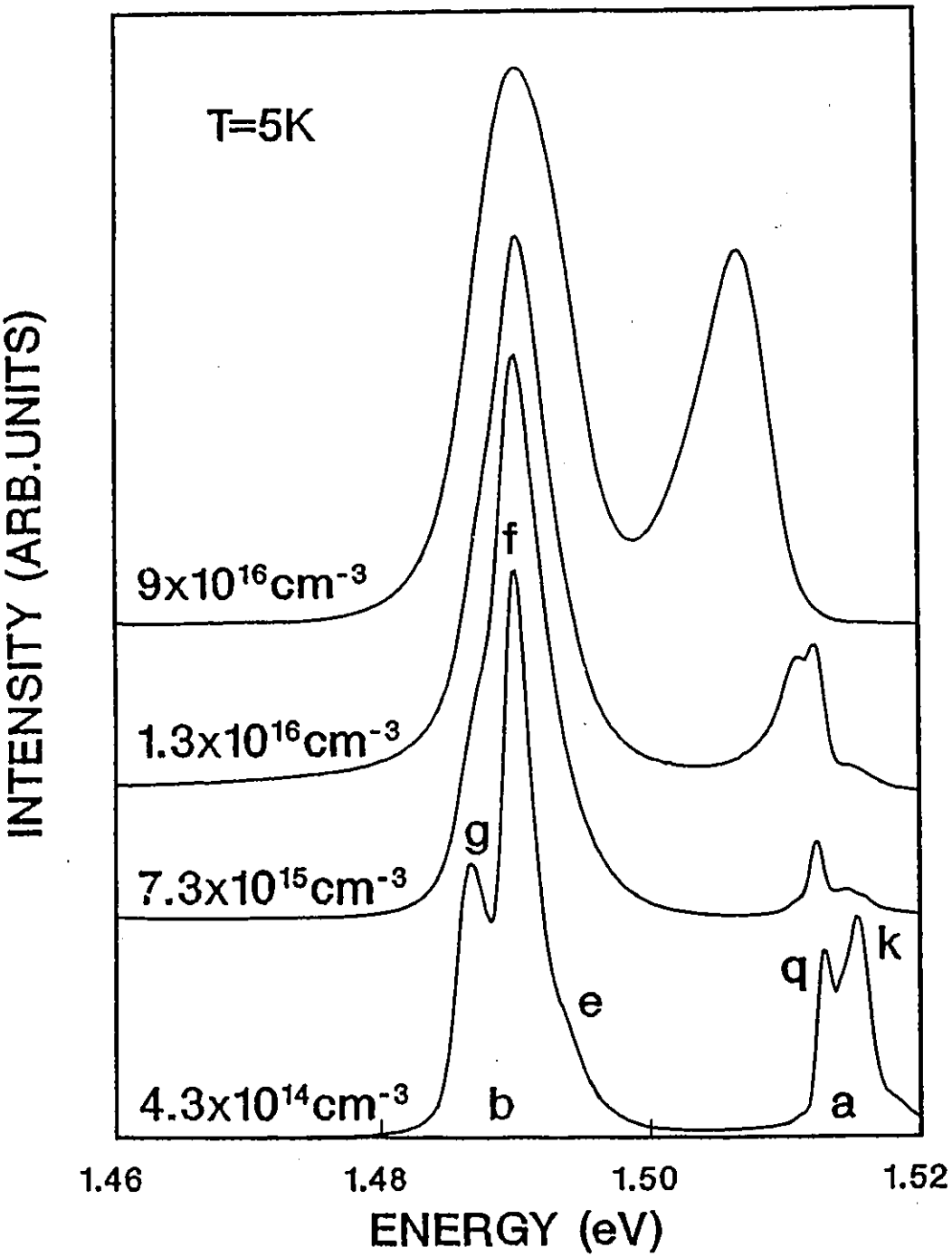

Figure 4.2.9. 5 K luminescence spectra of Zn-doped GaAs at various hole concentrations.

a = k (D^0,X), q (Zn^0,X)

b = e (e,C^0), f (e,Zn^0), g (D^0,Zn^0)

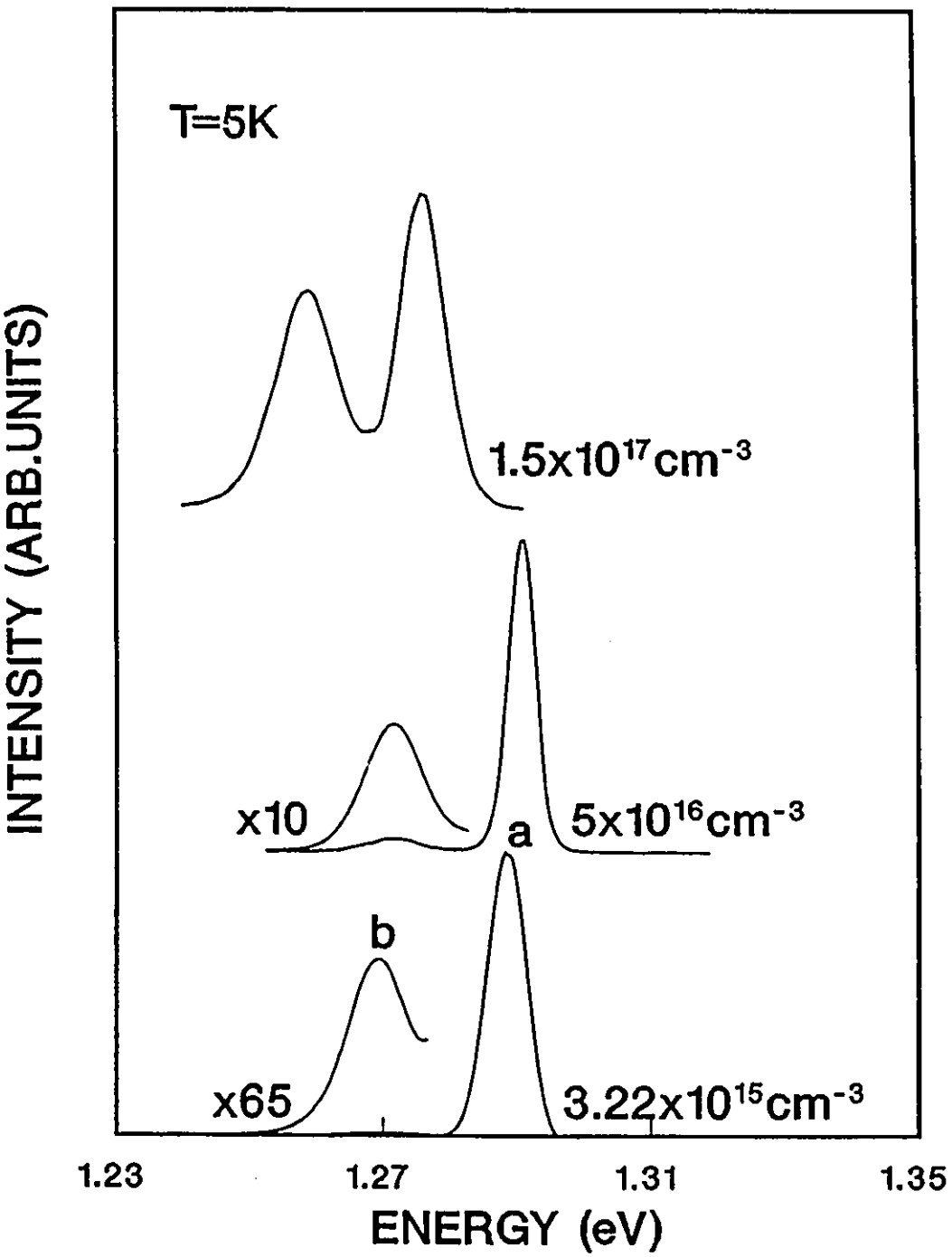

Figure 4.2.10. 5 K luminescence spectra of Zn-doped $Ga_{0.85}In_{0.15}As$ at various hole concentrations.

a = unresolved exciton recombinations

b = (e,Zn^0), (D^0,Zn^0)

GaAs, along with $E_{x,1}$=3.25 meV and $E(Zn^0)$=25 meV for $Ga_{0.85}In_{0.15}As$, E_g at T=5 K has been calculated for samples 3 and 4 (GaAs) and 9 and 10 ($Ga_{0.85}In_{0.15}As$). The results are reported in tables 4.2.3 and 4.2.4. For these GaAs and $Ga_{0.85}In_{0.15}As$ epilayers, we have neglected illumination heating effects in calculating the band gap at T=5 K, because the band gap obtained for these samples will not be used in the calculation of the band gap shrinkage (see section 4.3.2). However, we point out that the error of the band gap for these samples is significantly larger than the corresponding error of other samples investigated in this work, due to the uncertainty in the value of the temperature (see tables 4.2.3 and 4.2.4).

At higher doping level, corresponding to hole concentrations ranging from p=9x10^{16} cm^{-3} to p=1.5x10^{17} cm^{-3}, the high energy structure (a) in figs.4.2.9 and 4.2.10 is no longer dominated by exciton recombinations. In this doping regime, hole screening of the acceptor potentials reduces the binding energy of the excitons. As the hole concentration increases, exciton resonances disappear and only band to band transitions are observed. The band gap is then simply related to the experimental peak energy by the relation

$$E_g = E_{peak} \tag{4.2.4}$$

Thus E_g at T=5 K has been calculated for samples 5 (GaAs) and 11 ($Ga_{0.85}In_{0.15}As$) using equ.(4.2.4) (for reasons already mentioned, illumination heating effects have been neglected). The results are also reported in tables 4.2.3

and 4.2.4. The band to band recombination line, for concentrations higher than ~ 10^{18} cm^{-3} merges with the (e,Zn^0) emission line to form a broad asymmetrical band. This is discussed in the next section.

4.3 HEAVILY DOPED GaAs AND $Ga_{0.85}In_{0.15}As$

4.3.1 GENERAL FEATURES OF THE DATA

In the following, we restrict our discussion to the experimental results obtained with concentrations higher than 10^{18} cm^{-3}, a range for which the merging of the impurity band with the valence band edge results in a band gap shrinkage which is clearly seen in the PL spectra.

Typical PL spectra for hole concentrations in the range of $p=1.6\times10^{18}$ cm^{-3}-$p=1.95\times10^{20}$ cm^{-3} for both GaAs and $Ga_{0.85}In_{0.15}As$ are shown in figs.4.3.1.1 to 4.3.1.7. As the temperature is decreased, a shoulder develops on the high energy side of the emission line corresponding to the Fermi energy E_F. This change of shape is observed in all the samples with concentrations higher than 10^{18} cm^{-3}, and has been previously reported for p-type GaAs[21]. However, for sample 6 a well defined optical structure is observed at the low energy end of the spectrum around 1.46 eV. This structure is due to a LO phonon replica of the $\vec{k}$-conserving transitions. We will use these data to determine the band gap shrinkage at $T=5$ K. However, as already mentioned, one cannot measure directly the true sample temperature under illumination with excitation power densities of 2 W/cm^2 at $T=5$ K. Therefore, we have determined for the heavily doped layers, the band gap at

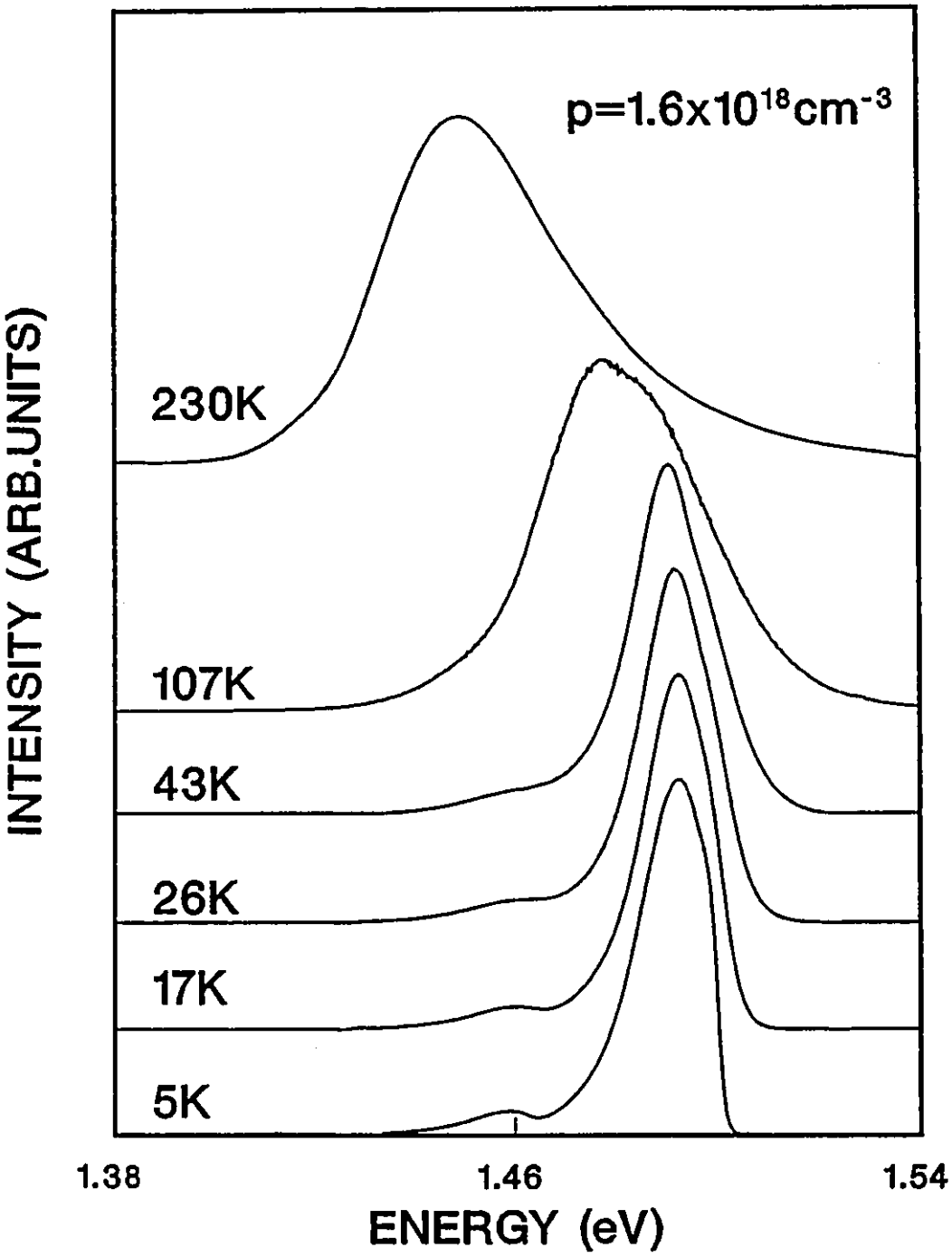

Figure 4.3.1.1. Luminescence spectra as a function of temperature of heavily Zn-doped GaAs with 1.6×10^{18} holes cm^{-3}.

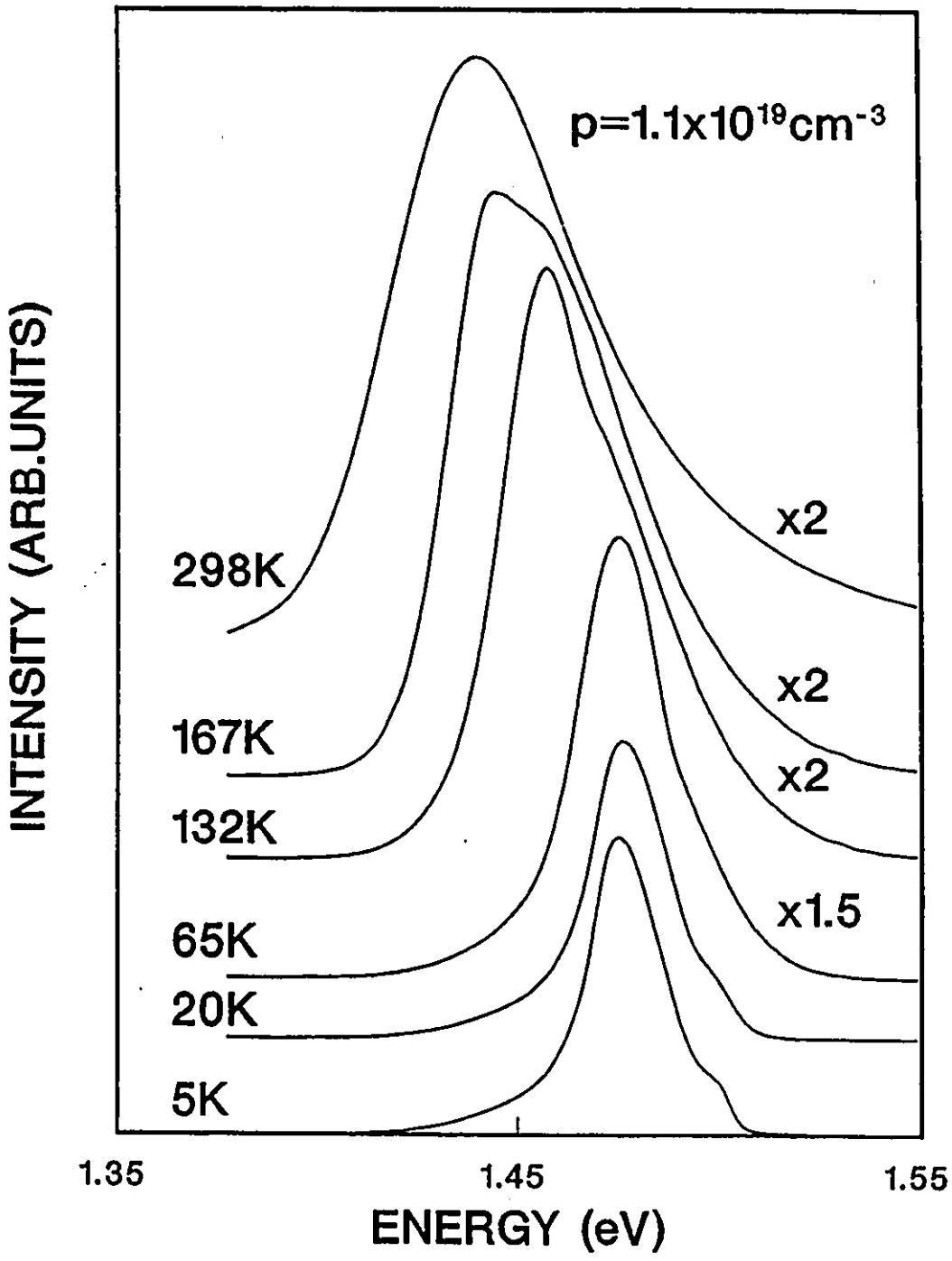

Figure 4.3.1.2. Luminescence spectra as a function of temperature of heavily Zn-doped GaAs with 1.1×10^{19} holes cm^{-3}.

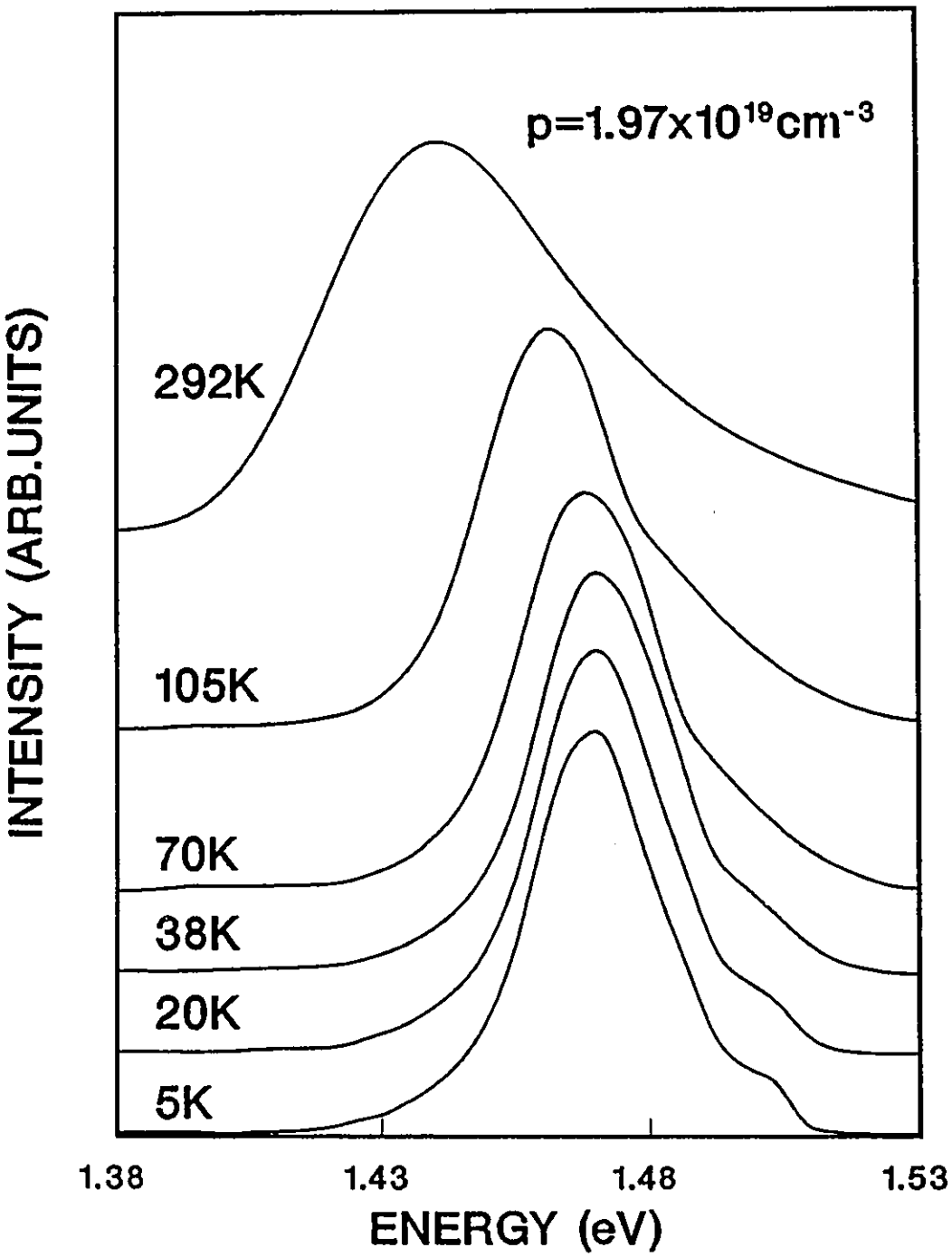

Figure 4.3.1.3. Luminescence spectra as a function of temperature of heavily Zn-doped GaAs with 1.97×10^{19} holes cm^{-3}.

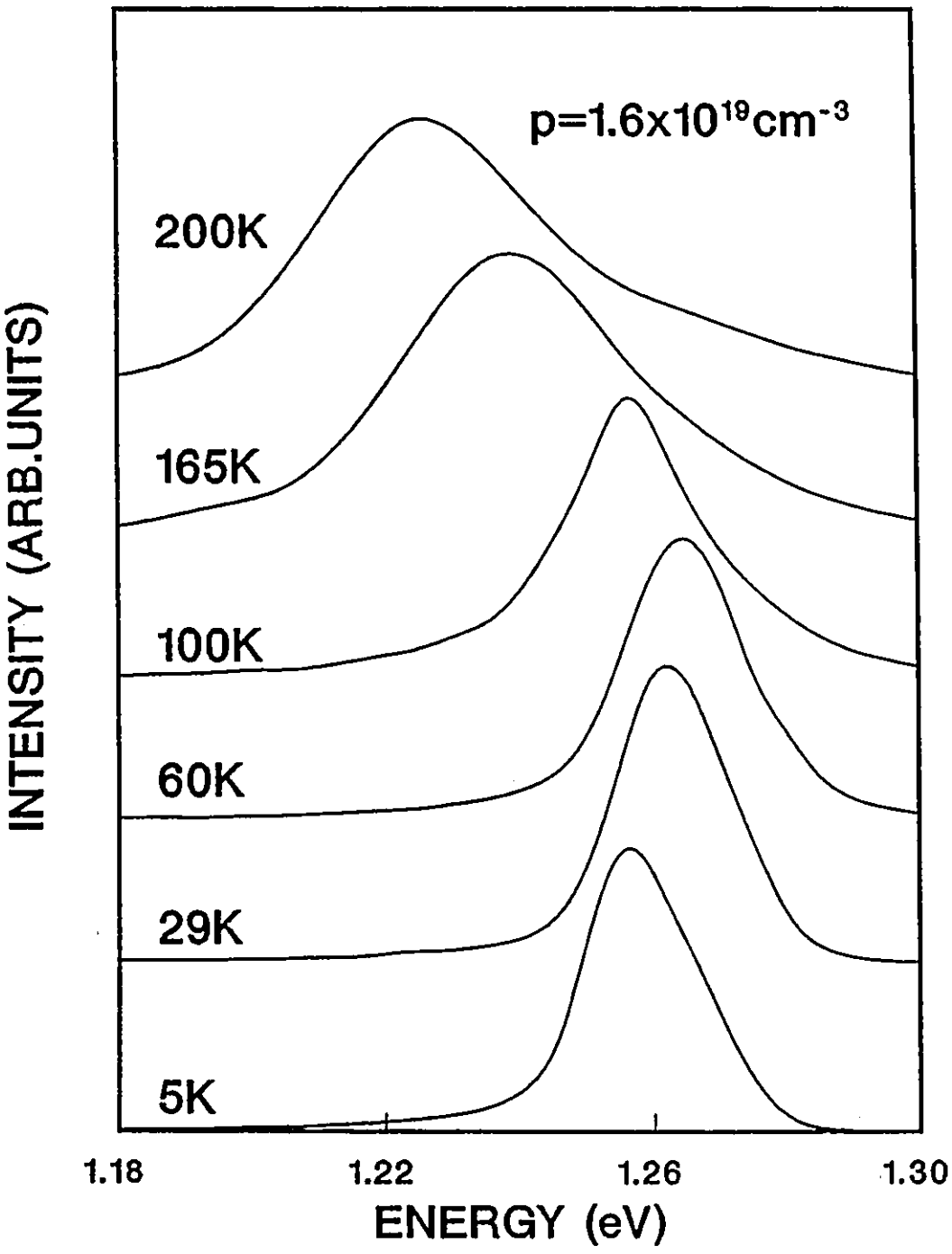

Figure 4.3.1.4. Luminescence spectra as a function of temperature of heavily Zn-doped $Ga_{0.85}In_{0.15}As$ with $1.6x10^{19}$ holes cm^{-3}

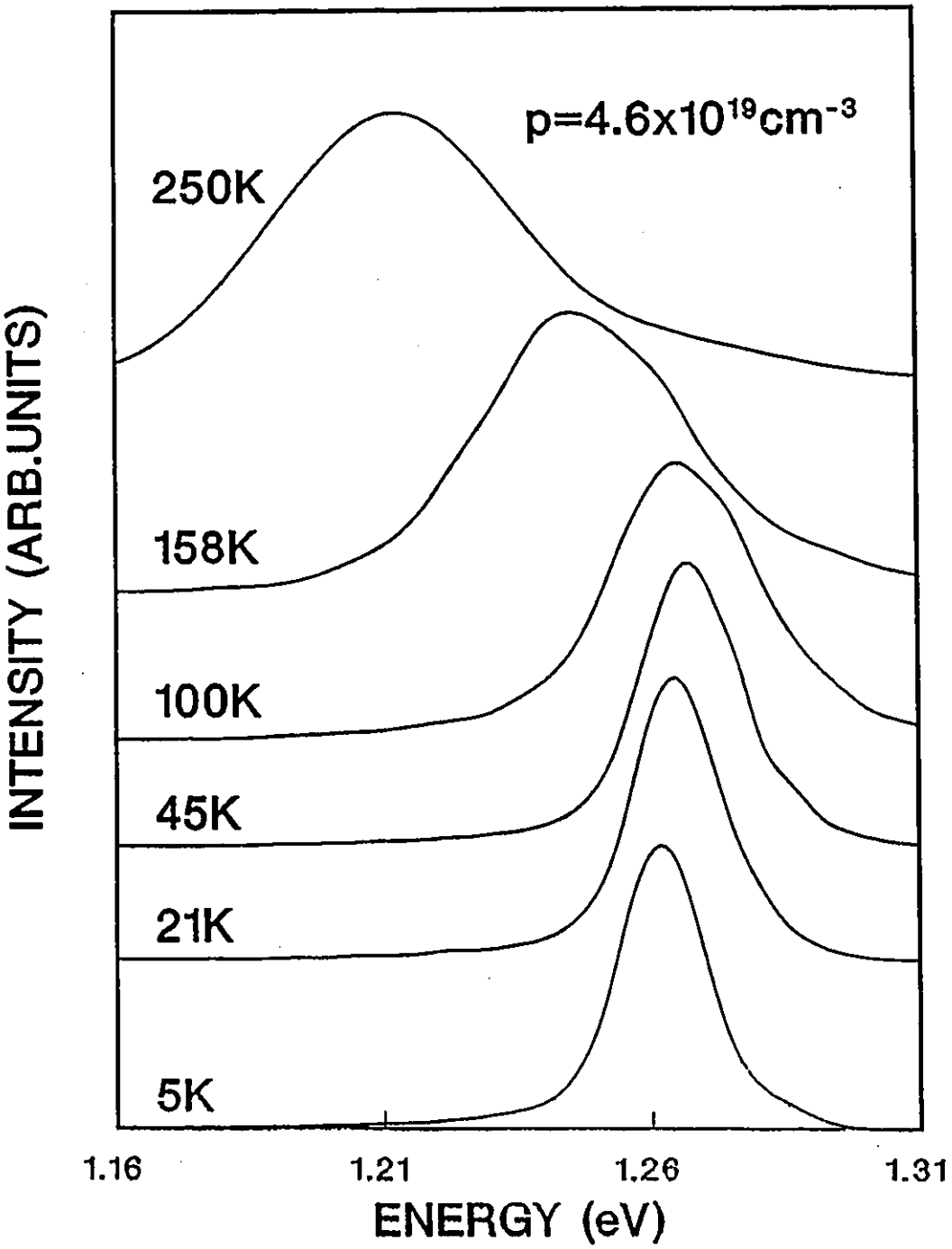

Figure 4.3.1.5. Luminescence spectra as a function of temperature of heavily Zn-doped $Ga_{0.85}In_{0.15}As$ with $4.6x10^{19}$ holes cm^{-3}

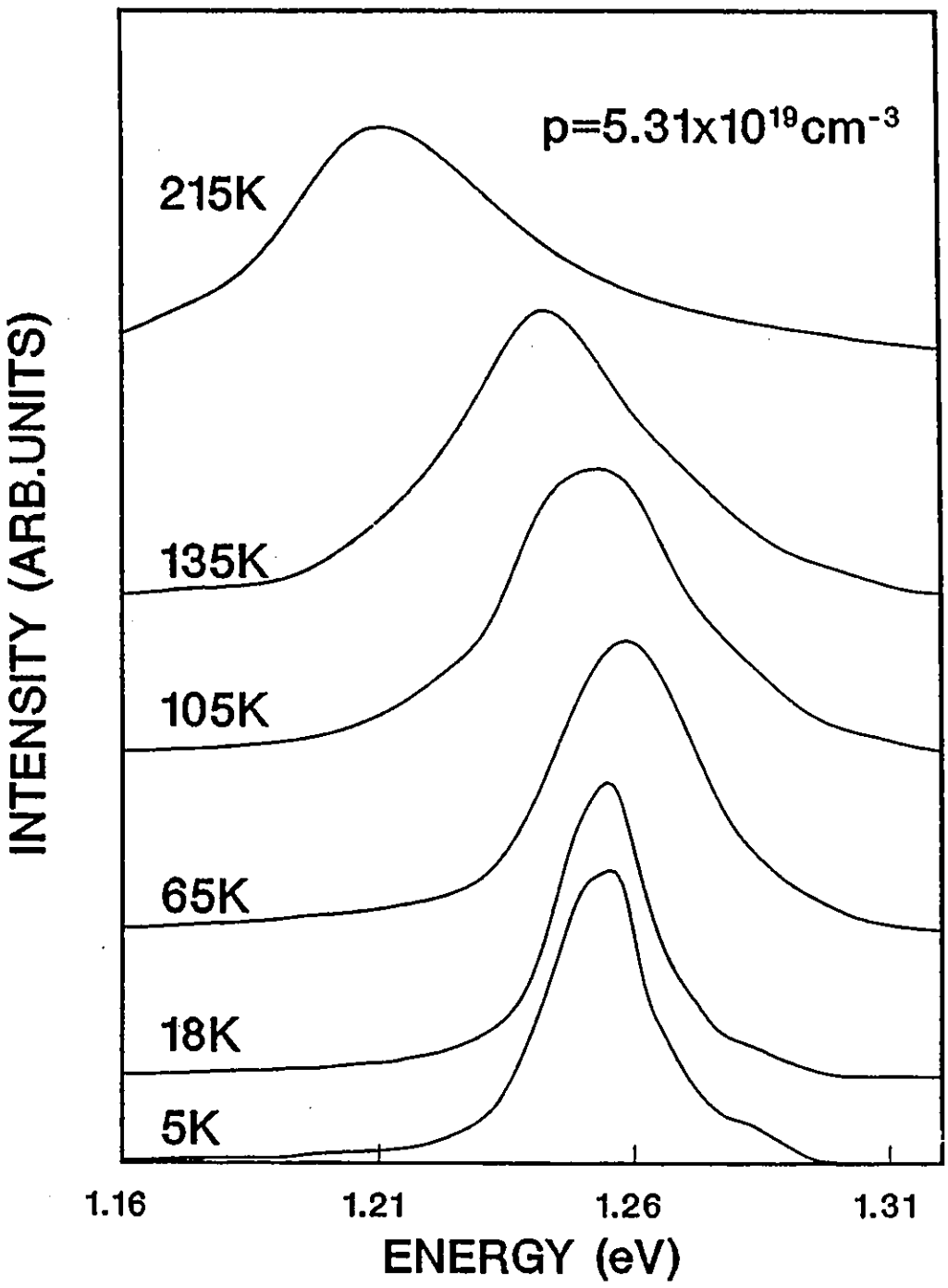

Figure 4.3.1.6. Luminescence spectra as a function of temperature of heavily Zn-doped $Ga_{0.85}In_{0.15}As$ with $5.31x10^{19}$ holes cm^{-3}

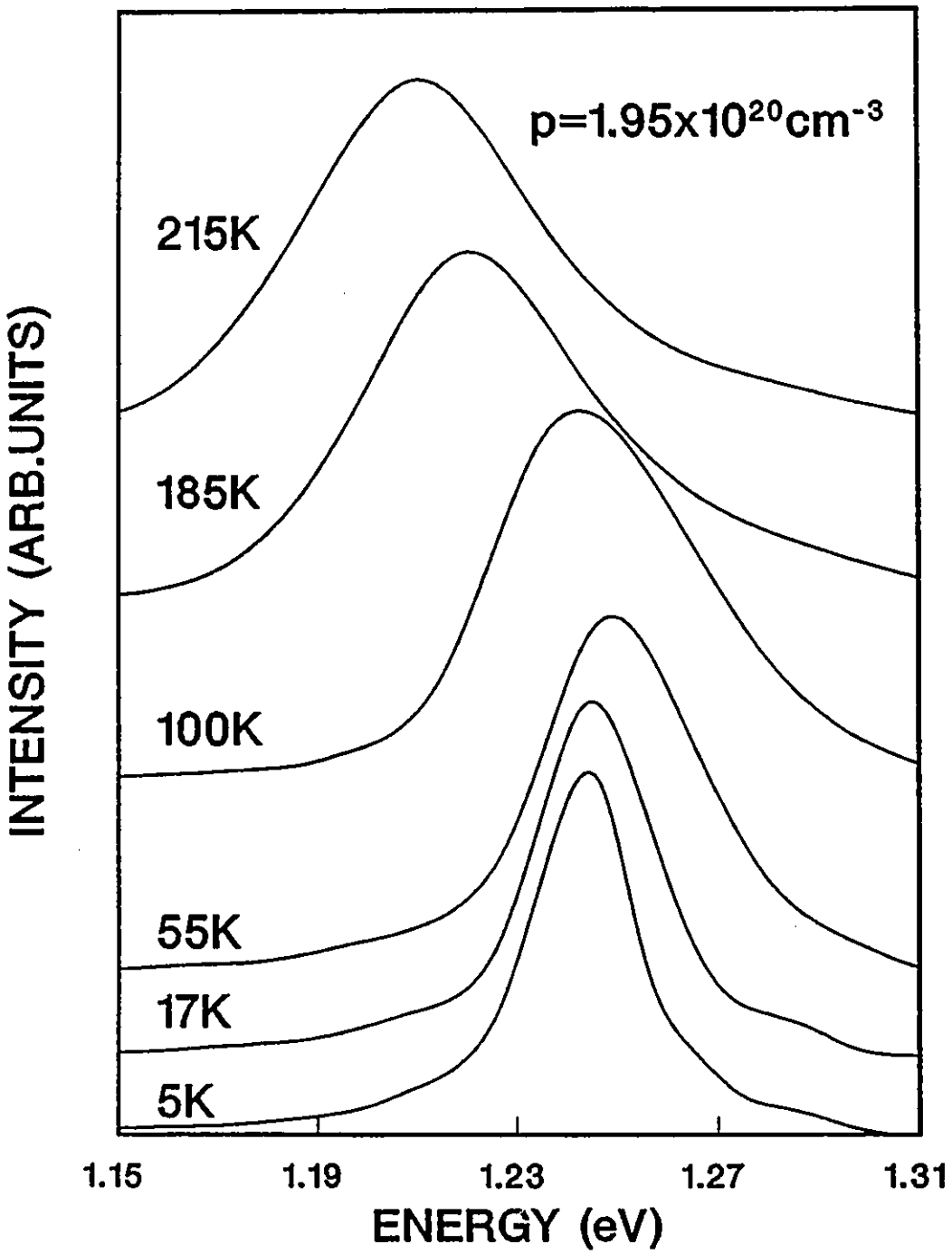

Figure 4.3.1.7. Luminescence spectra as a function of temperature of heavily Zn-doped $Ga_{0.85}In_{0.15}As$ with $1.95x10^{20}$ holes cm^{-3}

T=5 K from a fit of its variation with temperature in the range of 20-300 K where illumination heating effects are less important.

4.3.2 DETERMINATION OF THE BAND GAP SHRINKAGE

The Varshni equation has been shown by Olego and Cardona[21] to remain valid in the case of heavily doped material, given that $E_g(0)$, α and β are still assumed as adjustable parameters. The function $E_g(T)$, corresponding to a particular sample, is provided by a set of PL spectra collected at different temperatures, as in figs.4.3.1.1 to 4.3.1.7. For a given temperature T, $E_g(T)$ is taken as the intersection between the tangent to the low energy tail of the emission band and the background[21]. The fitting of equ.(4.2.3) to the experimental $E_g(T)$ provides $E_g(0)$, α and β for each sample. Figs.4.3.2.1 to 4.3.2.7 produce the temperature dependence of $E_g(T)$ for a series of hole concentrations in the range of p=1.6x10^{18} cm^{-3}-p=1.95x10^{20} cm^{-3}. The dashed and solid lines are, as already mentioned, theoretical fits obtained using the Varshni equation in the temperature range of 5-300 K and of 20-300 K, respectively. In tables 4.2.1 and 4.2.2, we list for a series of hole concentrations, the parameters $E_g(0)$, α and β obtained in the temperature range of 20-300 K. In tables 4.2.3 and 4.2.4, we display the measured hole concentration and E_g at T=5 K, as calculated from equ.(4.2.3), for a set of heavily doped GaAs (samples 6 to 8) and $Ga_{0.85}In_{0.15}As$ (samples 12 to 15) epilayers. The band gap shrinkage, also reported in tables 4.2.3 and 4.2.4, is given by

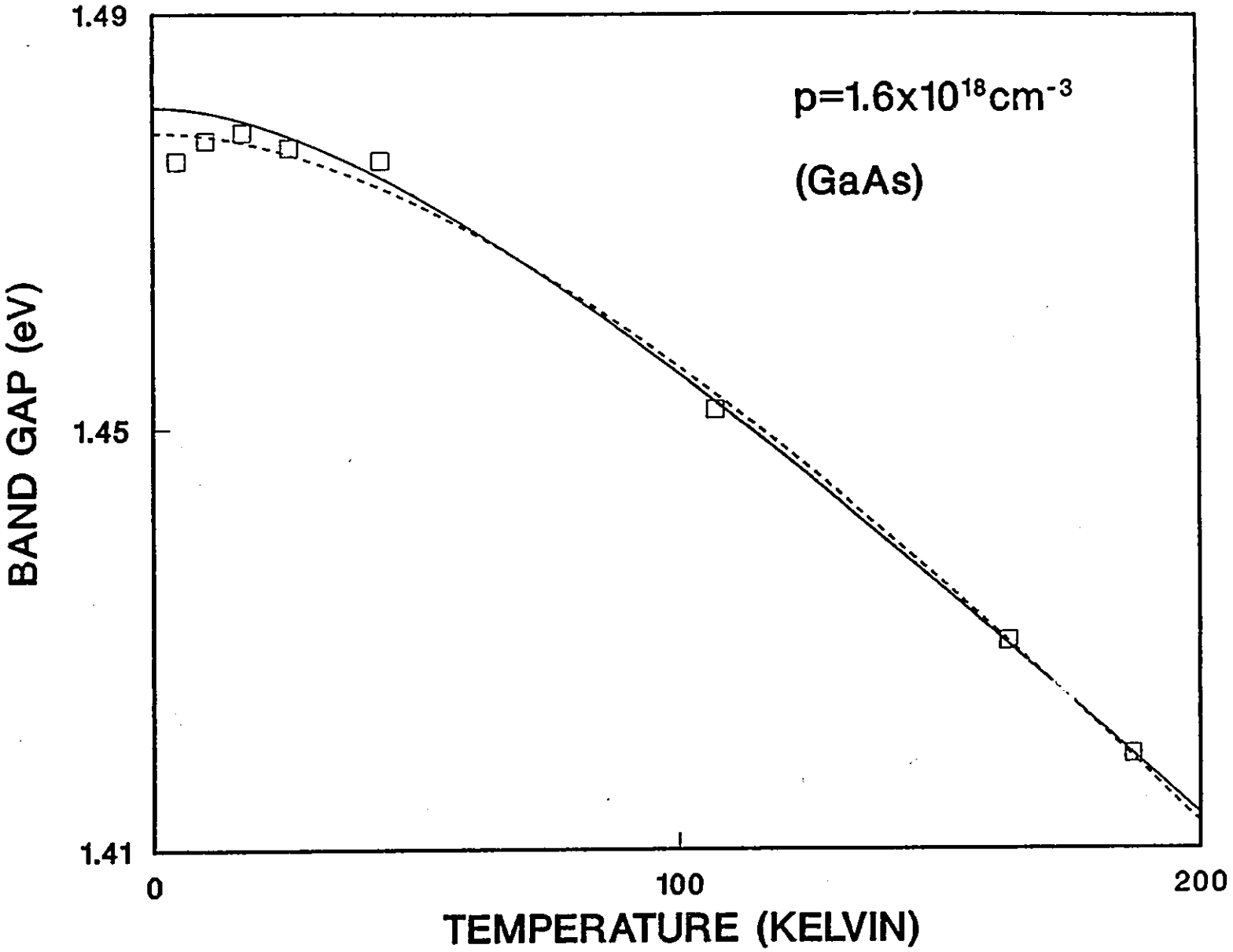

Figure 4.3.2.1. Temperature dependence of the band gap (open squares) of Zn-doped GaAs with 1.6×10^{18} holes cm^{-3}. The dashed and solid lines represent fits with Varshni's equation in the temperature range of 5-300 K and of 20-300 K, respectively.

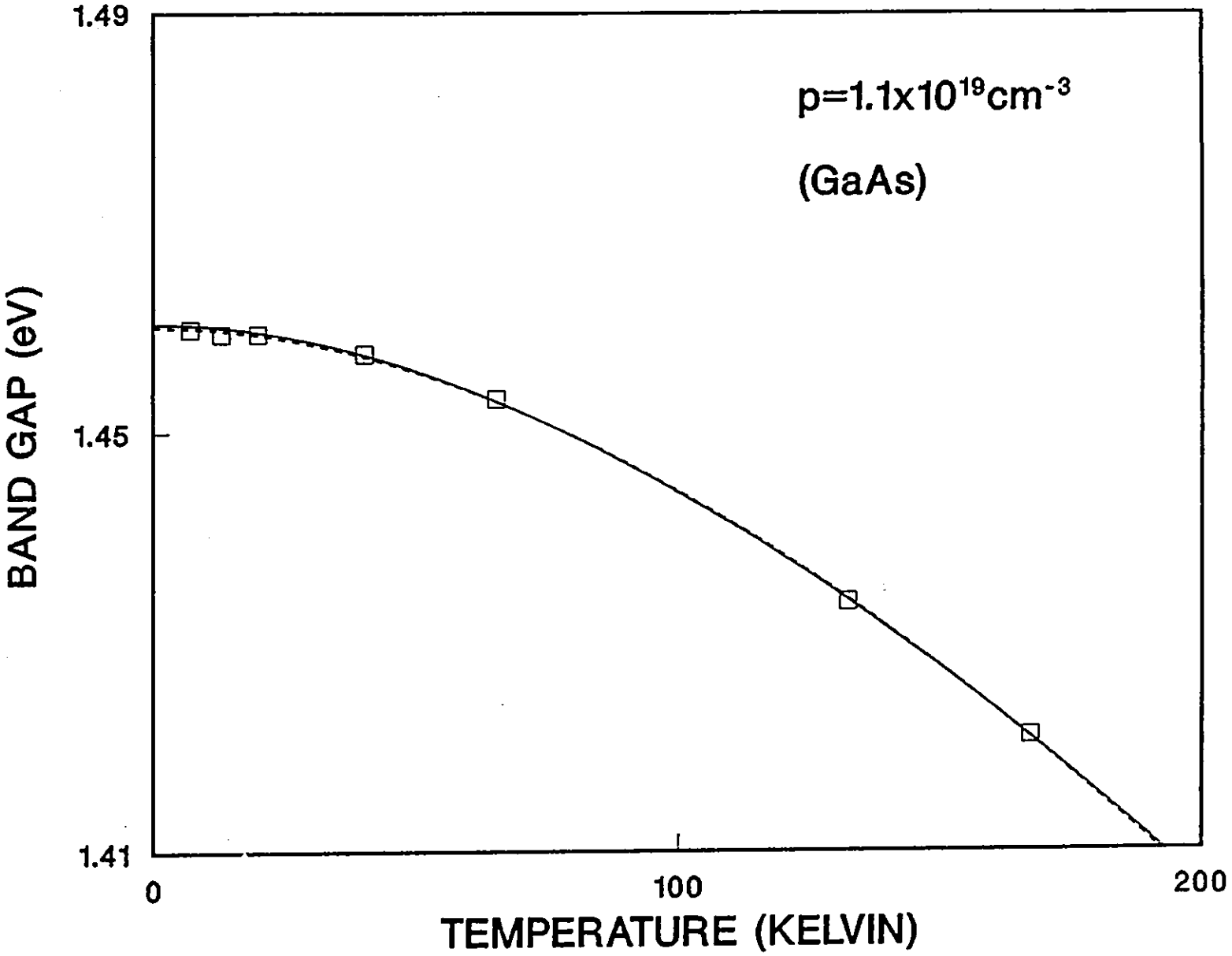

Figure 4.3.2.2: Temperature dependence of the band gap (open squares) of Zn-doped GaAs with 1.1×10^{19} holes cm^{-3}. The dashed and solid lines represent fits with Varshni's equation in the temperature range of 5-300 K and of 20-300 K, respectively.

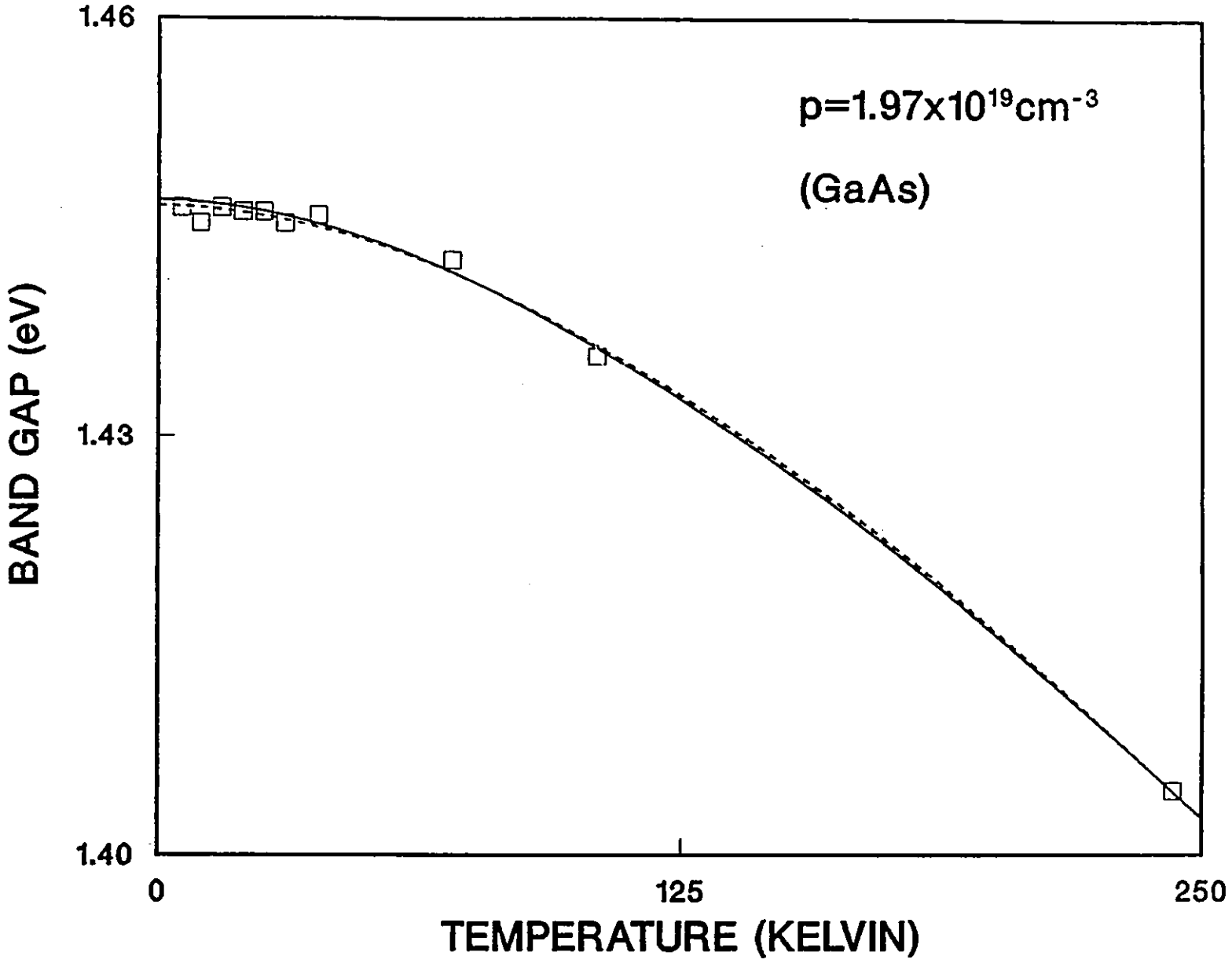

Figure 4.3.2.3. Temperature dependence of the band gap (open squares) of Zn-doped GaAs with 1.97×10^{19} holes cm^{-3}. The dashed and solid lines represent fits with Varshni's equation in the temperature range of 5-300 K and of 20-300 K, respectively.

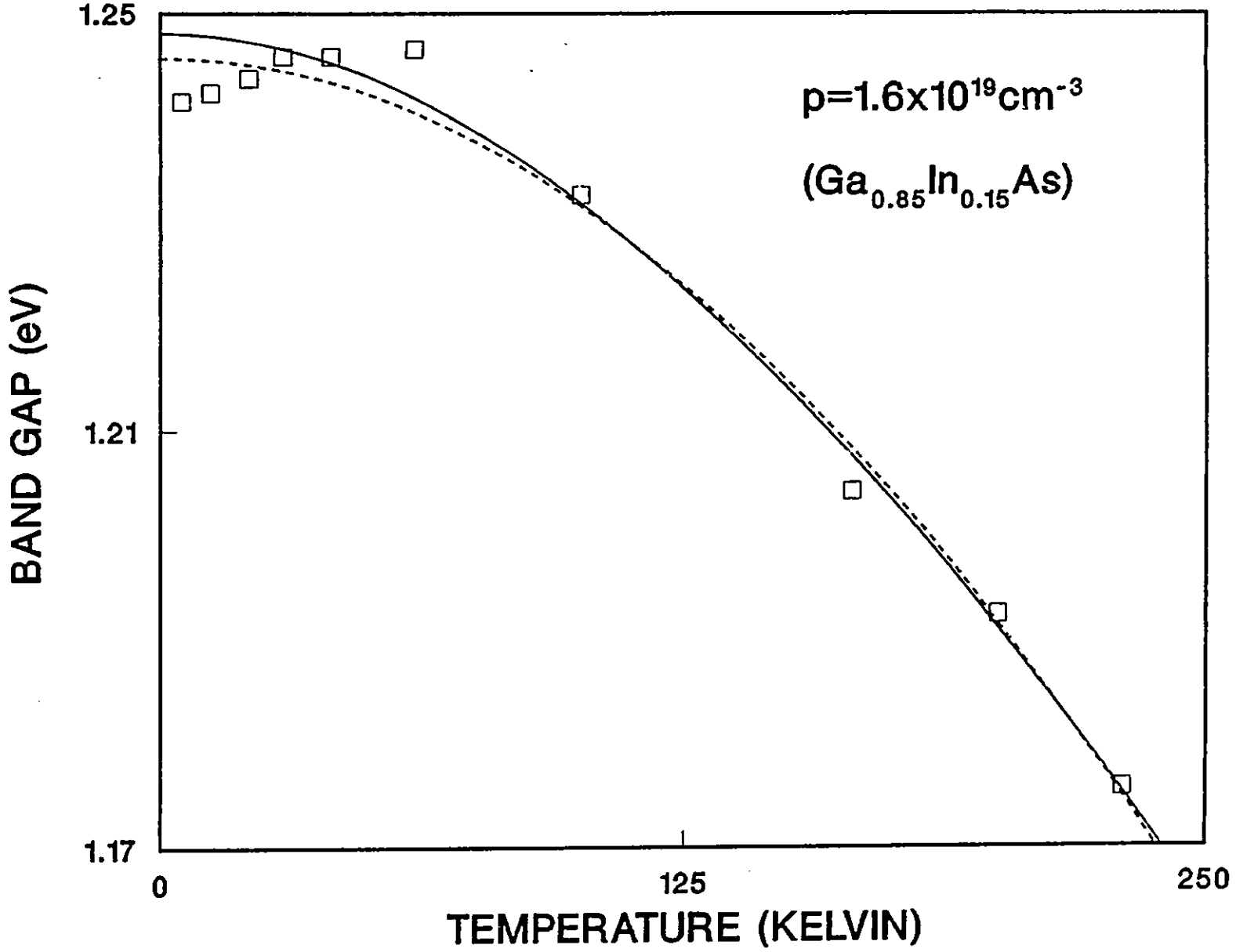

Figure 4.3.2.4. Temperature dependence of the band gap (open squares) of Zn-doped $Ga_{0.85}In_{0.15}As$ with 1.6×10^{19} holes cm^{-3}. The dashed and solid lines represent fits with Varshni's equation in the temperature range of 5-300 K and of 20-300 K, respectively.

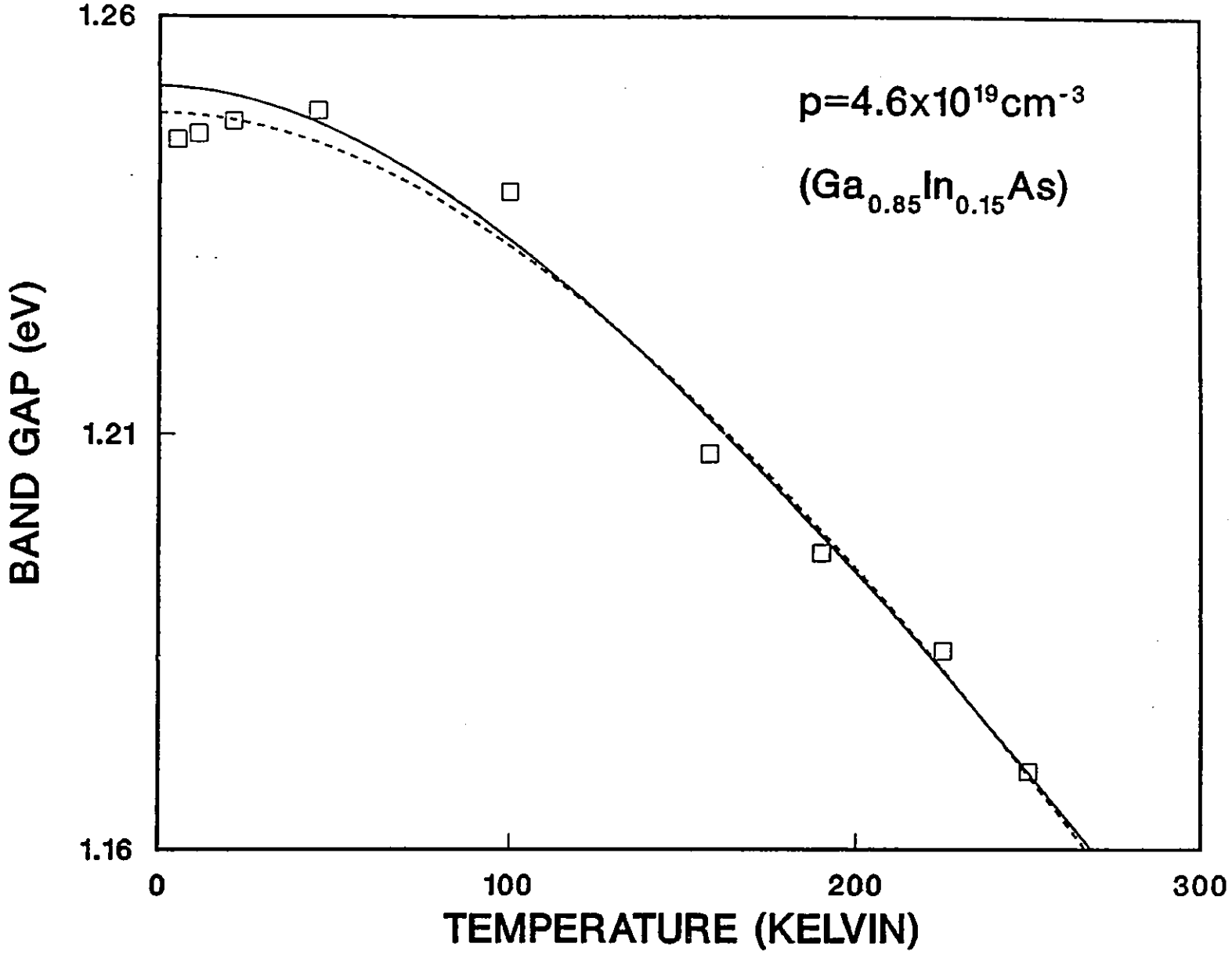

Figure 4.3.2.5. Temperature dependence of the band gap (open squares) of Zn-doped $Ga_{0.85}In_{0.15}As$ with $4.6x10^{19}$ holes cm^{-3}. The dashed and solid lines represent fits with Varshni's equation in the temperature range of 5-300 K and of 20-300 K, respectively.

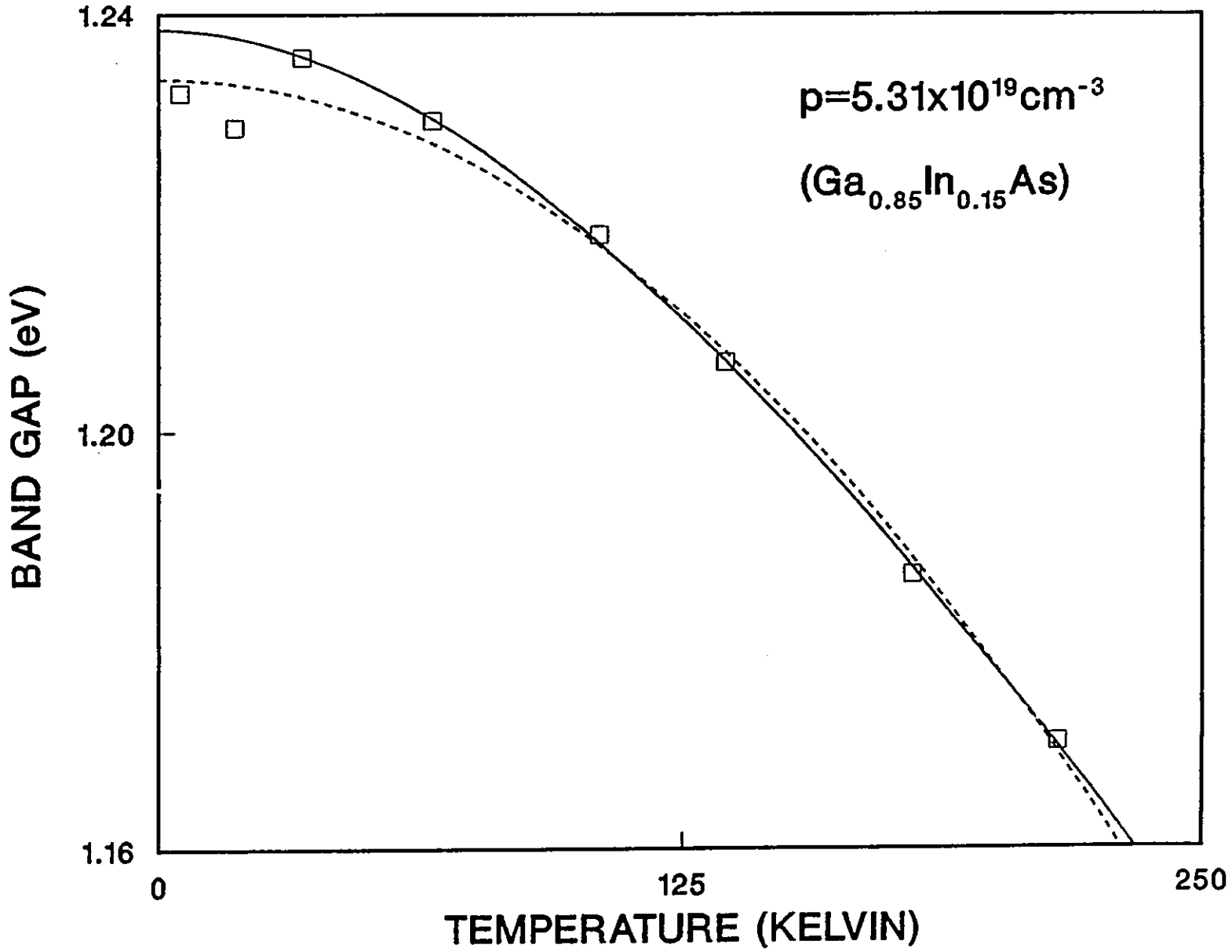

Figure 4.3.2.6. Temperature dependence of the band gap (open squares) of Zn-doped $Ga_{0.85}In_{0.15}As$ with 5.31×10^{19} holes cm^{-3}. The dashed and solid lines represent fits with Varshni's equation in the temperature range of 5-300 K and of 20-300 K, respectively.

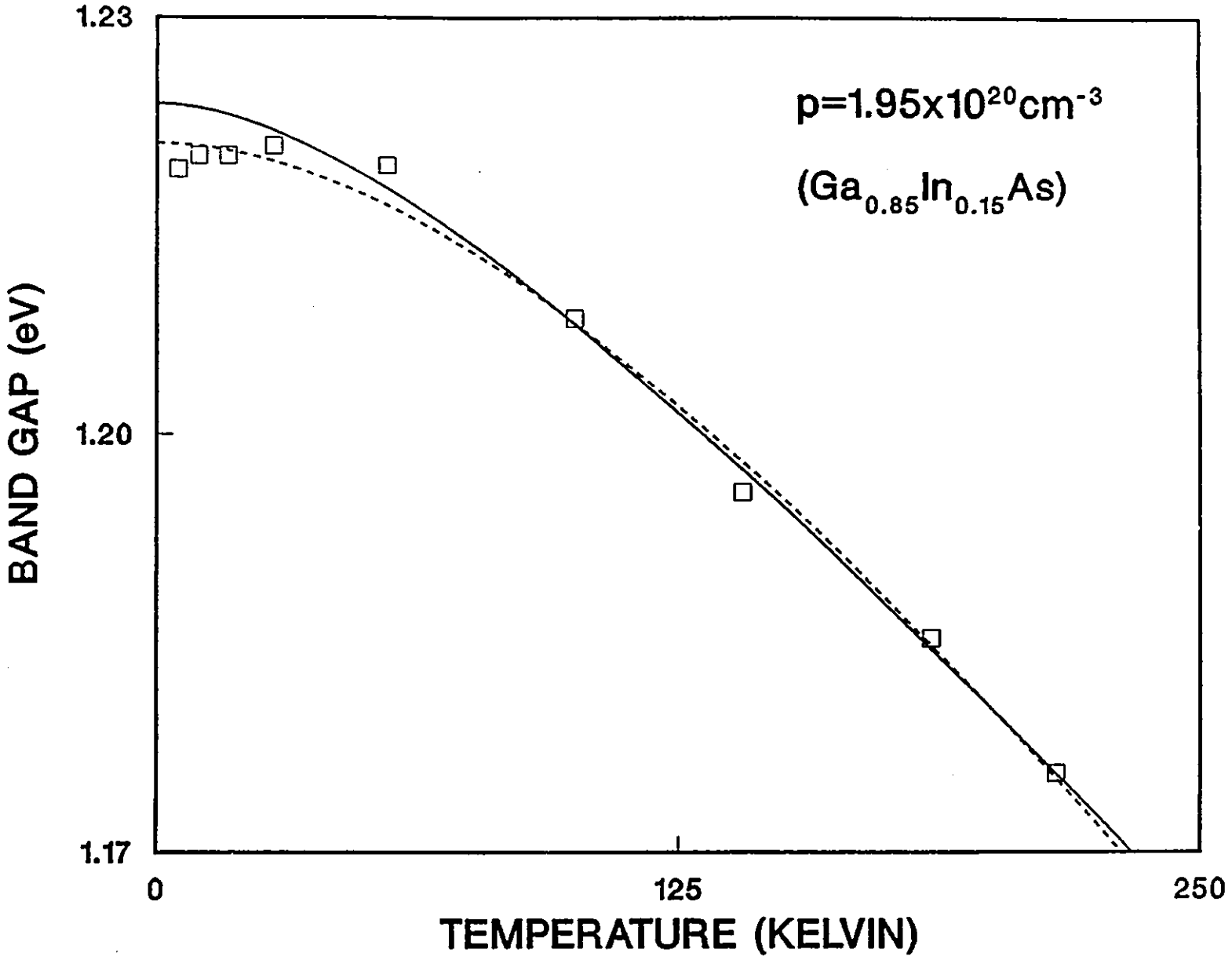

Figure 4.3.2.7. Temperature dependence of the band gap (open squares) of Zn-doped $Ga_{0.85}In_{0.15}As$ with 1.95×10^{20} holes cm^{-3}. The dashed and solid lines represent fits with Varshni's equation in the temperature range of 5-300 K and of 20-300 K, respectively.

$$|\Delta E_g| = |E_g^d - E_g^u| \qquad (4.3.2.1)$$

where E_g^u corresponds to the band gap of undoped material ($E_g^u(5)=(1.519 \pm 0.001)$ eV[7] for GaAs and $E_g^u(5)=(1.296 \pm 0.003)$ eV for $Ga_{0.85}In_{0.15}As$, as shown in table 4.2.3 for sample 9) and E_g^d is taken as the band gap of doped material.

The dependence of the band gap shrinkage on carrier concentration has been considered by many authors[31-35]. Most early calculations of the band gap shrinkage neglected some of the factors which contribute to $|\Delta E_g|$ (such as dielectric screening, distribution of impurity centres, etc) and the agreement between experiment and calculations was fortuitous due to cancelling effects. However, some model calculations[20,32,35,36,37] are more complete, but only apply satisfactorily for concentrations higher than 10^{18} cm^{-3}. In these calculations, which are all based on a weakly interacting hole gas-model (p-type material) at $T=0$ K, the band gap shrinkage is proportional to $p^{1/3}$, at least in a first approximation. We have thus determined the free hole dependence of heavily doped GaAs and $Ga_{0.85}In_{0.15}As$, using the relation

$$|\Delta E_g| = A\,p^{1/3} \qquad (4.3.2.2)$$

where A has been adjusted to give the measured value of $|\Delta E_g|$ at high p. The results of tables 4.2.3 and 4.2.4 are presented graphically in fig.4.3.2.8. A semi-empirical least-squares fit using equ.(4.3.2.2) of the points corresponding to $p \geq 10^{18}$ cm^{-3}[22] gives

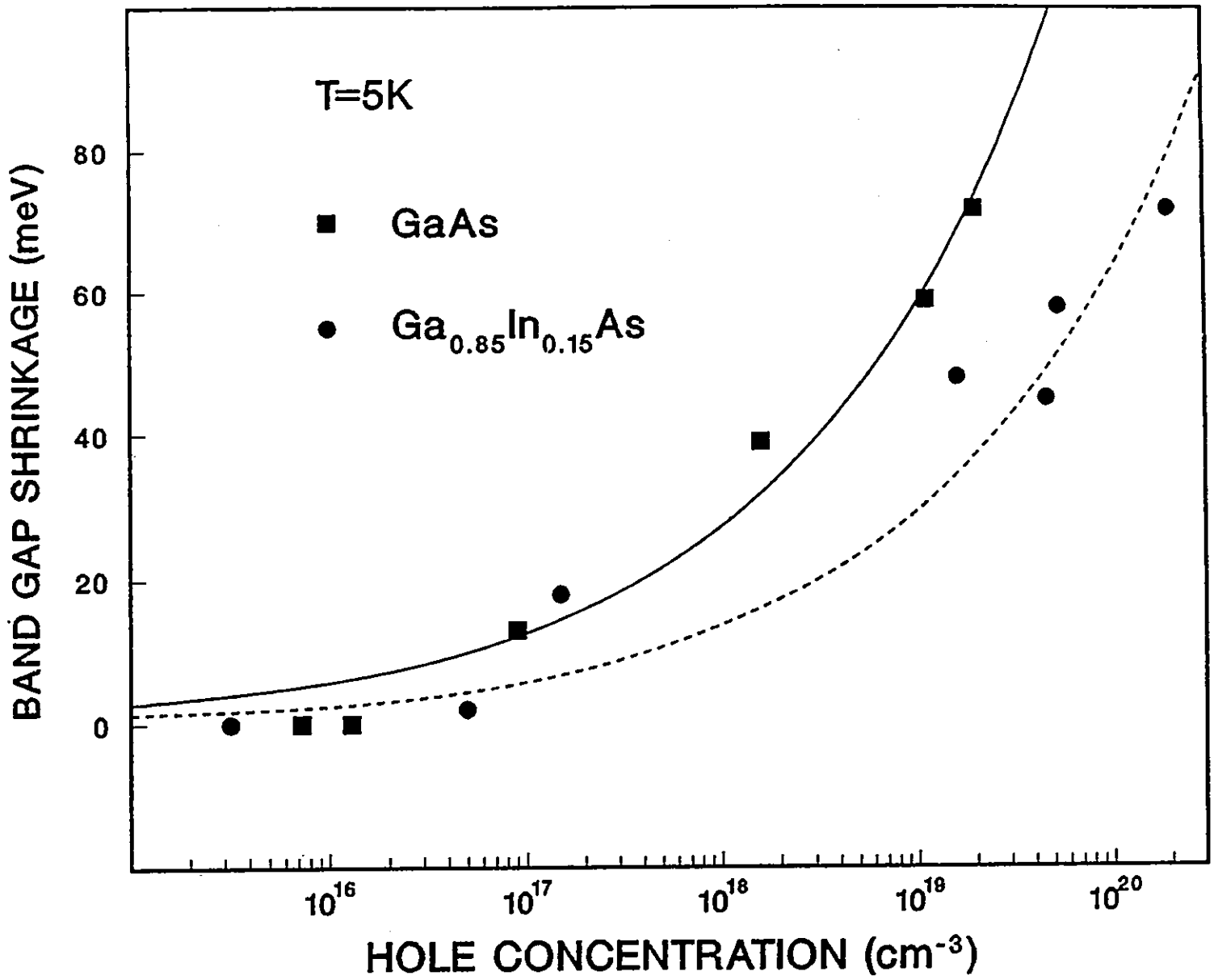

Figure 4.3.2.8. Band gap and band gap shrinkage as a function of hole concentration of Zn-doped GaAs (full squares) and $Ga_{0.85}In_{0.15}As$ (full circles) at 5 K. The solid and dashed lines represent a least-squares fit of the points corresponding to $p \geq 10^{18}$ cm^{-3} for GaAs and $Ga_{0.85}In_{0.15}As$, respectively.

Table 4.2.1. Coefficients $E_g(0)$, α, and β of Varshni's equ.(4.2.3) obtained in the temperature range of 20-300 K for various $Ga_{0.85}In_{0.15}As$ samples.

p (cm^{-3})	$E_g(0)$ (eV)	α (10^{-4} eV K^{-1})	β (K)
$3.22x10^{15}$	1.296 (3)	7.7 (4)	638 (25)
$1.60x10^{19}$	1.248 (3)	12.0 (4)	623 (25)
$4.60x10^{19}$	1.252 (3)	7.0 (4)	286 (25)
$5.31x10^{19}$	1.238 (3)	8.3 (4)	344 (25)
$1.95x10^{20}$	1.224 (3)	3.5 (4)	119 (25)

Table 4.2.2. Coefficients $E_g(0)$, α, and β of Varshni's equ.(4.2.3) obtained in the temperature range of 20-300 K for various GaAs samples.

p (cm^{-3})	$E_g(0)$ (eV)	α (10^{-4} eV K^{-1})	β (K)
$1.60x10^{18}$	1.480 (2)	4.9 (3)	94 (20)
$1.10x10^{19}$	1.460 (2)	7.8 (3)	379 (20)
$1.97x10^{19}$	1.447 (2)	3.9 (3)	310 (20)

Table 4.2.3. 5 K band gap and band gap shrinkage of various $Ga_{0.85}In_{0.15}As$ samples.

p (cm^{-3})	E_g (eV)	$\lvert\Delta E_g\rvert$ (meV)
3.22×10^{15}	1.296 (3)	0 (6)
5.00×10^{16}	1.298 (5)	2 (8)
1.50×10^{17}	1.278 (4)	18 (7)
1.60×10^{19}	1.248 (3)	48 (6)
4.60×10^{19}	1.251 (3)	45 (6)
5.31×10^{19}	1.238 (3)	58 (6)
1.95×10^{20}	1.224 (3)	72 (6)

Table 4.2.4. 5 K band gap and band gap shrinkage of various GaAs samples. The 30 K band gap shrinkage $|\Delta E_g|^*$ of GaAs obtained by Borghs[18] is also presented.

p (cm^{-3})	E_g (eV)	$\|\Delta E_g\|$ (meV)	$\|\Delta E_g\|^*$ (meV)
7.30×10^{15}	1.519 (5)	0 (6)	5 (2)
1.30×10^{16}	1.519 (5)	0 (6)	6 (2)
9.00×10^{16}	1.506 (4)	13 (5)	11 (2)
1.60×10^{18}	1.480 (2)	39 (3)	31 (2)
1.10×10^{19}	1.460 (2)	59 (3)	58 (2)
1.97×10^{19}	1.447 (2)	72 (3)	70 (2)

$$|\Delta E_g|_{GaAs} = 2.7x10^{-8}\, p^{1/3} \qquad (4.3.2.3)$$

$$|\Delta E_g|_{Ga_{0.85}In_{0.15}As} = 1.4x10^{-8}\, p^{1/3} \qquad (4.3.2.4)$$

with $|\Delta E_g|$ in eV and p in cm^{-3}. The solid and dashed lines in fig.4.3.2.8 are plots of equs.(4.3.2.3) and (4.3.2.4), respectively. The average relative error is 9 % for GaAs and 14 % for $Ga_{0.85}In_{0.15}As$. The variation of $|\Delta E_g|$ for GaAs is in very good agreement with previously published results by Borghs[18] and co-workers (see table 4.2.4). The corresponding result for $Ga_{0.85}In_{0.15}As$ is to the best of our knowledge the first of the kind. However, this result appears surprising, as one expects more overlap between impurity atoms in $Ga_{0.85}In_{0.15}As$ than in GaAs due to smaller binding energies. This can be understood on the basis of simple qualitative considerations. The binding energy (see equ.(1.4.4), Chapter 1) depends on m_{lh}^*, m_{hh}^*, and κ for a given material. In $Ga_{0.85}In_{0.15}As$, m_{lh}^* and m_{hh}^* are both smaller than in GaAs, and κ is larger than the corresponding GaAs value (see table 1.3.1, Chapter 1). This yields a smaller binding energy in the $Ga_{0.85}In_{0.15}As$ alloy than in GaAs. The wavefunctions of holes occupying such levels in $Ga_{0.85}In_{0.15}As$ are thus spatially more extended than in GaAs and the overlap between impurity atoms is more significant. Consequently, as the impurity concentration increases, the impurity band in $Ga_{0.85}In_{0.15}As$ broadens and eventually merges with the valence band at a lower impurity concentration than in GaAs. A larger band gap shrinkage is thus expected in $Ga_{0.85}In_{0.15}As$. This is in contradiction with our result of a smaller band gap shrinkage. A possible

explanation for this apparent contradiction lies in the fact that $Ga_{0.85}In_{0.15}As$ is an alloy, and therefore, more disorder is expected in the distribution of impurities, which leads to stronger carrier localization.

We have shown that the variation of the band gap shrinkage $|\Delta E_g|$ for both GaAs and $Ga_{0.85}In_{0.15}As$ may be approximated by the free hole concentration to the one third ($p^{1/3}$). The variation of $|\Delta E_g|$ for $Ga_{0.85}In_{0.15}As$ seems to be smaller than in GaAs. One can suspect that disorder effects make an essential contribution to the surprisingly low $|\Delta E_g|$ in $Ga_{0.85}In_{0.15}As$. Unfortunately the empirical nature of equ.(4.3.2.2) makes it difficult to compare the effects of different contributions to $|\Delta E_g|$ such as dielectric screening, distribution of impurities etc. It is hoped that extension of band gap shrinkage measurements to materials such as $Ga_{0.85}In_{0.15}As$ will help better quantify the physical source of band gap shrinkage in heavily doped alloy semiconductors.

4.3.3 FITTING OF THE LINE SPECTRA

All the PL spectra obtained at T=5 K of heavily doped GaAs (samples 6 to 8) and $Ga_{0.85}In_{0.15}As$ (samples 12 to 15) have been fitted using equ.(2.6.6). The results are displayed in figs.4.3.3.1 to 4.3.3.7. The solid line and open square symbols correspond respectively to the experimental and calculated curves. Because of the large number of free holes and the asymmetry of electron and hole masses (p-type material) most of the oscillator strength is concentrated in the $\vec{k}$-

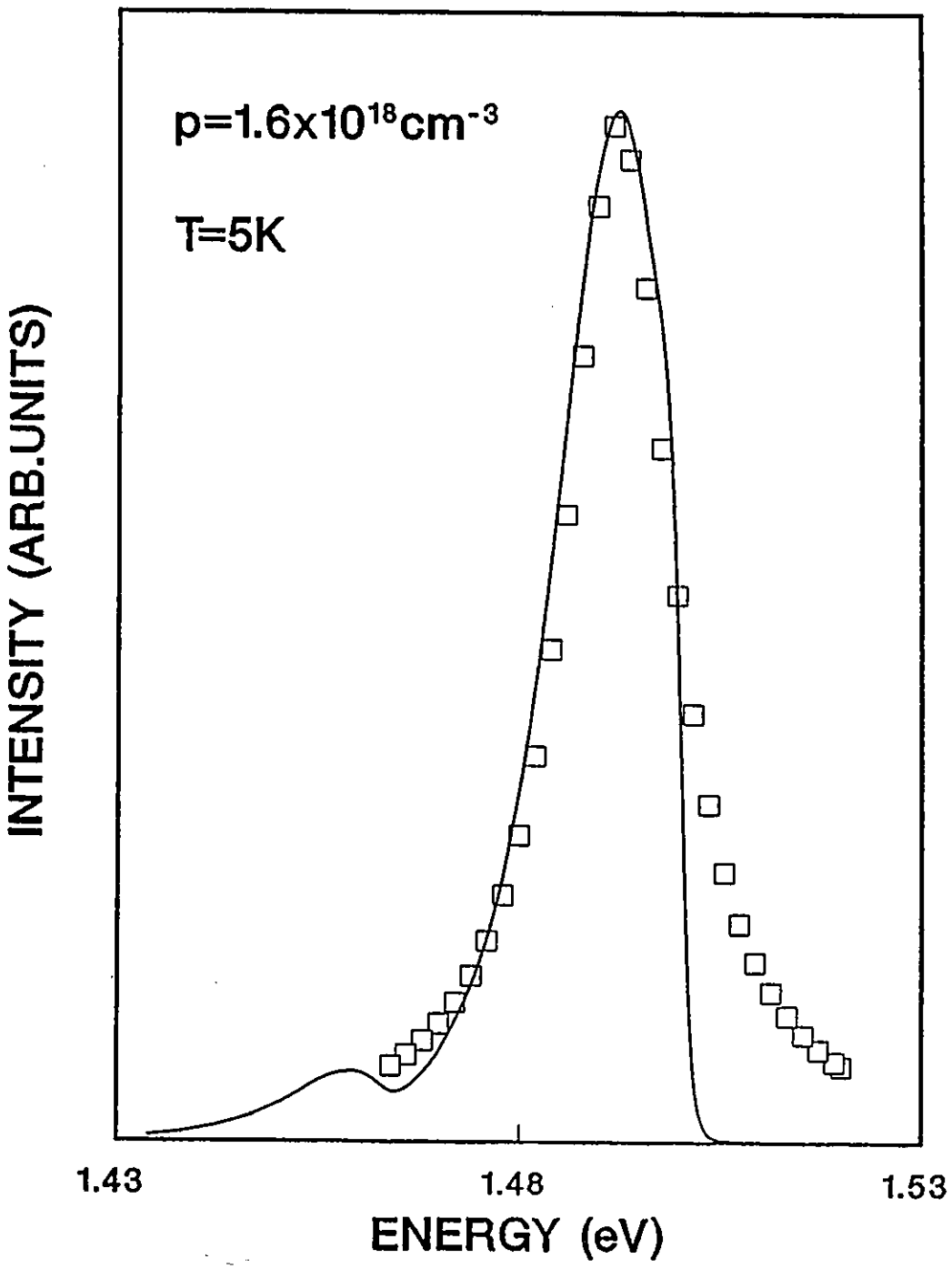

Figure 4.3.3.1. Experimental luminescence spectrum (solid line) of Zn-doped GaAs with 1.6×10^{18} holes cm^{-3} at 5 K and theoretical calculation (open squares).

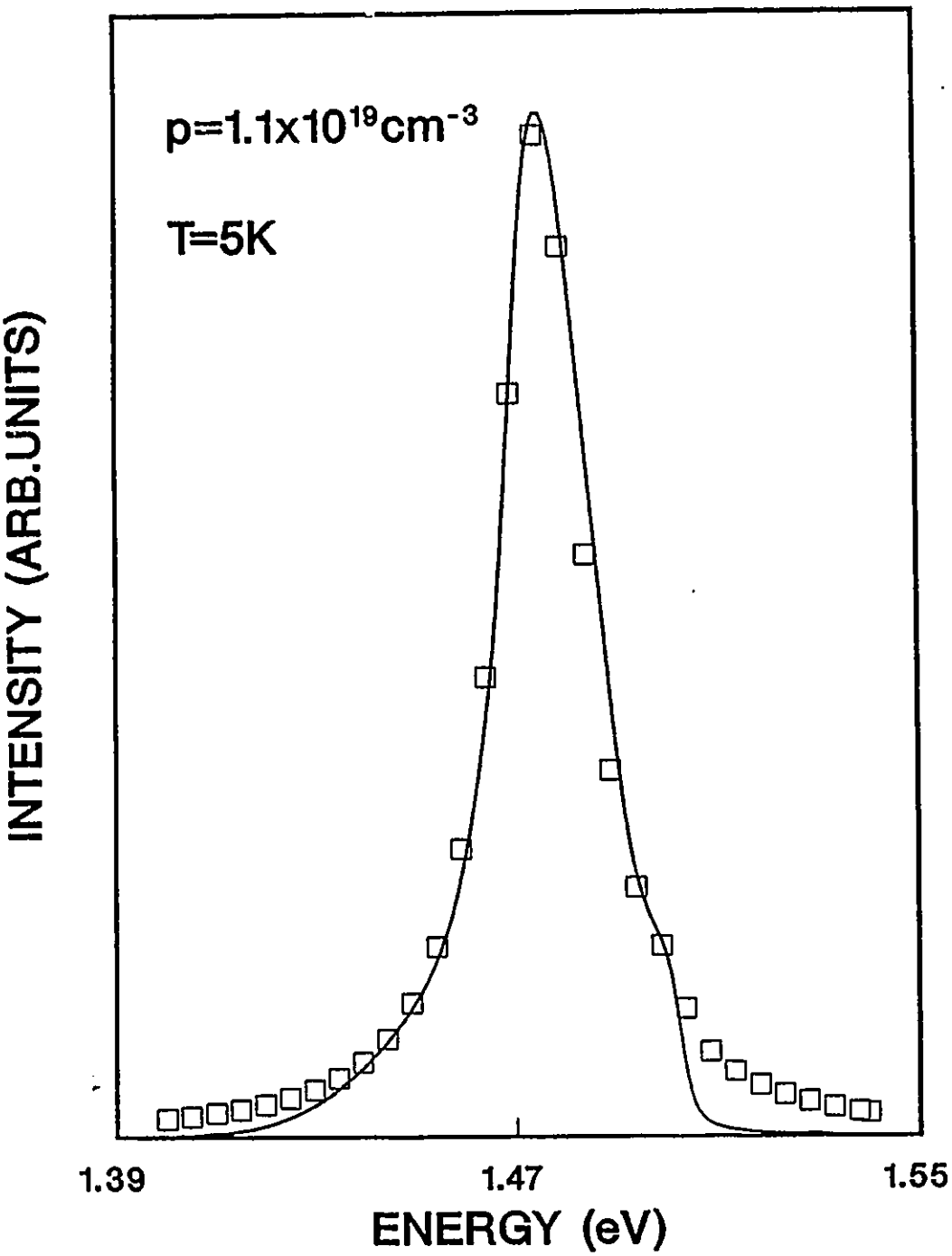

Figure 4.3.3.2. Experimental luminescence spectrum (solid line) of Zn-doped GaAs with 1.1×10^{19} holes cm^{-3} at 5 K and theoretical calculation (open squares).

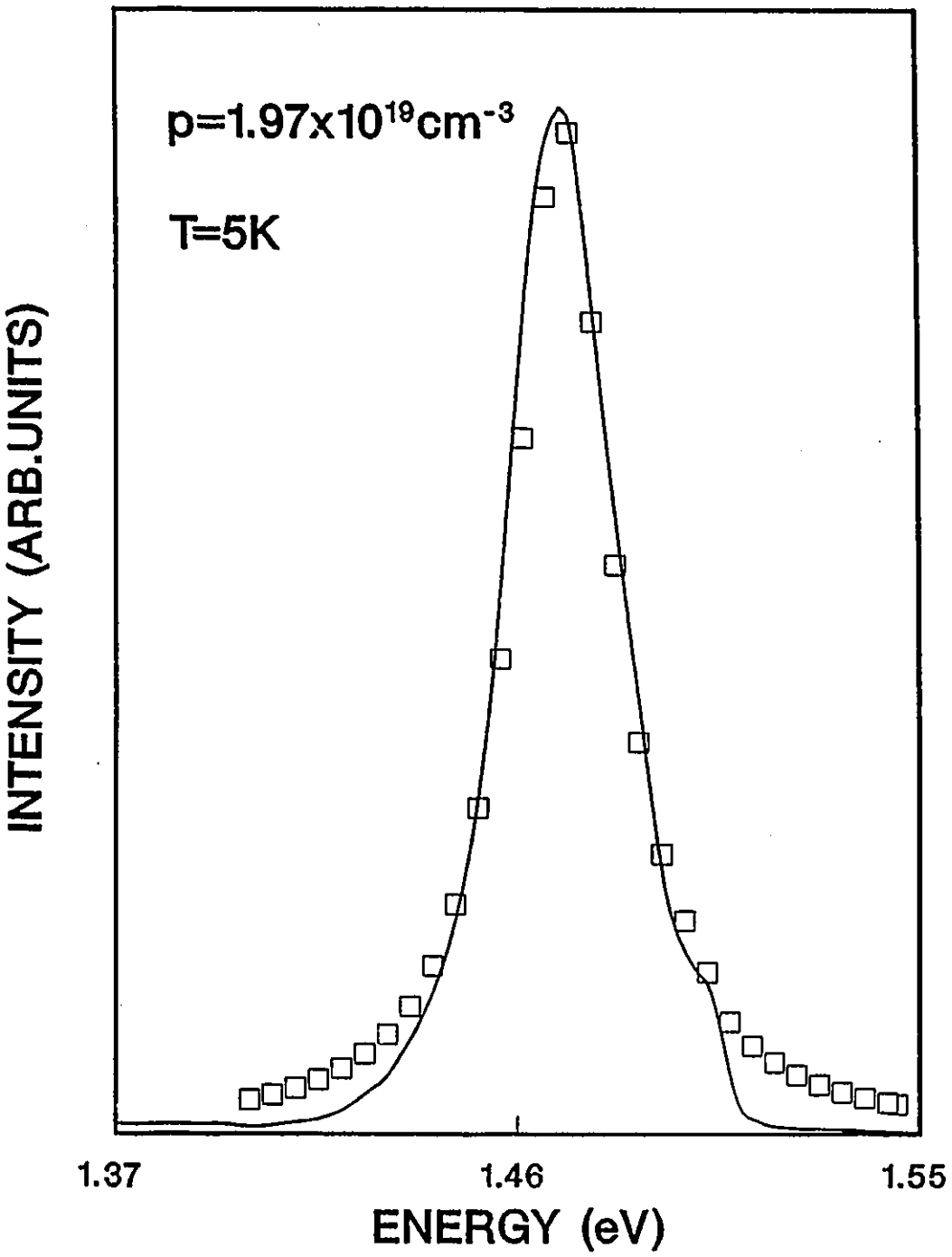

Figure 4.3.3.3. Experimental luminescence spectrum (solid line) of Zn-doped GaAs with 1.97×10^{19} holes cm^{-3} at 5 K and theoretical calculation (open squares).

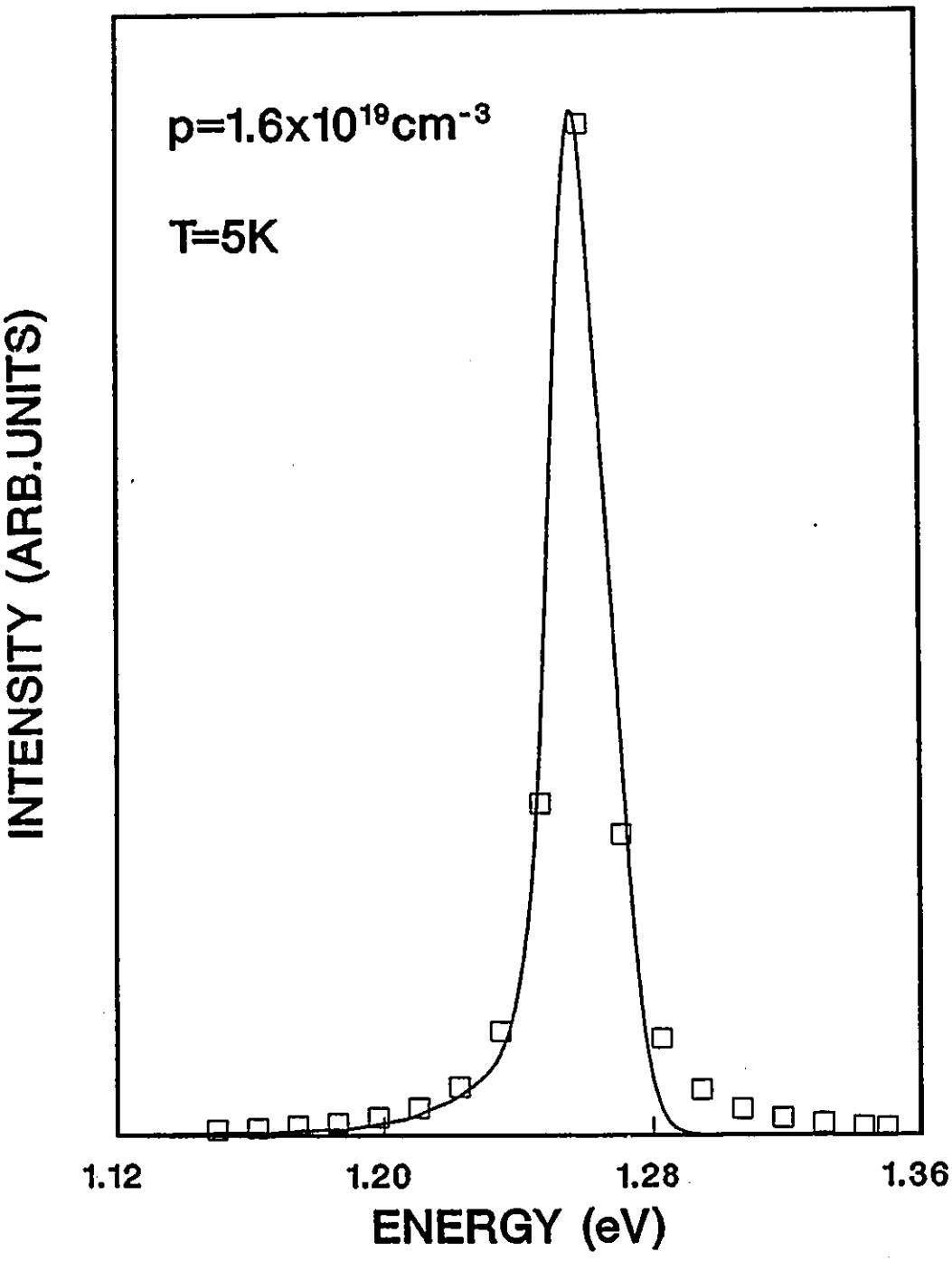

Figure 4.3.3.4. Experimental luminescence spectrum (solid line) of Zn-doped $Ga_{0.85}In_{0.15}As$ with $1.6x10^{19}$ holes cm^{-3} at 5 K and theoretical calculation (open squares).

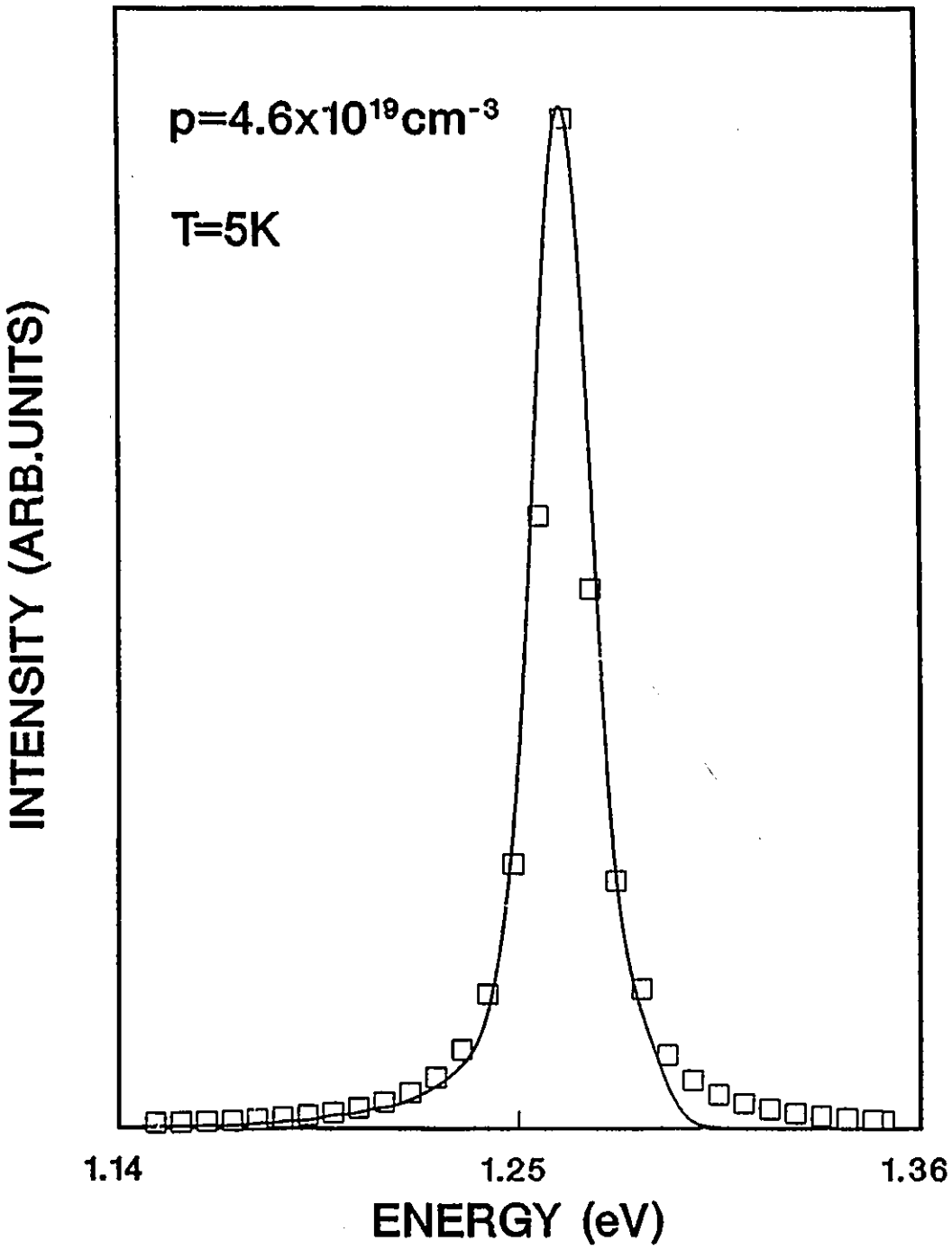

Figure 4.3.3.5. Experimental luminescence spectrum (solid line) of Zn-doped $Ga_{0.85}In_{0.15}As$ with $4.6x10^{19}$ holes cm^{-3} at 5 K and theoretical calculation (open squares).

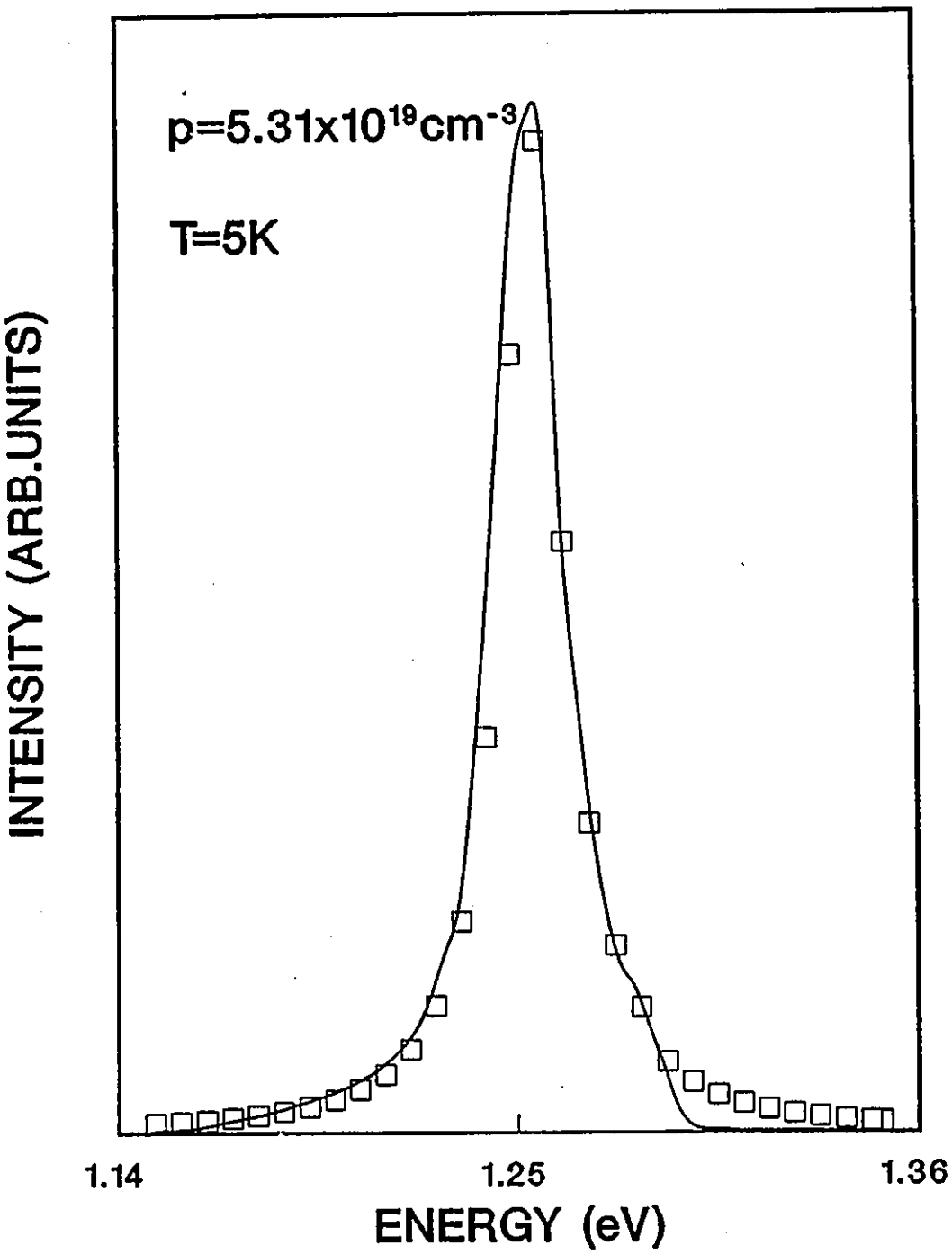

Figure 4.3.3.6. Experimental luminescence spectrum (solid line) of Zn-doped $Ga_{0.85}In_{0.15}As$ with $5.31x10^{19}$ holes cm^{-3} at 5 K and theoretical calculation (open squares).

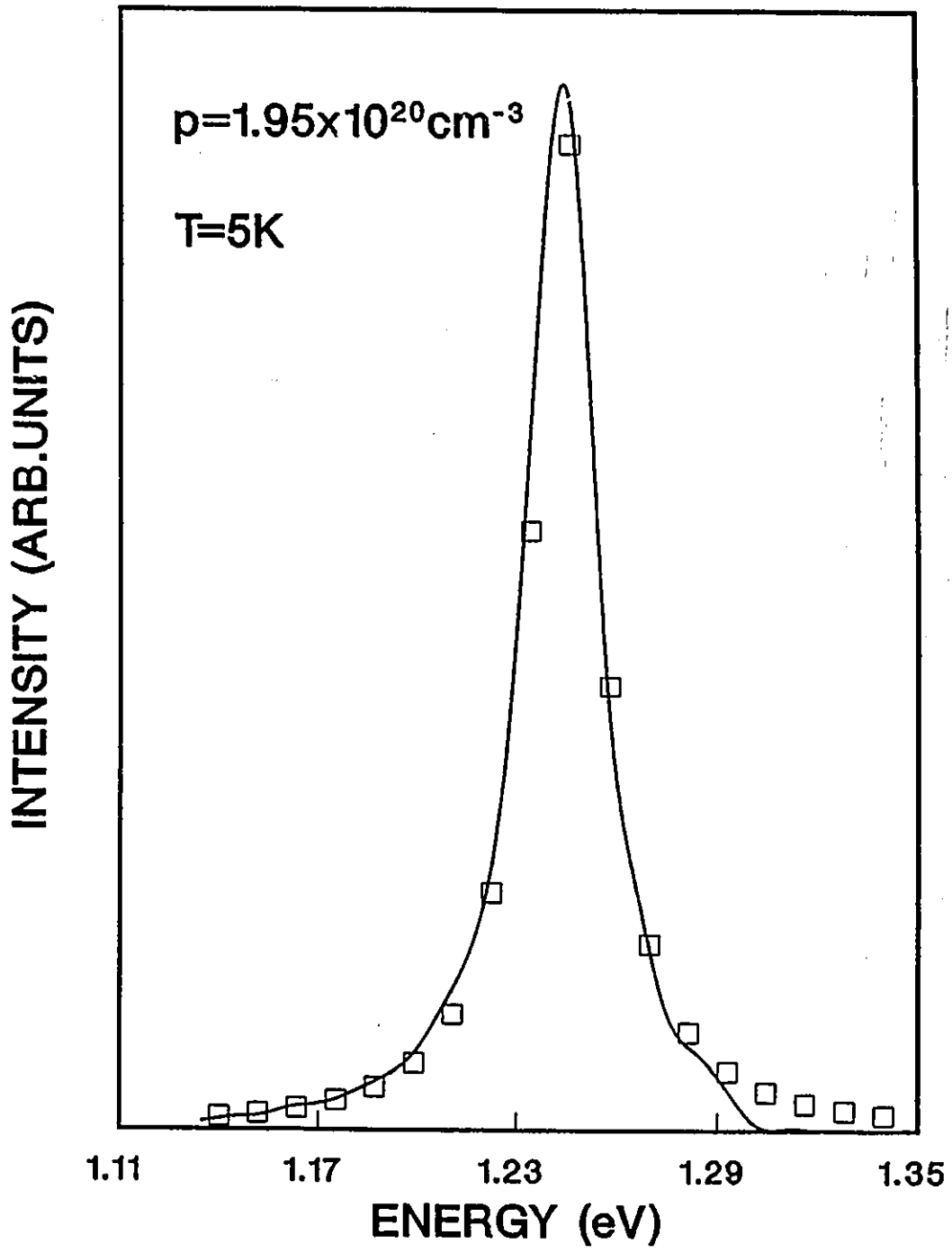

Figure 4.3.3.7. Experimental luminescence spectrum (solid line) of Zn-doped $Ga_{0.85}In_{0.15}As$ with $1.95x10^{20}$ holes cm^{-3} at 5 K and theoretical calculation (open squares).

conserving processes. The shoulder at higher energy represents the $\vec{k}$-nonconserving transitions. The fitting parameters were the temperature T, the Fermi energy E_F, the broadening parameter C_0, the peak maximum B_0 and the band tail parameter η. These are reported in tables 4.3.3.1 and 4.3.3.2.

The temperature of the carriers found by the analysis of the spectra (see tables 4.3.3.1 and 4.3.3.2) is much higher than the temperature measured by the Si sensor attached to the sample holder. In fact, we have not been able to fit any PL spectra with temperatures of less than T=15 K. This is due to illumination heating effects caused by the laser light (excitation power density 2 W/cm^2). The experimental values of the Fermi energy and of the peak maximum B_0, both of which are directly deduced from figs.4.3.3.1 to 4.3.3.7 are in good agreement with the corresponding fitted values obtained from the line shape analysis (see tables 4.3.3.1 and 4.3.3.2). Furthermore, as doping increases, the $\vec{k}$-conserving transitions shift to lower photon energies, this being an indication of the doping-induced band gap shrinkage (see tables 4.3.3.1 and 4.3.3.2). The overall agreement between experimental and fitted line shapes is good for the whole series of spectra analyzed. However, on the high energy side of the spectrum, the calculated line shape significantly overestimates the luminescence intensity observed in the experiment. This could be attributed to an incomplete thermalization of the electrons before recombination occurs. Indeed, because our samples are fully degenerate with $E_F < E_v$, electrons excited high into the conduction band (~0.40 eV above the conduction band minimum for GaAs) have

Table 4.3.3.1 Experimental (Expt.) values directly deduced from the spectrum and calculated (Calc.) values using equ.(2.6.6) of various heavily doped GaAs samples.

p (cm^{-3})	T (Expt.) (K)	E_F (Expt.) (eV)	B_0 (Expt.) (eV)	T (Calc.) (K)	E_F (Calc.) (eV)	B_0 (Calc.) (eV)	C_0 (Calc.) (meV)	η (Calc.) (meV)
1.60×10^{18}	5 (1)	1.500 (1)	1.492 (1)	15 (3)	1.500 (2)	1.492 (3)	8 (2)	24 (2)
1.10×10^{19}	5 (1)	1.500 (1)	1.474 (1)	15 (3)	1.502 (5)	1.475 (3)	10 (2)	24 (2)
1.97×10^{19}	5 (1)	1.503 (1)	1.471 (1)	15 (3)	1.502 (5)	1.470 (3)	13 (2)	25 (2)

Table 4.3.3.2 Experimental (Expt.) values directly deduced from the spectrum and calculated (Calc.) values using equ.(2.6.6) of various heavily doped $Ga_{0.85}In_{0.15}As$ samples.

p (cm^{-3})	T (Expt.) (K)	E_F (Expt.) (eV)	B_0 (Expt.) (eV)	T (Calc.) (K)	E_F (Calc.) (eV)	B_0 (Calc.) (eV)	C_0 (Calc.) (meV)	η (Calc.) (meV)
$1.60x10^{19}$	5 (1)	1.278 (1)	1.257 (1)	20 (3)	1.277 (2)	1.258 (3)	8 (2)	30 (2)
$4.60x10^{19}$	5 (1)	1.291 (1)	1.262 (1)	15 (3)	1.285 (5)	1.262 (3)	8 (2)	30 (2)
$5.31x10^{19}$	5 (1)	1.289 (1)	1.254 (1)	15 (3)	1.285 (5)	1.254 (3)	10 (2)	40 (2)
$1.95x10^{20}$	5 (1)	1.293 (1)	1.246 (1)	15 (3)	1.293 (5)	1.244 (3)	12 (2)	32 (2)

an increased probability of recombining with holes in the valence band before they have a chance to thermalize. In addition, as already mentioned, it is well known that Kane's theory overestimates the magnitude of the band tail.

The PL spectra of heavily doped GaAs (sample 7) and $Ga_{0.85}In_{0.15}As$ (samples 12 and 15) have been fitted in the temperature range of 5-300 K using equ.(2.6.6). The results which are qualitatively the same for all the samples with concentrations higher than 10^{18} cm^{-3} are displayed in figs.4.3.3.8 to 4.3.3.10.

The temperature dependence of the carriers found by the analysis of the PL spectra (see tables 4.3.3.3 to 4.3.3.5) is in good agreement with the experimental temperature as measured by the Si sensor, but only in the temperature range of 20-300 K. For example, in GaAs (Sample 7), the PL spectrum obtained at 132 K has been fitted with a temperature of 145 K (this corresponds to a relative temperature deviation of less than 9%), giving good results as can be appreciated in fig.4.3.3.8. Consequently, the fitted temperature values seem to indicate that illumination heating effects due to the laser light become negligible for temperatures above 20 K (see tables 4.3.3.3 to 4.3.3.5). The experimental Fermi energy which can be directly deduced from the PL spectra (up to 167 K for GaAs (sample 7) and up to ~60 K for $Ga_{0.85}In_{0.15}As$ (samples 12 and 15) are in good agreement with the corresponding fitted values (see tables 4.3.3.3 to 4.3.3.5). Furthermore, the peak maximum moves to lower photon energies upon heating as expected due to the reduction of the band gap with heating (see tables 4.3.3.3 to 4.3.3.5).

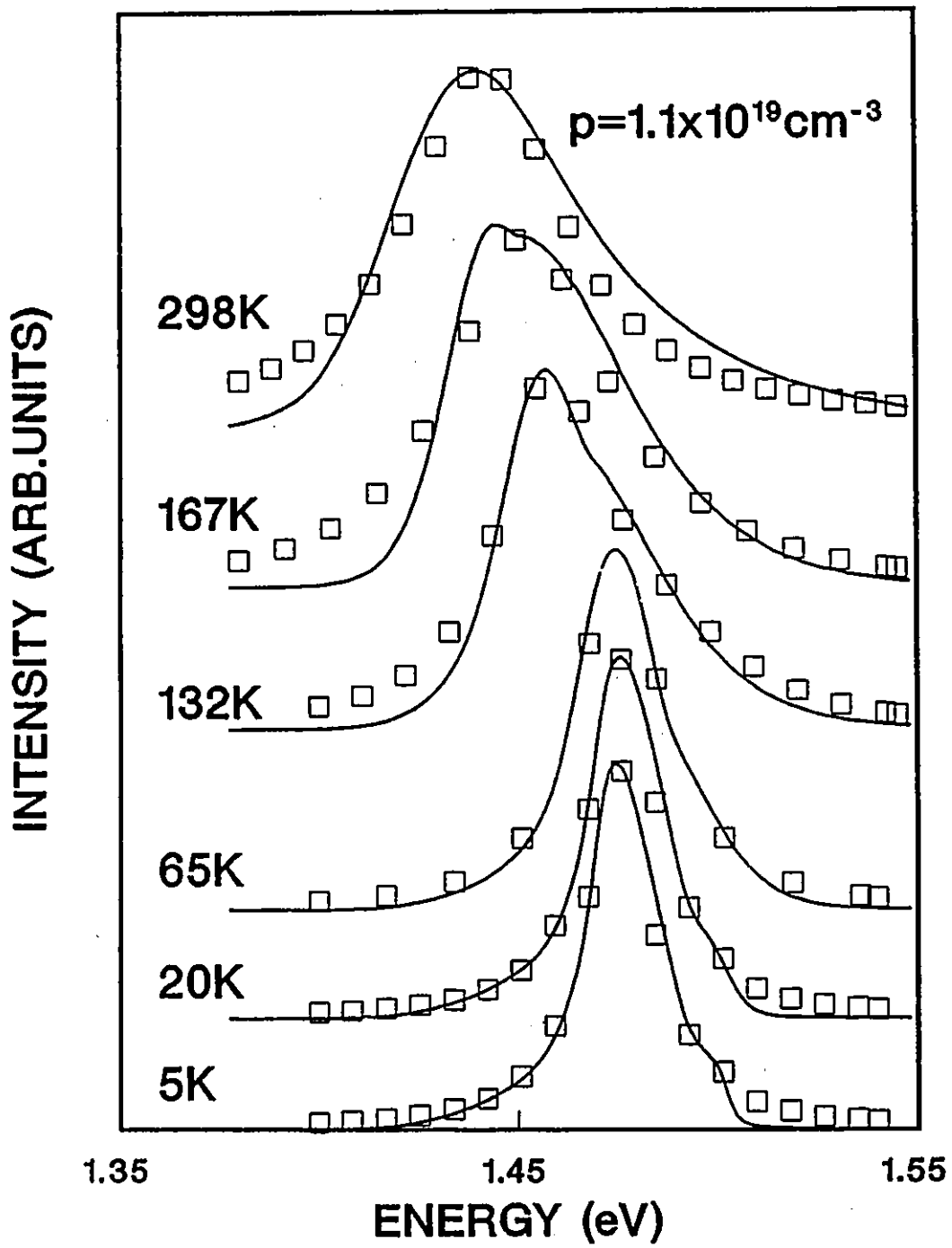

Figure 4.3.3.8. Experimental luminescence spectra (solid line) of Zn-doped GaAs with 1.1×10^{19} holes cm^{-3} as a function of temperature and theoretical calculation (open squares).

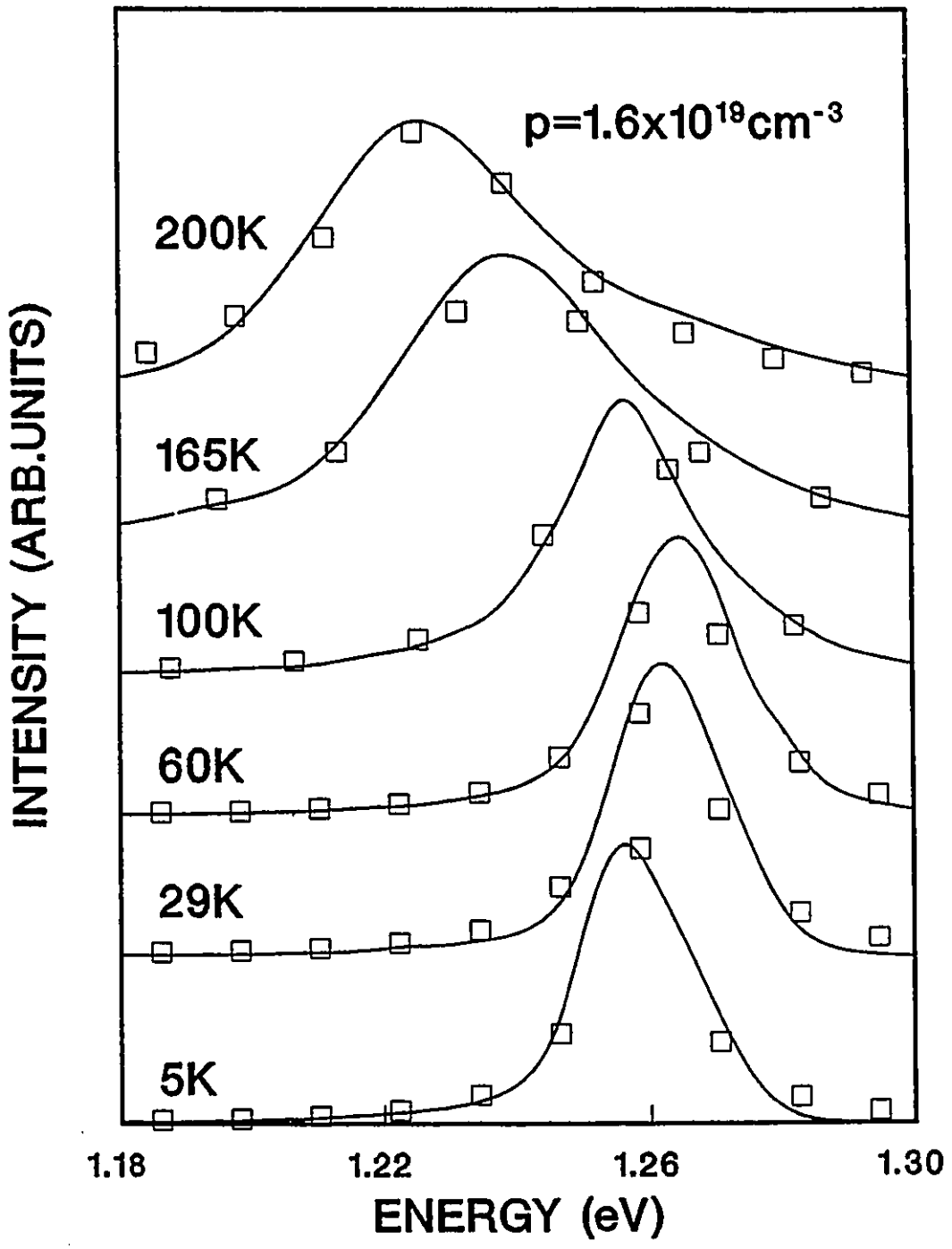

Figure 4.3.3.9. Experimental luminescence spectra (solid line) of Zn-doped $Ga_{0.85}In_{0.15}As$ with $1.6x10^{19}$ holes cm^{-3} as a function of temperature and theoretical calculation (open squares).

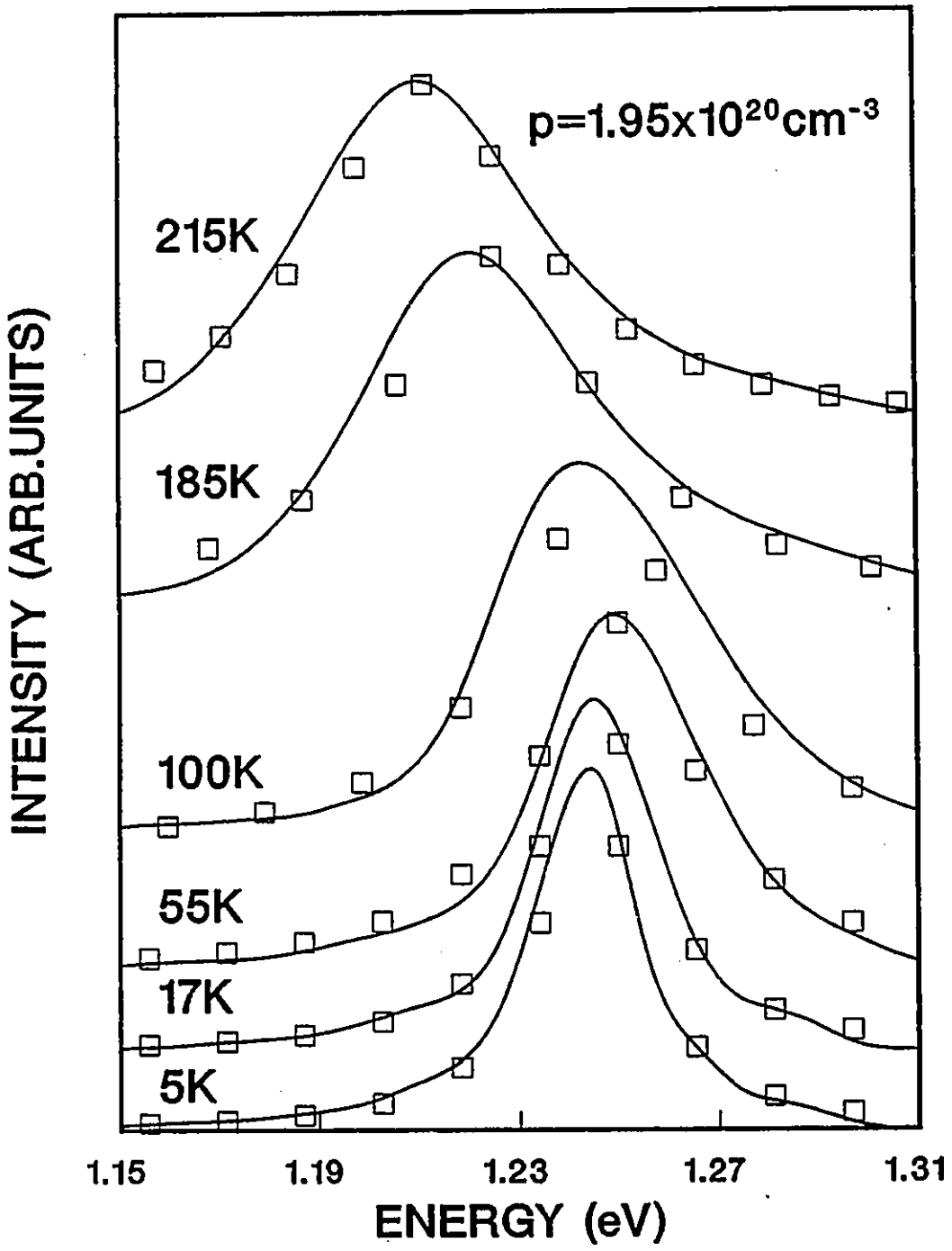

Figure 4.3.3.10. Experimental luminescence spectra (solid line) of Zn-doped $Ga_{0.85}In_{0.15}As$ with $1.95x10^{20}$ holes cm^{-3} as a function of temperature and theoretical calculation (open squares).

Table 4.3.3.3 Experimental (Expt.) values directly deduced from the spectrum and calculated (Calc.) values using equ.(2.6.6) at various temperatures for a typical heavily doped GaAs sample.

p (cm^{-3})	T (Expt.) (K)	E_F (Expt.) (eV)	B_0 (Expt.) (eV)	T (Calc.) (K)	E_F (Calc.) (eV)	B_0 (Calc.) (eV)	C_0 (Calc.) (meV)	η (Calc.) (meV)
1.10×10^{19}	5 (1)	1.500 (1)	1.474 (1)	15 (3)	1.502 (2)	1.475 (3)	10 (2)	24 (2)
	20 (1)	1.500 (1)	1.476 (1)	23 (3)	1.499 (5)	1.476 (3)	10 (2)	24 (2)
	65 (1)	1.497 (1)	1.474 (1)	65 (3)	1.490 (5)	1.475 (3)	12 (2)	27 (2)
	132 (1)	1.476 (1)	1.457 (1)	145 (3)	1.480 (5)	1.458 (3)	16 (2)	38 (2)
	167 (1)	1.450 (1)	1.444 (1)	195 (3)	1.450 (5)	1.452 (3)	22 (2)	50 (2)
	298 (1)	...	1.440 (1)	320 (3)	1.450 (5)	1.442 (3)	23 (2)	55 (2)

Table 4.3.3.4 Experimental (Expt.) values directly deduced from the spectrum and calculated (Calc.) values using equ.(2.6.6) at various temperatures for a typical heavily doped $Ga_{0.85}In_{0.15}As$ sample.

p (cm^{-3})	T (Expt.) (K)	E_F (Expt.) (eV)	B_0 (Expt.) (eV)	T (Calc.) (K)	E_F (Calc.) (eV)	B_0 (Calc.) (eV)	C_0 (Calc.) (meV)	η (Calc.) (meV)
$1.60x10^{19}$	5 (1)	1.278 (1)	1.257 (1)	20 (3)	1.277 (2)	1.258 (3)	8 (2)	30 (2)
	29 (1)	1.280 (1)	1.262 (1)	30 (3)	1.275 (5)	1.262 (3)	9 (2)	31 (2)
	60 (1)	...	1.264 (1)	65 (3)	1.273 (5)	1.264 (3)	9 (2)	31 (2)
	100 (1)	...	1.256 (1)	110 (3)	1.270 (5)	1.256 (3)	12 (2)	38 (2)
	165 (1)	...	1.236 (1)	170 (3)	1.265(5)	1.240 (3)	18 (2)	48 (2)
	200 (1)	...	1.225 (1)	215 (3)	1.260 (5)	1.282 (3)	20 (2)	52 (2)

Table 4.3.3.5 Experimental (Expt.) values directly deduced from the spectrum and calculated (Calc.) values using equ.(2.6.6) at various temperatures for a typical heavily doped $Ga_{0.85}In_{0.15}As$ sample.

p (cm^{-3})	T (Expt.) (K)	E_F (Expt.) (eV)	B_0 (Expt.) (eV)	T (Calc.) (K)	E_F (Calc.) (eV)	B_0 (Calc.) (eV)	C_0 (Calc.) (meV)	η (Calc.) (meV)
$1.95x10^{20}$	5 (1)	1.293 (1)	1.246 (1)	15 (3)	1.293 (2)	1.244 (3)	12 (2)	32 (2)
	17 (1)	1.289 (1)	1.244 (1)	20 (3)	1.293 (5)	1.245 (3)	13 (2)	32 (2)
	55 (1)	1.285 (1)	1.246 (1)	60 (3)	1.279 (5)	1.249 (3)	19 (2)	36 (2)
	100 (1)	...	1.236 (1)	105 (3)	1.270 (5)	1.246 (3)	23 (2)	40 (2)
	185 (1)	...	1.219 (1)	200 (3)	1.265 (5)	1.225 (3)	25 (2)	45 (2)
	215 (1)	...	1.210 (1)	230 (3)	1.262 (5)	1.212 (3)	25 (2)	45 (2)

A model taking into account band tailing effects has been fitted both as a function of temperature in the range of 5-300 K, and of carrier concentration in the range of $p=1.6\times10^{18}$ cm^{-3}-$p=1.95\times10^{20}$ cm^{-3}, to the PL spectra of heavily doped GaAs and $Ga_{0.85}In_{0.15}As$. The overall agreement between calculated and experimental line shapes is good for the whole series of spectra analyzed. In addition, this simple model was used to compare the sample temperature as measured by the Si sensor to the fitted temperature. This enabled us to determine the temperature range at which illumination heating effects become negligible.

CONCLUSION

We have performed temperature dependent PL experiments on a series of GaAs and $Ga_{0.85}In_{0.15}As$ epilayers grown by LP-MOVPE. The samples were zinc doped p-type, with hole concentrations in the range of $n=1x10^{14}$ (nominally undoped)-$p=1.95x10^{20}$ cm^{-3}.

At low doping levels there are well defined bound states associated with each dopant ion. A low doped $Ga_{0.85}In_{0.15}As$ sample ($p=3.22x10^{15}$ cm^{-3}) provided a reference band gap at $T=5$ K ($E_g(5)=(1.296 \pm 0.003)$ eV) and the binding energy of the zinc acceptor ($E(Zn^0)=(0.025 \pm 0.003)$ eV). As the dopant density increases, the bound states broaden into a distinct impurity band because of the overlap among the dopant-ion orbits. As the density increases still further, the impurity band merges with the valence band above the Mott transition[11]. At the same time, the conduction band edge moves downward and the valence-band edge moves upward. On the whole, the band gap narrows and the density of state curve is distorted because the states in each band do not shift with the same amount. This gives rise to a density of states band tail extending into the gap and containing both extended and localised states.

At high doping levels, the band gap shrinkage, expected from band tailing effects caused by the random distribution of the impurities, has been studied as a function of the free hole concentration. The free hole dependence of the 5 K band gap shrinkage has been provided to the best of our knowledge for the first

time in $Ga_{0.85}In_{0.15}As$, $|\Delta E_g| = 1.4 \times 10^{-8} p^{1/3}$ where it appears to be smaller than in GaAs, $|\Delta E_g| = 2.7 \times 10^{-8} p^{1/3}$, with $|\Delta E_g|$ in eV and p in cm^{-3}.

A model based on the presence of Kane[2] band tails and on the assumption of a constant matrix element for the relevant optical transitions has been fitted to all the PL spectra of heavily doped GaAs and $Ga_{0.85}In_{0.15}As$ obtained at $T=5$ K in the range of $p=1.6 \times 10^{18}$-$p=1.95 \times 10^{20}$ cm^{-3}. The model has also been fitted in the temperature range of 5-300 K to three typical hole concentrations. This model provided a good description of the experimental data. However, on the high energy side of the PL spectra of heavily doped GaAs and $Ga_{0.85}In_{0.15}As$, the calculated line shape significantly overestimates the experimental line shape. This was attributed to an incomplete thermalization of the minority carriers before recombining with the holes left behind upon excitation. In addition, illumination heating effects caused by the laser light (power excitation density 2 W/cm^2) made it impossible to fit any PL spectra obtained at $T=5$ K with temperatures of at least 15 K. Nevertheless, the agreement between the sample temperature as measured by the Si sensor and the fitted temperature is good in the temperature range of 20-300 K. This indicates that illumination heating effects are negligible for temperatures higher than 20 K.

LIST OF TABLES

LIST OF FIGURES

REFERENCES

[1] N.F. Mott, and E.A. Davis. Electronic processes in non-crystalline materials. Clarendon Press, Oxford. 1971.

[2] E.O. Kane. Phys. Rev. **131**, 79 (1963).

[3] W.J. Schaff, P.J. Tasker, M.C. Foisy, and L.F. Eastman. Semiconductors and Semimetals, Vol. 33. Edited by T.P. Pearsall. Academic Press Inc, San Diego, 1991. p.128.

[4] J. Wagner. Solid-State Electron. **28**, 25 (1985).

[5] F. Bloch. Zeit. Phys. **52**, 555 (1928).

[6] E.O. Kane. J. Phys. Chem. Solids. **1**, 249 (1957).

[7] Landolt-Bornstein. Numerical data and functional relationship in science and technology, Vol.22a. Edited by O. Madelung. Springer-Verlag, Berlin. 1987.

[8] W. Kohn. Solid-State Phys. **5**, 257 (1957).

[9] O. Madelung. Introduction to solid state theory. Springer-Verlag, Berlin. 1978.

[10] H.B. Bebb and E.W. Williams. Semiconductors and Semimetals, Vol.8. Edited by R.K. Willardson and A.C. Beer. Academic Press Inc, New-York, 1972. p.279.

[11] P.J. Dean and D.C. Herbert. In Topics in current Physics, Vol.14. Edited by K. Cho. Springer-Verlag, Berlin. 1979.

[12] R.J. Elliot. Introduction to the theory of excitons in Polarons and excitons in

polar semiconductors and Ionic crystals. Edited by J.T. Devreese and F. Peeters. Nato ASI Series, Series B: Physics. **108**, Antwerp (1982).

[13] J.J. Hopfield. Proc. 7th Int. Conf. Phys. Semicond. Dunod, Paris. 1964. p.725.

[14] D.C. Herbert. J. Phys. C. **10L**, 131 (1977).

[15] F. Williams. Phys. Status Solidi. **25**, 493 (1968).

[16] D.G. Thomas, M. Gershenzon, and F.A. Trumfore. Phys. Rev. **133**, A269 (1964).

[17] D.M. Eagles. J. Phys. Chem. Solids. **16**, 76 (1960).

[18] G. Borghs, K. Bhattacharyyva, K. Deneffe, P. Van Mieghem, and R. Mertens. J. Appl. Phys. **66**, 4381 (1989).

[19] R. Benzaquen, T. Erland, C. Lacelle, E. Fortin, and A.P. Roth. Can. J. Phys. Accepted for publication.

[20] R.A. Abram, G.J. Rees, and B.L.H. Wilson. Adv. Phys. **27**, 779 (1978).

[21] D. Olega and M. Cardona. Phys. Rev. B. **22**, 886 (1980).

[22] H.C. Casey and F. Stern. J. Appl. Phys. **47**, 631 (1976).

[23] G. Lasher and F. Stern. Phys. Rev. **133**, A553 (1964).

[24] A.P. Roth, M.A. Sacilotti, R.A. Masut, A. Machado, and P.J. D'Arcy. J. Appl. Phys. **60**, 2003 (1986).

[25] U. Heim, and P. Hiesinger. Phys. Status Solidi. **B66**, 461 (1974).

[26] D.J. Ashen, P.J. Dean, D.T.J. Hurle, J.B. Mullin, A.M. White, and P.D. Green. J. Phys. Chem. solids. **36**, 1041 (1975).

[27] A.P. Roth, M.A. Sacilotti, R.A. Masut, D. Morris, J. Young, C. Lacelle, E. Fortin, and J.L. Brebner. Can. J. Phys. **67**, 330 (1989).

[28] J.R. Haynes. Phys. Rev. Lett. **4**, 361 (1960).

[29] K.H. Goetz, D. Bimberg, H. Jürgensen, J. Selders, A.V. Solomonov, G.F. Glinskii, and M. Razeghi. J. Appl. Phys. **54**, 8 (1983).

[30] Y.P. Varshni. Physica (Utrecht). **39**, 149 (1967).

[31] A.P. Roth, J.B. Webb, and D.F. Williams. Phys. Rev. B. **25**, 7836 (1982).

[32] P.E. Schmid. Phys. Rev. B. **23**, 5531 (1980).

[33] I. Hamberg, C.G. Granqvist, K.F. Berggren, B.E. Sernelius, and L. Engström. Phys. Rev. B. **30**, 3240 (1984).

[34] J. Wagner. Phys. Rev. B. **29**, 2002 (1983).

[35] K.F. Berggren, and B.E. Sernelius. Phys. Rev. B. **24**, 1971 (1981).

[36] G.D. Mahan. J. Appl. Phys. **51**, 2634 (1980).

[37] J. Serre, A. Ghazali, and P. Leroux-Hugon. Phys. Rev. B. **23**, 1979 (1981).

APPENDIX I

THE EXCITON PROBLEM IN THE EFFECTIVE MASS APPROXIMATION

Let us consider a bulk semiconductor and assume that one can approximate its band structure by a single spherical conduction band with dispersion relation

$$E_c(\vec{k}) = E_g + \frac{\hbar^2 \vec{k}^2}{2m_e^*} \tag{I.1}$$

separated by the band gap, E_g, from a single spherical valence band with dispersion relation

$$E_v(\vec{k}) = -\frac{\hbar^2 \vec{k}^2}{2m_h^*} \tag{I.2}$$

Our problem consists of solving Schrödinger's equation for the stationary states $\psi(\vec{r}_e,\vec{r}_h)$ of the exciton system

$$\left(-\frac{\hbar^2}{2m_e^*}\vec{\nabla}_e^2 - \frac{\hbar^2}{2m_h^*}\vec{\nabla}_h^2 - \frac{e^2}{\kappa|\vec{r}_e - \vec{r}_h|} \right) \Psi(\vec{r}_e,\vec{r}_h) = E\Psi(\vec{r}_e,\vec{r}_h) \tag{I.3}$$

Since the Coulombic term only affects the relative electron-hole coordinates, it is convenient to make the following change of variables

$$\vec{r} = \vec{r}_e - \vec{r}_h \tag{I.4}$$

$$\vec{R} = \frac{m_e^* \vec{r}_e + m_h^* \vec{r}_h}{\left(m_e^* + m_h^*\right)} \tag{I.5}$$

Solving equs.(I.4) and (I.5) for $\vec{r}_e$ and $\vec{r}_h$ gives

$$\vec{r}_e = \vec{R} + \frac{\mu}{m_e^*} \vec{r} \tag{I.6}$$

$$\vec{r}_h = \vec{R} - \frac{\mu}{m_h^*} \vec{r} \tag{I.7}$$

where $\mu^{-1} = (m_e^*)^{-1} + (m_h^*)^{-1}$ is the reduced mass.

By carrying out chain rule differentiation with respect to the electron and hole coordinates, the Laplacian operators $\vec{\nabla}_e^2$ and $\vec{\nabla}_h^2$, are given by

$$\vec{\nabla}_e^2 = \vec{\nabla}_r^2 + \frac{\mu^2}{m_h^*} \vec{\nabla}_R^2 + \frac{2\mu}{m_h^*} \vec{\nabla}_R \cdot \vec{\nabla}_r \tag{I.8}$$

$$\vec{\nabla}_h^2 = \vec{\nabla}_r^2 + \frac{\mu^2}{m_e^*} \vec{\nabla}_R^2 - \frac{2\mu}{m_e^*} \vec{\nabla}_R \cdot \vec{\nabla}_r \tag{I.9}$$

Replacing equs.(I.8) and (I.9) into equ.(I.3) yields

$$\left(-\frac{\hbar^2}{2M} \vec{\nabla}_R^2 - \frac{\hbar^2}{2\mu} \vec{\nabla}_r^2 - \frac{e^2}{\kappa r} \right) \Psi(\vec{r}, \vec{R}) = E \Psi(\vec{r}, \vec{R}) \tag{I.10}$$

where $M = m_e^* + m_h^*$.

Let us now separate equ.(I.10) into two distinct partial differential equations of the variables $\vec{r}$ and $\vec{R}$, respectively, by introducing

$$\Psi(r,\vec{R}) = \eta(r)\chi(\vec{R}) \tag{I.11}$$

where $\eta(r)$ is the exciton wavefunction of relative motion and $\chi(\vec{R})$ represents the wavefunction describing the motion of the centre of mass of the exciton.

Replacing equ.(I.11) into equ.(I.10) gives

$$-\frac{1}{\eta(r)}\frac{\hbar^2}{2\mu}\vec{\nabla}_r^2\eta(r) - \frac{e^2}{\kappa r} = \frac{1}{\chi(\vec{R})}\frac{\hbar^2}{2M}\vec{\nabla}_R^2\chi(\vec{R}) + E = \lambda \tag{I.12}$$

where λ is the separation parameter.

Equ.(I.12) represents, in fact, the following two distinct partial differential equations

$$-\frac{\hbar^2}{2\mu}\vec{\nabla}^2\eta(r) - \frac{e^2}{\kappa r}\eta(r) = \lambda\,\eta(r) \tag{I.13}$$

$$\frac{\hbar^2}{2M}\vec{\nabla}^2\chi(\vec{R}) + (E-\lambda)\,\chi(\vec{R}) = 0 \tag{I.14}$$

Equ.(I.13) is the well known hydrogen-like Schrödinger's equation with eigenfunctions and eigenvalues given by

$$\eta(r) = R_{n,l}(r)\,Y_l^m(\theta,\phi) \tag{I.15}$$

$$\lambda = -\frac{\mu e^4}{2\hbar^2\kappa^2 n^2} \tag{I.16}$$

where $R_{n,l}(r)$ and $Y_l^m(\theta,\phi)$ are the well known radial and spherical harmonic wavefunctions, respectively. n, l and m are the principal quantum numbers.

The solution of equ.(I.14) is straightforward with eigenfunctions and eigenvalues

given by

$$\chi(\vec{R}) = \exp(i\vec{K}\cdot\vec{R}) \tag{I.17}$$

$$\vec{K}^2 = \frac{2M}{\hbar^2}(E-\lambda) \tag{I.18}$$

Combining equ.(I.11) along with equs.(I.15) to (I.18) one finally obtains for the eigenfunction solutions

$$\Psi_{n,l,m}(\vec{r},\vec{R}) = \exp(i\vec{K}\cdot\vec{R})\, R_{n,l}(r)\, Y_l^m(\theta,\phi) \tag{I.19}$$

and for the eigenvalue solutions

$$E_n(\vec{K}) = -\frac{\mu e^4}{2\hbar^2\kappa^2 n^2} + \frac{\hbar^2\vec{K}^2}{2M} \tag{I.20}$$

where $E_{x,n}(\vec{K})$ is measured from the bottom of the conduction band.

APPENDIX II

LEAST-SQUARES TECHNIQUE

Consider a set of p data points defined by the variables x_r, y_r with $r=1, p$. Let $F(x,\bar{q})$ be a vector function of $\bar{q}=(q_i,\ i=1,n)$ to be fitted to the previous p data points.

Our problem is to determine the vector function $F(x,\bar{q})$ which minimizes the following expression

$$\chi^2 = \sum_{r=1}^{p} (y_r - F(x_r,\bar{q}))^2 \qquad \text{(II.1)}$$

which gives, for every q_l

$$\frac{\partial \chi^2}{\partial q_l} = -2 \sum_{r=1}^{p} [\, y_r - F(x_r,\bar{q}) \,] \left(\frac{\partial F}{\partial q_l} \right)_{x=x_r} = 0 \qquad \text{(II.2)}$$

Let

$$q_l = q_l^0 + \eta_l \qquad \text{(II.3)}$$

the q_l represent the actual solutions and the corresponding q_l^0 are the initial trial values.

$F(x,\bar{q})$ can now be expanded into a Taylor's series of n variables near q_l^0, then equ.(II.2) can be written as

$$\sum_{r=1}^{p}\left[y_r - F(x_r,q^0) - \sum_{j=1}^{n}\eta_j\left(\frac{\partial F}{\partial q_j}\right)_{x=x_r,q=q^0}\right]\left(\frac{\partial F}{\partial q_i}\right)_{x=x_r,q=q^0} = 0 \qquad \text{(II.4)}$$

which can be rewritten as

$$\sum_{r=1}^{p}\left[(y_r - F(x_r,q^0))\left(\frac{\partial F}{\partial q_i}\right)_{x=x_r,q=q^0} - \sum_{j=1}^{n}\eta_j\left(\frac{\partial F}{\partial q_i}\right)_{x=x_r,q=q^0}\left(\frac{\partial F}{\partial q_j}\right)_{x=x_r,q=q^0}\right] = 0 \quad \text{(II.5)}$$

regrouping the various sums gives

$$\sum_{r=1}^{p}[y_r - F(x_r,q^0)]\left(\frac{\partial F}{\partial q_i}\right)_{x=x_r,q=q^0} - \sum_{r=1}^{p}\sum_{j=1}^{n}\eta_j\left(\frac{\partial F}{\partial q_j}\right)_{x=x_r,q=q^0}\left(\frac{\partial F}{\partial q_i}\right)_{x=x_r,q=q^0} = 0 \text{ (II.6)}$$

Letting

$$d_i = \sum_{r=1}^{p}[y_r - F(x_r,q^0)]\left(\frac{\partial F}{\partial q_i}\right)_{x=x_r,q=q^0} \qquad \text{(II.7)}$$

and

$$A_{ij} = \sum_{r=1}^{p}\left(\frac{\partial F}{\partial q_j}\right)_{x=x_r,q=q^0}\left(\frac{\partial F}{\partial q_i}\right)_{x=x_r,q=q^0} \qquad \text{(II.8)}$$

we get

$$d_i = \sum_{j=1}^{n} A_{ij}\,\eta_j \qquad \text{(II.9)}$$

which can be written in matrix form as follows

$$\vec{D} = A\,\vec{\eta} \qquad \text{(II.10)}$$

We can now carry out an iterative procedure:

1 - Evaluation of the matrix elements defined by equs. (II.7) and (II.8) given the parameters x_r, y_r, $F(x,q)$, $\left(\frac{\partial F}{\partial q_i}\right)_{x=x_r,q=q^0}$ and q^0.

2 - Numerical solution of the $n \times n$ linear system equ.(II.10) using Gaussian elimination.

3 - Correction of the initial trial values q^0.

4 - Reiteration of the iterative procedure up to the required precision.

APPENDIX III

LOW-PRESSURE METAL ORGANIC VAPOUR PHASE EPITAXY SETUP

In recent years, there has been a rapid development in the production of electronic and opto-electronic devices based on thin single crystal semiconductor films. The growth of such layers on single crystal substrates, with the atom in the layer duplicating the arrangement of the atoms in the substrate, is known as epitaxy.

Epitaxy is divided into three general categories: liquid phase epitaxy (LPE), vapour phase epitaxy (VPE), and solid phase epitaxy (SPE). VPE includes as sub-categories metal-organic vapour phase epitaxy (MOVPE) and molecular beam epitaxy (MBE), among others.

The MOVPE growth technique is emerging as one of the most promising of all the epitaxial growth techniques currently in use. This is primarily due to the versatility of this technique. It is capable of producing a large number of high purity semiconductor materials including multilayer structures. Advanced digital and optical devices based on thin film structures have been successfully fabricated using this technique. This versatility, combined with the possibility of relatively cheap mass production of thin films by this method, suggests that the MOVPE technique will play an increasingly important role in device fabrication in the future.

MOVPE is a deposition technique where metal-organic compounds and hydrides serve respectively as the sources of the metal and non-metal

components of the semiconductor to be formed. The desired reaction of these sources is pyrolysis of the compounds near the hot substrate followed by incorporation into the crystal epilayer. The metal-organics commonly used are high vapour pressure liquids or solids at room temperature, while the hydrides are gases or liquids. A schematic of the MOVPE system is shown in fig.III.1.

The GaAs layers investigated in this work have been grown on semi-insulating Cr-doped (100) GaAs substrates, in a horizontal low-pressure MOVPE reactor (see fig.III.1) heated by infrared radiation. The $Ga_{0.85}In_{0.15}As$ layers were also grown by LP-MOVPE but on GaAs substrates oriented 2° off (001) towards [011]. The effect of cutting the substrate 2° off (001) towards [011] is to create steps on the surface in two orthogonal [110] directions. These steps reduce the mobility of dislocations along the [011] direction, therefore limiting their multiplication as the layer thickness increases. The gas mass flow rates are controlled by electronic mass flow controllers, independently of the pressure in the reactor. The pressure can be reduced by a vacuum pump and automatically adjusted by a pressure controller connected to a capacitance manometer and an electrical butterfly valve. The pressure in the gas manifold is kept at 600 Torr by two micro-valves, independently of the pressure in the reactor. The layers were grown at a pressure of 80 Torr (GaAs) or 40 Torr ($Ga_{0.85}In_{0.15}As$) from the reaction of (AsH_3), diluted (5%) in H_2 and TMG (GaAs) or TMI ($Ga_{0.85}In_{0.15}As$). The liquid TMG or TMI is kept at a constant temperature of -12° C in a stainless steel bubbler, and carried to the reactor by palladium-purified H_2. The typical growth

parameters are the growth temperature (575-700° C), growth rate 2-3 monolayers/s.

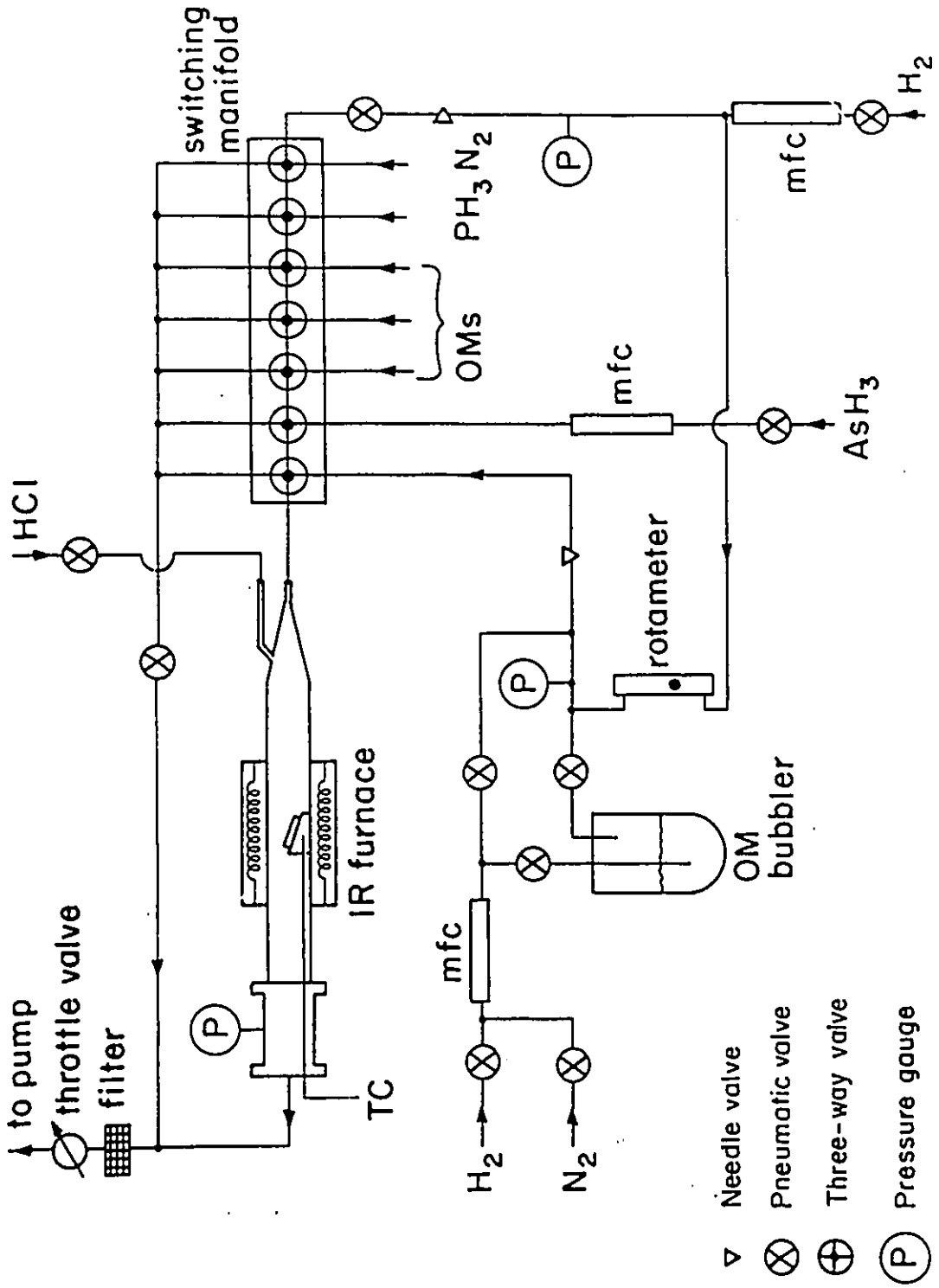

Figure III.1. Low-pressure metal organic vapour phase epitaxy setup.